BNWL-340

AEC RESEARCH and DEVELOPMENT REPORT

REACTOR PHYSICS DEPARTMENT TECHNICAL ACTIVITIES QUARTERLY REPORT JULY, AUGUST, SEPTEMBER, 1966

OCTOBER 15, 1966

BATTELLE-NORTHWEST
BATTELLE MEMORIAL INSTITUTE / PACIFIC NORTHWEST LABORATORY

LEGAL NOTICE

PACIFIC NORTHWEST LABORATORY
RICHLAND, WASHINGTON
operated by
BATTELLE MEMORIAL INSTITUTE
for the
UNITED STATES ATOMIC ENERGY COMMISSION UNDER CONTRACT AT(45-1)-1830

PRINTED BY/FOR THE U. S. ATOMIC ENERGY COMMISSION

AEC-RLOO RICHLAND, WASH.

BNWL-340
UC-80, Reactor Technology

REACTOR PHYSICS DEPARTMENT TECHNICAL ACTIVITIES QUARTERLY REPORT JULY, AUGUST, SEPTEMBER, 1966

By

THE REACTOR PHYSICS DEPARTMENT STAFF

F. G. Dawson, Manager

October 15, 1966

PACIFIC NORTHWEST LABORATORY
RICHLAND, WASHINGTON

Printed in USA. Price $3.00. Available from the
Clearinghouse for Federal Scientific and Technical Information,
National Bureau of Standards,
U.S. Department of Commerce,
Springfield, Virginia 22151

REACTOR PHYSICS DEPARTMENT
TECHNICAL ACTIVITIES QUARTERLY REPORT
JULY, AUGUST, SEPTEMBER, 1966

FOREWORD

The Technical Activities Quarterly Report replaces the Physics Research Quarterly Report previously published by Battelle-Northwest's Reactor Physics Department. The objective of the report is to inform the scientific community in a timely manner of the technical progress made on the many phases of work within the department. The report contains brief technical discussions of accomplishments in all areas where significant progress has been made during the quarter. The results presented should be considered preliminary, and do not constitute final publication of the work. A list of publications and papers by the department staff is given in the report. Anyone wishing to obtain additional information on the work presented is encouraged to contact the author directly.

PREVIOUS REPORTS IN THIS SERIES

HW-42181	October, November, December	1955
HW-43441	January, February, March	1956
HW-44525	April, May, June	1956
HW-47012	July, August, September	1956
HW-48893	October, November, December	1956
HW-50598	January, February, March	1957
HW-51983	April, May, June	1957
HW-53492	July, August, September	1957
HW-54591	October, November, December	1957
HW-55879	January, February, March	1958
HW-56191	April, May, June	1958
HW-57861	July, August, September	1958
HW-59126	October, November, December	1958
HW-60220	January, February, March	1959
HW-61181	April, May, June	1959
HW-62727	July, August, September	1959
HW-63576	October, November, December	1959
HW-64866	January, February, March	1960
HW-66215	April, May, June	1960
HW-67219	July, August, September	1960
HW-68389	October, November, December	1960
HW-69475	January, February, March	1961
HW-70716	April, May, June	1961
HW-71747	July, August, September	1961
HW-72586	October, November, December	1961
HW-73116	January, February, March	1962
HW-74190	April, May, June	1962
HW-75228	July, August, September	1962
HW-76128	October, November, December	1962
HW-77311	January, February, March	1963
HW-77871	April, May, June	1963
HW-79054	July, August, September	1963
HW-80020	October, November, December	1963
HW-81659	January, February, March	1964
HW-83187	April, May, June	1964
HW-84369	July, August, September	1964
HW-84608	October, November, December	1964
BNWL-95	January, February, March	1965
BNWL-149	April, May, June	1965
BNWL-193	July, August, September	1965
BNWL-222	October, November, December	1965
BNWL-284	January, February, March	1966
BNWL-315	April, May, June	1966

TABLE OF CONTENTS

SUMMARY 1

REACTOR THEORY 4

Effective Cross Sections for Resonances in HGR - J. L. Carter 4

BNW Master Cross Section Library - Status Report - K. B. Stewart . . . 5

THERMAL REACTORS 6

Thermalization Calculational Study - Comparison of Results Obtained Using the RBU Monte Carlo, THERMOS, and Program S-XIII Codes - D. H. Thomsen 6

Critical Experiments with PuO_2-UO_2 Fuel Rods - V. O. Uotinen and and L. D. Williams 9

Results of Thermalization Calculations for PuO_2-UO_2-H_2O Lattices - R. C. Liikala and W. L. Purcell 10

Three-Dimensional Analysis of Plutonium Fuel MTR Cores: Preliminary Results - W. W. Porath 17

Measurements of k_∞ for a Pu-Al Thoria Supercell - N. A. Hill 20

A Thermal Column Study in The PCTR - G. E. Hanson and N. A. Hill 22

FAST REACTORS 32

Physics Characteristics of an 800 Liter Oxide FTR Reference Core - R. W. Hardie 32

Preliminary Evaluation of Cross-Section Data - W. W. Little, L. L. Maas, and R. W. Hardie 33

Algorithms for Collapsing Fast Reactor Cross Sections - W. W. Little, Jr and R. W. Hardie 35

Planning of FTR Critical Experiment Program - R. A. Bennett and R. A. Harris 36

FTR Shield Calculations - D. R. Marr and W. L. Bunch 38

Shield Analyses for Irradiated FTR Fuel Handling - W. L. Bunch. . . . 39

A Study of Fast-Thermal Reactor Experiment - R. M. Humes and D. A. Bitz 39

CRITICAL MASS PHYSICS 43

Resolving Time of a Pulsed Neutron Source Data Acquisition System - S. R. Bierman and K. L. Garlid* 43

Neutron Spectra Experiments - S. R. Bierman, L. E. Hansen G. L. Woodruff,** R. C. Lloyd and G. M. Hess III 46

Pulsed Neutron Source Measurements - $Pu(NO_3)_4$ Solutions - G. M. Hess III and S. R. Bierman. 49

Least Squares Data Reduction Code - G. M. Hess III. 50

Neutron Interaction Experiments with Bottles of U^{233} Solution - R. C. Lloyd and E. D. Clayton. 51

Basic Criticality Experiments with Plutonium Nitrate Solutions in Slab Geometry - R. C. Lloyd and E. D. Clayton 56

*Department of Nuclear Engineering, University of Washington, Consultant to Battelle-Northwest Critical Mass Laboratory.

**Department of Nuclear Engineering, University of Washington, Summer Faculty Appointment Program Professor at the Critical Mass Laboratory.

NEUTRON PHYSICS 59
Existence of the 2.86 MeV Level in B^{10} - D. W. Glasgow and D. G. Foster, Jr. 59
The n-d Total Cross Section, the Di-Neutron, and Charge Independence - D. W. Glasgow and D. G. Foster, Jr. 62
High-Resolution Monochromatization of Neutrons and X Rays by Multiple Bragg Reflections - D. A. Kottwitz 63
Scattering Law Measurements for Light Water at 95 °C - R. B. Smith. 64
COMPUTER CODE ABSTRACTS 65
PUBLICATIONS 69
PAPERS ACCEPTED FOR PRESENTATION. 70
PAPERS ACCEPTED FOR PUBLICATION 70

REACTOR PHYSICS DEPARTMENT
TECHNICAL ACTIVITIES QUARTERLY REPORT
JULY, AUGUST, SEPTEMBER, 1966

SUMMARY

REACTOR THEORY

A recent revision in HRG (Hanford Revised Gam), a neutron slowing down code, modifies the calculation of the effective resonance integral of individual resonance by using for normalization an approximation to the flux used in the resonance integral calculation itself rather than a 1/E flux.

Since publication of a description of data in the BNW Master Library (BNWL-CC-325), 32 isotopes have been updated and three system modifications have been completed.

THERMAL REACTORS

A calculational study of thermalization within a simple cell has been made using the RBU Monte Carlo, THERMOS, and Program S-XIII codes. A comparison of the results shows the RBU Monte Carlo thermalization routine is formulated correctly and free from detectable numerical error.

Experiments have been conducted in the PRCF using 2 wt% PuO_2-UO_2 fuel in H_2O. These experiments are directed towards determining the physics properties of plutonium-fueled H_2O moderated reactor systems. Results are given for a two-zone critical experiment. Also given are results of measurements in a single-zone loading of fuel which contains 24 wt% Pu^{240}.

A calculational study of thermalization in PuO_2-UO_2 fueled H_2O moderated lattices has been performed. The purpose of the study is to determine whether errors are incurred in making assumptions pertaining to scattering processes, boundary conditions, and the source of thermal neutrons. The results of the study show that the assumptions do lead to errors and should not be made to accurately compute thermalization events for these lattices.

Measurements have been made in the PCTR with a mixed lattice of Pu-Al fuel and thoria targets in alternating cells. New techniques were developed to adapt the PCTR type of measurement to this lattice array of supercells. The results include values of k_∞ for the array with and without water coolant surrounding the fuel and targets.

Neutron activation of gold foils in the thermal column of the PCTR have been made to measure the relative neutron flux intensities for various thermal column conditions. The addition of a polyethylene reflector to the graphite stack was found to improve the thermal neutron intensity and to reduce the fast neutron component of the total flux. The presence of a small cavity in the center of the thermal column did not appreciably reduce

the neutron flux gradient in the standard foil irradiation position.

FAST REACTORS

Neutronics calculations were performed for an 800 liter, PuO_2-UO_2 FTR "reference" core. Principal physics statics and kinetics parameters were determined.

To assess the accuracy of the present cross-section set in use for design calculations, numerous critical assembly results have been analyzed. In general, the computed fissile fuel fission ratios are in reasonable agreement with experiment, whereas, the computed U^{238}/U^{235} fission ratios are consistently higher than experimental values.

A new group cross-section "collapsing algorithm" has been devised which makes use of a pseudo absorption cross section in each coarse group. The use of such "perturbation" cross sections is much more accurate for computing moderator reactivity coefficients than corresponding models using flux weighted sections.

Critical experiments in support of FTR are being planned. The first series of these experiments will probably be carried out in ZPR-III, Assembly 48. Calculations for these experiments are under way.

The removal-diffusion code MAC has been used to compare four different axial shield arrangements for the FTR. Energy and spatial distributions of both neutron and gamma fluxes have been obtained.

Basic shielding requirements for a number of FTR fuel processing and handling facilities have been specified.

CRITICAL MASS PHYSICS

Subcritical neutron interaction experiments were performed with bare and Plexiglas reflected arrays of bottles containing aqueous solution of U^{233}. The critical numbers of bottles in arrays were determined for various spacings. In addition, the effects of internal moderation brought about by positioning Lucite sheet in various thicknesses between the bottles comprising several arrays were studied. The concentration of uranium in the experiments was 330 g U^{233}/liter. The experiments provide data for nuclear safety guidance in handling, storage, and shipment of the material and for checking interaction calculations.

A series of criticality experiments were begun, using a vessel of unique design, for determining bare and reflected critical thicknesses of plutonium solution in slab geometry. The slab vessel was designed to permit adjustment of its thickness over the range 3 to 9 in. Criticality experiments were performed, bare and water reflected, in the thickness range 4.5 to 6.5 in. with plutonium nitrate solution containing ~58 g Pu/liter with an acid molarity of 2.3. Infinite slab thicknesses are estimated from the measurement data.

To permit studying the fundamental behavior of neutrons in plutonium-fueled systems, critical approach, pulsed neutron source and foil activation measurements were made on three PuO_2-polystyrene-fueled assemblies.

Some initial results are reported; however, the major portion of the data remain to be analyzed.

Pulsed neutron measurements were performed concurrently with the critical experiments on $Pu(NO_3)_4$ solution in an expandable slab tank. For the water reflected 4.6 in. thick slab of 58 g Pu/liter solution, β/liter was found to be 95 ± 3 sec^{-1}.

To account properly for coincidence losses at the very high counting rates often encountered in making pulsed neutron measurements, it is necessary to determine how closely a perfectly paralyzable or completely nonparalyzable system represents the real detection system used in the measurements. A "maximum observed counting rate" technique was developed which, in conjunction with a double pulse method, permits the system to be characterized relative to these two theoretically limiting models.

A least squares code has been assembled to facilitate reduction of data from pulse neutron and reactor noise experiments.

NEUTRON PHYSICS

The spectrum of neutrons from the $Be^9(d,n)B^{10}$ reaction was studied by time-of-flight techniques at deuteron energies of 1.7 and 2.0 MeV. A study of this spectrum shows no evidence for the existence of an excited state in B^{10} at 2.86 MeV which has been reported in some other investigations.

The neutron total cross section of deuterium has been measured continuously over the energy range 2.25 to 15.0 MeV with good resolution and accuracy. The results of this measurement are consistent with recent theoretical calculations which assume charge independence and derive n-d scattering lengths in agreement with experimental measurements.

A method of obtaining highly monochromatic, reproducible beams of slow neutrons or X rays at fixed wavelength by means of crystal diffraction is described. Detailed computer calculations have been carried out to ascertain potentially useful wavelengths for a germanium monochromator.

The abstract of a report on the Scattering Law for neutrons on H_2O at 95 °C is presented.

REACTOR THEORY

EFFECTIVE CROSS SECTIONS FOR RESONANCES IN HRG

J. L. Carter

One of the distinguishing features of the GAM-I calculational scheme for determining the energy spectrum of epithermal neutrons is the method of treating resonance contributions of the principal resonance absorbers. The resonances are found and these are converted into effective fine group cross sections by dividing by a fine energy group flux. GAM, and HRG until recently, has used a 1/E flux for this conversion. This procedure has not correctly allowed for spatial and energy self-shielding effects. A recent revision in HRG (Hanford Revised Gam) has modified this σ_{eff} calculation by using, instead of the 1/E flux, an approximation to the flux used in the resonance integral calculation itself. It is also assumed that unbroadened cross sections and the Wigner rational approximation to the collision probability could be used. The resulting divisor of the resonance integral, instead of the value 0.25 previously used, becomes

$$\int_n dE\ \phi(E) = 0.25 - \frac{N_{cell}}{N_{fuel}} \frac{b}{(b+1)(1+c^2)} \cdot [0.25 + 2c \tan^{-1} 0.1243530c] \quad \ldots(1)$$

with $b = \frac{\sigma_o}{\sigma_p + \sigma_\ell}$ NR

$= \frac{\Gamma_a}{\Gamma} \frac{\sigma_o}{\sigma_m + \sigma_\ell}$ IM

$$c = \frac{2E_i}{\Gamma(b+1)^{1/2}}$$

and other quantities as defined in the GAM-I document, GA-1850.

Numerical evaluation of Equation (1) in representative cases of a moderate concentration of Pu^{240} gives a revised σ_{eff} for the strong 1.056 eV resonance 5 to 10% larger than the unrevised value in a usual homogenized cell calculation, and 20 to 40% larger in a one-region calculation for the fuel rod itself. The accuracy of these calculations was 0.5 to 1% and 3 to 4% in the respective cases, when compared to a form of the flux integral in which exact collision probabilities and Doppler broadened cross sections were used.

These comparisons show that the HRG modifications to σ_{eff} can be appreciable for strong resonances and can be calculated with acceptable accuracy. The effect of the revised σ_{eff} on the nuclear parameters of the cell depends, of course, on the flux spectrum. Since the corrections are largest for the strong, low energy resonances of isotopes such as U^{238} and Pu^{240}, their influence is strongest for thermal or near thermal reactors. For such reactors, calculated changes in reactivity of 10 to 15 mk are typical. The revisions have also improved the correlation between HRG calculations and Hellstrand's experimental measurements of resonance integrals.

BNW MASTER CROSS-SECTION LIBRARY - STATUS REPORT

K. B. Stewart

Since the BNW Master Library (BNWL-CC-325) was last described on September 1, 1965, a description of improvements incorporated into the library system during the last year is appropriate. In addition to improvements in the data for numerous isotopes, three major modifications have been made in the library system itself. The system modifications are:

- Dating each record on the library tape
- Storing resonance parameter tables in the even numbered records of each isotope instead of in the second record of the library tape with allowance for use of bound state resonances ($E < 0$)
- Allowing Legendre expansion coefficients at each energy point instead of the previous fifty point limit.

Additional and more accurate data have been incluses for the following isotopes:

1. Carbon 12
2. Nitrogen 14
3. Oxygen 16
4. Fluorine 19
5. Sodium 23
6. Aluminum 27
7. Chromium 52
8. Iron 54, 56, 57, and 58
9. Nickel 58
10. Copper 63 and 65
11. Indium 115
12. Samarium 149
13. Europium 151 and 153
14. Lutetium 175 and 176
15. Gold 197
16. Thorium 230
17. Thorium 232
18. Protactinium 231
19. Protactinium 233
20. Uranium 233
21. Uranium 234
22. Uranium 235
23. Uranium 236
24. Uranium 238
25. Neptunium 237
26. Plutonium 239
27. Plutonium 240
28. Plutonium 241
29. Plutonium 242
30. Plutonium 243
31. Plutonium 244
32. Americium 241

A brief description of the changes made to each of the isotopes along with a listing of source references will be published shortly.

THERMAL REACTORS

THERMALIZATION CALCULATIONAL STUDY COMPARISON OF RESULTS OBTAINED USING THE RBU MONTE CARLO, THERMOS, AND PROGRAM S-XIII CODES

D. H. Thomsen

INTRODUCTION

Thermalization calculations for a simple cell were performed using the RBU Monte Carlo,[1] THERMOS,[2] and Program S-XIII[3] codes and the results compared. The purpose of the comparison was to check the formulation and numerics of the RBU Monte Carlo thermalization routine.

SUMMARY

The results obtained from the RBU Monte Carlo and Program S-XIII codes are in excellent agreement. The results obtained from the THERMOS code do not agree with the RBU results. The discrepancy is attributed to the isotropic scattering limitation in the THERMOS code.

ANALYSIS

The problem was to compute the thermalization within a two region cylindrical cell consisting of a boron aluminum rod in light water. The material compositions and cell dimensions are given in Table I. The energy range studied was from 0.0 to 0.683 eV. The analysis with the RBU Monte Carlo code was based upon the following. The scattering model used for all materials was the ideal gas model. Mirror reflection cell boundary conditions were used. A 1.0 eV monoenergenic isotropic source was used. The source was spatially constant in the water.

The conditions on the problem solved using the THERMOS code were the same with the following exceptions. The scattering cross sections and transfer kernel were calculated using the Brown St. John model of the THERMOS code. In the THERMOS transport calculation scattering is treated isotropically. The source of thermal neutrons was spatially constant in the water and the energy distribution was proportional to the width of the energy group.

TABLE I. Description of Two Region Cylinerical Cell Studied

Region	Radius, cm	Material(s)	Concentration, atoms/barn-cm	Mass, a.m.u.	Cross Section, barn σ_a^{2200}	σ_{fa}
1	0.47245	Boron	8.73058×10^{-4}		4020	
		Aluminum	5.3265×10^{-2}	27	0.241	1.45
2	1.52427	Hydrogen	6.686×10^{-2}	1	0.332	20.3
		Oxygen	3.343×10^{-2}	16	0.0002	3.7

Program S-XIII accommodates both zeroth (Po) and first moment (P_1) scattering. The P_o and P_1 total scattering cross sections and transfer kernels were calculated using the IDEAL GAS [4] code. To insure the correct total scattering cross section the in-group transfers $\sigma(i \rightarrow i)$ were calculated by the equation,

$$\sigma(i \rightarrow i)\ \Delta E_i = \sigma_t(i) - \sum_{\substack{j \\ i \neq j}} \sigma(i \rightarrow j)\ \Delta E_j .$$

The P_1 kernel was used only for hydrogen. The other conditions in the problem were the same as used in THERMOS.

Other details of the problem are given in Table II for each code. The space points in Program S-XIII were distributed at closer intervals near the interface of the two regions while the THERMOS calculation used a uniform spatial mesh in each region. To speed up Program S-XIII convergence three axial angles were used for the first iterations and then five axial angles were used in a restart to obtain the final values.

COMPARISON

The quantities obtained from the calculations are flux averaged* cross section values for boron absorption, $\bar{\sigma}_a^B$, hydrogen absorption, $\bar{\sigma}_a^H$, and hydrogen scattering, $\bar{\sigma}_s^H$, along with the flux disadvantage factor, ϕ_{H_2O}/ϕ_B, (the ratio of the average flux in the water to the average flux in the boron rod). A statistical analysis was made on the values of $\bar{\sigma}_a^B$, $\bar{\sigma}_a^H$, and ϕ_{H_2O}/ϕ_B for the results obtained from the RBU Monte Carlo Code. All results are shown in Table III.

* $\bar{\sigma} = \dfrac{\int \sigma(E)\ \phi(E)\ dE}{\int \phi(E)\ dE}$

TABLE II. Comparison of Problem Input for RBU, Program S and Thermos

	RBU	Program S	THERMOS
Total Numbers of Energies	63	30	30
Number of Energies Below 0.683 eV	58	30	30
Number of Space Points in Boron Rod		15	7
Number of Space Points in Water		14	13
Number of Polar Angles		2	
Number of Axial Angles		3 or 5	

TABLE III.

Case	$\bar{\sigma}_s$ Hydrogen	$\bar{\sigma}_a$ Hydrogen	$\bar{\sigma}_a$ Boron	ϕ_{H_2O}/ϕ Boron Rod
1. RBU Monte Carlo	27.43	0.2625 ± 0.0009	2613 ± 14	2.684 ± 0.034
2. THERMOS, Flat Source	27.57	0.2657	2615	2.964
3. Sn, Pl, Flat Source	27.49	0.2638	2611	2.609
4. Sn, No Pl, Flat Source	27.53	0.2650	2605	2.93
5. THERMOS, Nonflat Source	27.57	0.2657	2623	2.987

Comparison of Cases 1 and 2 shows that the cross sections calculated using THERMOS are within 1.2% of those calculated using RBU while the flux disadvantage factor differs by 12%. These results are not close enough to provide an adequate check for the RBU Monte Carlo calculation. Comparing Cases 1 and 3 shows that the cross sections calculated using Program S-XIII are within 0.5% of the RBU Monte Carlo values and the disadvantage factor differs by 2.9%. These results are in satisfactory agreement.

To check the validity of the Program S results, two additional calculations were made. The first calculation was made using Program S with isotropic scattering only.

The comparison of results for Cases 2 and 4 shows that when given the same input Program S and THERMOS give nearly the same answers.

The other calculation was made using THERMOS. The source in the RBU calculation was not spatially constant below 0.683 eV and to see the effect of this THERMOS was used with a space dependent source. The space dependence was obtained by using the Program S fluxes for the highest energy group. Comparing the results of these calculations, Cases 2 and 5 in Table III, shows that there is a 0.8% effect in the disadvantage factor due to the space dependence of the source.

If the correction indicated by the THERMOS run due to the source is applied to the Program S value for the disadvantage factor the value becomes 2.629.

CONCLUSION

The comparison of the results from RBU and Program S-XIII show that the RBU Monte Carlo ideal gas routine is both formulated correctly and free from detectable numerical error. It should be safe to use RBU for similar calculations with confidence in its reliability.

The ideal gas model was used for these calculations. A method of treating the scattering in water more accurately is needed. One approximate method will be tried with a similar series of calculations.

REFERENCES

1. *J. R. Tripplet, E. T. Merrill, and J. R. Burr. The RBU Reactor-Burnup Code: Formulation and Operating Procedures, HW-70049, General Electric Company, Richland, Washington. July 1961.*

2. *H. C. Honeck. THERMOS, A Thermalization Transport Theory Code for Reactor Lattice Calculations, BNL-5826, Brookhaven National Laboratory, also J. R. Worden, W. L. Purcell, and R. C. Liikala, "Modifications to the Computer Code, THERMOS and Comparative Studies on Scattering Kernels," Physics Research Quarterly Report, July, August, September, 1965, BNWL-193, pp. 5-15. October 15, 1965.*

3. *B. H. Duane. Neutron and Photon Transport Plane-Cylinder-Sphere GE-ANPD Program S Variational Optimum Formulation, XDC 59-9-118. January 9, 1959.*

4. *D. R. Skeen. Ideal Gas Program, HW-76945, General Electric Company, Richland, Washington. March 14, 1963.*

CRITICAL EXPERIMENTS WITH PuO_2-UO_2 FUEL RODS

V. O. Uotinen and L. D. Williams

Critical experiments are being conducted in the PRCF using H_2O moderator and 1/2 in. diam 2 wt% PuO_2-UO_2 fuel rods. Criticality has been achieved with a two-zone loading in which the inner zone contained plutonium with 24 wt% Pu^{240} and the outer zone contained plutonium with 16 wt% Pu^{240}. The inner zone contained 121 rods and the total number of rods required for criticality was 353.4.

The data obtained in the single-zone loading of 24 wt% Pu^{240} rods is being analyzed. Cosine functions have been fitted to axial copper activation data using program GLEX. The function that best fits the experimental points is $\phi = A_{cos}\ 0.07720\ (H - 17.30)$, where ϕ is the flux and H is the height measured from the bottom of the fuel. The axial buckling as determined from this fit is $(9.24 \pm 0.28) \times 10^{-4}\ cm^{-2}$, and the reflector savings is 6.0 cm. Data from spatial scans of the gamma ray activity from fuel rods are being analyzed in the same way. A preliminary analysis of reactor noise data yields a value of ∿135 for the quantity β/ℓ; a calculation using the transport theory code Program S predicted a value of 127. Moderator level coefficients of reactivity have been analyzed and a value of $44 \pm 11\ cm^2$ is deduced for the migration area; a diffusion-theory calculation using HFN predicted a value of $40.5\ cm^2$. Dysprosium activation data have been analyzed to give relative flux distributions in the central cell with various materials occupying the central lattice position. The results are shown in Figure 1.

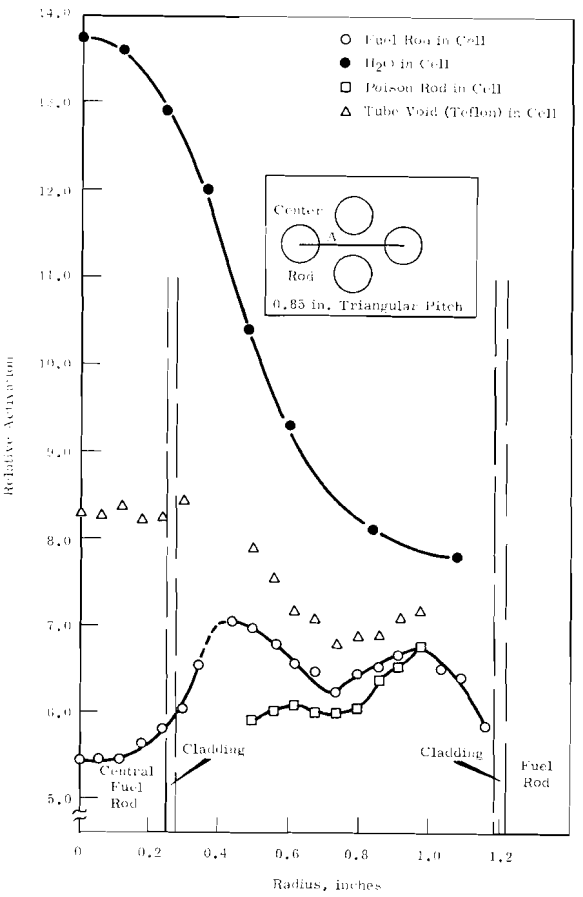

FIGURE 1. Dy-Activation, 24 wt% Pu^{240} Fuel Rods with Various Materials Occupying the Central Lattice Position [The radius was measured along path A (see insert) from center rod.]

RESULTS OF THERMALIZATION CALCULATIONS FOR PuO_2-UO_2-H_2O LATTICES

R. C. Liikala and W. L. Purcell

INTRODUCTION

Earlier reports on theoretical thermalization in plutonium light water systems gave results comparing; various spectral models for H_2O[1,2] and, methods of obtaining lattice constants for the homogenized unit lattice cell[3]. The THERMOS code[4] was used extensively in the latter study. Assumptions were made in the THERMOS problems in this study. Specifically, we assumed that the 1.056 eV resonance of Pu^{240} did not effect the thermal flux shapes in the lattice cell. In addition, the THERMOS code has some inherent approximations built into it, namely, the birth rate density is isotropic and the reflecting boundary condition on a cylindrical cell. The purpose of this study is to investigate what effects these approximations have on the results (thermal lattice parameters) for the lattices covered in the previous study[3] as well as for other PuO_2-UO_2-H_2O lattices.

LATTICES

The lattices investigated are systems for which critical masses and bucklings have been experimentally determined.[6,7,8] The fuel is PuO_2-UO_2 clad with zircaloy tubing at enrichments of 1.5 wt% PuO_2 in depleted UO_2 (EBWR FUEL),[6] 2.0 wt% PuO_2 in natural UO_2,[7] and 6.6 wt% PuO_2 in natural UO_2(SAXTON FUEL).[8] The 1.5 and 2.0 wt% PuO_2-UO_2 fueled experiments are uniform arrays of rods in a hexagonal pattern. The experiments using 6.6 wt% PuO_2-UO_2 are uniform square arrays of rods. Each set of experiments covers a wide range of moderator to fuel volume ratios. The Pu^{240} concentration is near 8 at.% for the 1.5 and 6.6 wt% PuO_2-UO_2 fueled experiments. The 2.0 wt% PuO_2-UO_2 fueled experiments have either ~8, 16, or 24 at.% Pu^{240}. Details of the experiments are given elsewhere.[6,7,8]. From this wide range of reactor systems, appropriate cases were selected to illustrate the points in question.

We shall discuss the results in terms of the effects the approximations have on the familiar thermal lattice parameters,

- disadvantage factor, $\bar{\phi}_{Mod}/\bar{\phi}_{Fuel}$
- thermal utilization, f(fuel absorptions/cell absorptions)
- thermal reproduction factor, $\bar{\eta}$ $\left(\frac{\text{fission neutrons produced}}{\text{cell absorptions}}\right)$
- reactivity, η_f.

APPROXIMATIONS

The THERMOS code for cylindrical cells in use at Pacific Northwest Laboratory (PNL) is limited to isotropic scattering. Also, the code has certain restrictions as to the boundary conditions which are applied to the outer edge of a unit lattice cell. Honeck has investigated the effects these restrictions have upon computing thermal utilizations and disadvantage factors for uranium/water lattices.[9] As a result, he has devised some approximate corrections for both the isotropic scattering and boundary condition limitations.

In the same manner, the source term in the THERMOS code assumes the energy variation of the neutron flux just above the highest energy point in the problem is 1/E (i.e., constant in lethargy). As stated above, the THERMOS code[4] was utilized in a previous study of cell homogenization. These THERMOS problems assumed the highest energy point as 0.683 eV. In lattices fueled with plutonium, the presence of Pu^{240} with its giant resonance at ~1 eV may perturb the neutron flux such that the energy variation just above 0.683 eV is not 1/E. The expanded version of the THERMOS code in use at PNL[5] enables avoiding this problem of the Pu^{240} perturbing the source term.

The approximate corrections devised by Honeck to include anisotropic scattering and to obtain the exact boundary conditions were used in THERMOS calculations for the unit lattice cell. The results of these calculations are compared to those obtained when these corrections are neglected.

Results of THERMOS problems for cases in which the Pu^{240} resonance is included in the thermalization calculation are compared to those cases where it is neglected.

RESULTS

Corrections for Anisotropy

The THERMOS code assumes that the neutron birth rate density is isotropic. If the gradients of the flux in the lattice cell are large, then it might be expected that neglecting anisotropic scattering effects would lead to significant errors. Honeck[9] devised an approximate correction to be made in generating the Nelkin[10] scattering kernel for H_2O to account for anisotrophy by substituting the transport cross section for the total scattering cross section.

Calculations of lattice reaction rates for thermal neutrons in the PuO_2-UO_2-H_2O cells were made using the THERMOS code. The energy range from 0.0 to 0.683 eV was spanned with 30 groups. The Nelkin scattering kernel for H_2O was used. The Brown-St. John scattering model was used for all other cell materials. Reflecting cell boundconditions were assumed. Twenty space points were employed in the three region unit lattice cell consisting of fuel, clad, and moderator. The results of the calculations which included the "transport correction" to account for anisotropic scattering are compared in Table I to the results obtained assuming only isotropic scattering.

In general, the relative differences in the thermal lattice parameters, $\bar{\eta}$, and f, are small with a few exceptions. A sizeable* discrepancy in f is shown for the loose lattices fueled with 2.0, and 6.0 wt% PuO_2-UO_2. The discrepancy in f is not strictly a function of either moderator to fuel volume ratio or hydrogen to plutonium atom ratio. The largest difference in f is for the 2 wt% PuO_2-UO_2-H_2O lattice which has a moderator-to-fuel volume ratio of 0.85. The most open lattice of the 6.6 wt% PuO_2-UO_2-H_2O system has a larger moderator to fuel volume ratio and the difference in f is smaller. Likewise, two systems which have approximately the

A priori we designate sizeable errors as those 1% or larger.

TABLE I. The Effect of Neglecting Anisotropy in Computing Thermal Lattice Parameters

Fuel	V_{Mod}/V_{Fuel}	H/Pu (Atom)	Percent Change in Lattice Parameter* (Isotropic Scattering/Anisotropic Scattering) $\bar{\phi}_{Mod}/\bar{\phi}_{Fuel}$	f	$\bar{\eta}$	$\bar{\eta}_f$
1.5 wt% PuO_2-UO_2	1.10	230	-3.1	+0.22	-0.07	+0.14
	2.71	567	-0.49	+0.10	-0.03	+0.07
	5.58	1169	+1.1	-0.30	0.0	-0.30
2.0 wt% PuO_2-UO_2	0.614	98	-6.0	+0.17	-0.30	-0.13
	1.49	237	-1.6	+0.13	-0.11	+0.02
	2.45	390	+0.39	-0.06	-0.04	-0.10
	4.35	692	+2.6	-0.52	-0.01	-0.53
	6.97	1110	+3.5	-1.2	+0.01	-1.1
	9.85	1567	+5.1	-1.9	+0.01	-1.8
6.6 wt% PuO_2-UO_2	1.68	76	-6.1	+0.21	-0.34	-0.13
	4.70	211	0.0	-0.07	-0.10	-0.17
	10.8	486	+4.0	-0.93	+0.07	-0.90

*e.g., $f_{Isotropic}/f_{Anisotropic\ Correction} \times 100$.

same H/Pu atom ratio do not have differences in f which are equivalent (e.g. the 1.5 wt% lattice of H/Pu = 1169 and the 2.0 wt% lattice of H/Pu = 1110). To what extent the differences in the disadvantage factor, $\bar{\phi}_{Mod}/\bar{\phi}_{Fuel}$ effect f is also shown to be lattice spacing dependent. For the same size discrepancy in $\bar{\phi}_{Mod}/\bar{\phi}_{Fuel}$, the perturbation of this difference in f is larger for loose lattices than for tight lattices.

If the "transport correction" does accurately account for the linear anisotropic scattering in the lattice cell, then the conclusion is reached that, upon neglecting anisotropy in the scattering

- sizeable errors in computing spatial flux variations will result
- sizeable errors in computing the thermal utilization f and the reactivity, $\bar{\eta}_f$ for loose lattices will result.

The results of a recent study by Takahashi[11] concerning this problem of anisotropic scattering indicates this "transport correction" to be quite accurate.

Cylindrical Cell Boundary Conditions

The rods in the lattices are in either regular triangular arrays or square arrays. The usual procedure utilized in defining the unit lattice cell is to assume the cell is cylindrical (commonly referred to as a Wigner-Seitz cell) and preserve the material concentrations. Moreover, the neutrons reaching the edge of this cylindrical cell are usually assumed to reflect from this boundary. Numerous authors have shown these approximations frequently lead to errors, especially for close packed lattices. Honeck[9] has given a method of simulating a boundary condition in one dimensional THERMOS problems which results in matching the thermal disadvantage factor computed using a two dimensional THERMOS code for U/H_2O lattices. The boundary condition

simulated is one which returns all neutrons incident on the cell boundary in an isotropic distribution. To simulate this isotropic boundary condition requires surrounding the one dimensional cell with a thick (2 mean free paths or greater), heavy mass, pure scattering region. The net effect is only the angular distribution of neutrons returning from this boundary are altered in the problem.

Unit cell calculations using the THERMOS code were made applying this isotropic boundary condition. Two calculations for each lattice cell considered were made using this boundary condition. One calculation included the "transport correction" to the H_2O scattering kernel (Nelkin) and the other neglected this correction for anisotropy. The results are compared in Table II to those in which reflecting boundary conditions were used.

The difference in disadvantage factor is largest for the 6.6 wt% PuO_2-UO_2 system. The differences in $\bar{\phi}_{Mod}/\bar{\phi}_{Fuel}$ are also lattice spacing dependent. As expected, the effect is largest for the tighter lattice shown in the results for the 2 wt% PuO_2-UO_2 systems. The effect of the boundary conditions in the reactivity $\bar{\eta}_f$ are small because the effects in $\bar{\eta}$ and f compensate. However, an interplay between the correction for anisotropy and the cell boundary correction is shown. The differences in all thermal lattice parameters due to the boundary condition correction is larger when the correction for anisotropy is included.

Thus, if surrounding the lattice cell by a source free, thick, pure scatter region represents an accurate correction to the boundary condition, then the conclusion is reached that upon neglecting this correction,

- sizeable errors in computing the spacial flux variations will result
- negligible errors in the computed reactivity occurs only because the errors in $\bar{\eta}$ and f compensate.

TABLE II. Comparison of Computed Thermal Neutron Lattice Parameters Using Different Cell Boundary Conditions

Fuel	V_{Mod}/V_{Fuel}	Anisotropic Correction	Percent Change in Lattice Parameter* (Isotropic Boundary/Reflecting Boundary) $\bar{\phi}_{Mod}/\bar{\phi}_{Fuel}$	f	$\bar{\eta}$	$\bar{\eta}_f$
1.5 wt% PuO_2-UO_2	1.10	Yes	- 4.9	+0.46	-0.19	+0.26
	1.10	No	- 2.9	+0.21	-0.05	+0.16
2.0 wt% PuO_2-UO_2 (8% Pu^{240})	0.614	Yes	-14.1	+0.44	-0.42	+0.02
	0.614	No	- 8.5	+0.27	-0.23	+0.04
	1.49	Yes	- 6.5	+0.49	-0.23	+0.26
	1.49	No	- 3.7	+0.28	-0.11	+0.17
6.6 wt% PuO_2-UO_2	1.68	Yes	-15.7	+0.59	-0.76	-0.17
		No	- 9.8	+0.35	-0.36	-0.01

*e.g., $f_{Isotropic\ Correction}/f_{Reflecting} \times 100$.

Effect of 1.056 eV Pu^{240} Resonance in Thermalization

The version of the THERMOS code[4] which was used for earlier studies[3,6,7] of these systems was limited to the use of 30 energy groups. Because of the low energy resonance of Pu^{239} (at ~0.683 eV) to adequately describe the events occurring in this energy region. With the advent, at PNL, of the Univac 1107 computing system, which has a larger memory capacity than the IBM-7090, an extended version of the THERMOS code was developed.[5] This extended version accomodates up to 40 energy groups and 25 space points. By using the version with 30 energy groups below 0.683 eV and 10 energy groups from 0.683 to 1.3 eV, the effects of the Pu^{240} resonance at 1.05 eV on the thermal flux shapes can be evaluated.

An attempt to generate the scattering kernel for H_2O using the GAKER code[4] for this 40 group energy mesh was made. A plot of the total scattering cross section versus energy showed slight oscillations in the energy region near the Pu^{240} resonance. Since the origin of these oscillations may be in the numerical methods employed in determining the scattering kernel rather than the physical model itself the Brown-St. John (B.S.J.) model[12] for H_2O was used.

Since the results given above are all based upon the Nelkin kernel for H_2O we first give a comparison of results obtained using the B.S.J. model to those obtained using the Nelkin model in THERMOS. No corrections were made to either model (Nelkin or B.S.J.) to account for anisotropy for this comparison and reflecting cell boundary conditions were utilized. The source of thermal neutrons was assumed as flat in the moderator and the energy variation of source neutrons above 0.683 eV was assumed constant in lethargy (i.e., 1/E). The comparison of computed thermal lattice parameters is shown in Table III.

The value of f computed using the Nelkin kernel is consistently larger than the value computed using the

TABLE III. Comparison of Computed Thermal Neutron Lattice Parameters Using the Nelkin and Brown-St. John Models for H_2O*

Fuel	V_{Mod}/V_{Fuel}	$\bar{\phi}_{Mod}/\bar{\phi}_{Fuel}$	Percent Change in Lattice Parameter** (Nelkin Model*/B.S.J. Model) f	$\bar{\eta}$	$\bar{\eta}f$
1.5 wt% PuO_2-UO_2	1.10	-0.02	+0.17	-0.22	-0.05
	2.71	-0.14	+0.29	-0.16	+0.13
	5.58	-0.27	+0.36	-0.11	+0.25
2.0 wt% PuO_2-UO_2	0.614	-0.12	+0.08	-0.37	-0.27
	1.49	-0.31	+0.19	-0.31	-0.12
	2.45	-0.52	+0.26	-0.25	+0.01
	4.35	-0.59	+0.34	-0.20	+0.14
	9.85	-0.84	+0.48	-0.14	+0.34
6.6 wt% PuO_2-UO_2	1.68	-0.23	+0.10	-0.49	-0.38
	4.70	-0.67	+0.27	-0.37	-0.09
	10.8	-0.88	+0.42	-0.18	+0.26

*No corrections for anisotropy

**e.g., $f_{Nelkin\ model}/f_{B.S.J.\ model} \times 100$.

B.S.J. kernel. The difference in f becomes larger as the moderator to fuel volume ratio increases. The same trend with lattice spacing is noted in the $\bar{\phi}_{Mod}/\bar{\phi}_{Fuel}$ except the values computed using the Nelkin kernel are all smaller relative to the B.S.J. kernel. The differences in $\bar{\eta}$ are the same sign as that noted for the $\bar{\phi}_{Mod}/\bar{\phi}_{Fuel}$ except the trend with lattice spacing is reversed. The differences in $\bar{\eta}$ and f are such that they tend to compensate in the product $\bar{\eta}f$. The differences in the lattice parameters are not so large as to cause large uncertainties in the comparison of the Pu^{240} resonance effect on thermal reaction rates.

Cell calculations were made for some of the above mentioned PuO_2-UO_2-H_2O systems using the 40 energy groups described above. The following conditions were assumed. Reflecting cell boundary conditions, a flat spatial and constant lethargy source above 1.3 eV, and the B.S.J. model for H_2O. The necessary integrals (i.e., the thermal lattice parameters) from 0.0 to 0.683 eV were obtained and the results compared to those where the Pu^{240} 1 eV resonance was neglected in the thermalization calculations. Table IV shows the comparison.

The two lattices considered were the tightest lattices for the 2 wt% PuO_2-UO_2-H_2O system containg ~24 at.% Pu^{240}. The latter system has more Pu^{240} however the 2.0 wt% PuO_2-UO_2 rods are larger in diameter. Thus, one or the other of these two systems should be the case in which the largest effect occurs.

From Table IV we see that the effect on all the thermal lattice parameters is small. The calculations using 40 groups were performed neglecting Doppler broadning of the Pu^{240} cross sections. A subsequent calculation for the 6.6 wt% PuO_2-UO_2-H_2O lattice which included Doppler broadning (0.0 to 293.2° K) gave essentially the same result as noted from Table IV.

Thus, for Pu-H_2O systems such as these, the effect of neglecting the 1.056 eV resonance of Pu^{240} in computing thermal lattice parameters does not produce large errors in these parameters.

TABLE IV. The Effect of Neglecting the Pu^{240} 1.056 eV Resonance in Computing Thermal Neutron Lattice Parameters

Fuel	V_{Mod}/V_{Fuel}	Percent Change in Lattice Parameters (Including the Resonance Neglecting the Resonance) $\bar{\phi}_{Mod}/\bar{\phi}_{Fuel}$	f	$\bar{\eta}$	$\bar{\eta}f$
2.0 wt% PuO_2-UO_2 (24% Pu^{240})	1.49	+0.55	-0.17	+0.04	-0.13
6.6 wt% PuO_2-UO_2	1.68				
Neglecting Doppler Broadening		+0.62	-0.07	+0.40	+0.33
Including Doppler Broadening		+0.63	-0.08	+0.44	+0.36

SUMMARY AND CONCLUSIONS

We have investigated some possible sources of error arising from assumptions made in solving for the distributions of thermal neutrons in PuO_2-UO_2-H_2O lattice cells. The study was made using the THERMOS code exclusively. The comparison has been made using "approximate corrections" to the given problem which supposedly represents the exact solution to the problem. If we assume that these corrections are accurate then the following conclusions are reached.

In order to accurately compute the spatial variation of thermal neutrons in a PuO_2-UO_2-H_2O lattice cell using the THERMOS code, one must account for anisotropy in the scattering and use an isotropic boundary condition.

Likewise, to accurately compute the parameters $\bar{\eta}$ and f these effects should be included. If they were neglected, trends in the reactivity, $\bar{\eta}_f$ as a function of H/Pu atom ratio may result which may lead to erroneous conclusions concerning the origin of these trends (i.e., possibly the resonance absorption).

The effect of the 1.056 eV resonance of Pu^{240} on thermal flux shapes is relatively small and probably can be neglected in reactor design computations for reactor systems such as covered in this study.

From the standpoint of reactor design, where the quantity of interest is generally the reactivity effect, $\bar{\eta}_f$ all of these effects can probably be neglected. The possible exception is to include the correction for anisotropy in loose lattice calculations. However, the design of thermal reactor systems generally does not consider lattices which are largely overmoderated and as such can neglect this effect in reactor design computations.

REFERENCES

1. *K. B. Stewart. "The Modified Heavy Gas Equation and Light Water Moderated Systems," Physics Research Quarterly Report, October, November, December, 1963, HW-80020, pp. 8-13. January 15, 1964.*

2. *R. C. Liikala. "Comparison of Thermalization Models," Physics Research Quarterly Report, January, February, March, 1964, HW-81659, pp. 20-25. April 15, 1964.*

3. *R. C. Liikala. "A Comparitive Study of Unit Cell Homogenization for PuO_2-UO_2-H_2O Lattices," Physics Research Quarterly Report, July, August, September, 1964, HW-84369, pp. 5-9. October 15, 1964.*

4. *H. C. Honeck. THERMOS, A Thermalization Transport Theory Code for Reactor Lattice Calculations, BNL-5826. Brookhaven National Laboratory.*

5. *J. R. Worden, W. L. Purcell, and R. C. Liikala. "Modifications to the Computer Code, THERMOS, and Comparative Studies on Scattering Kernels," Physics Research Quarterly Report, July, August, September, 1965, BNWL-193, pp. 5-15. October 15, 1965.*

6. *L. C. Schmid, et.al. "Critical Masses and Bucklings of PuO_2-UO_2-H_2O Systems," Trans. Am. Nucl. Soc. vol. 7, p. 216. 1964; also Physics Research Quarterly Report April, May, June, 1964, HW-83187, pp. 4-6. July 15, 1964.*

7. *R. C. Liikala and W. P. Stinson. "Experimental and Analytical Results for PuO_2-UO_2-H_2O Lattices," Trans. Am. Nucl. Soc., vol. 9, p. 127. 1966.*

8. *E. G. Taylor, et. al. Saxton Plutonium Program Critical Experiments for the Saxton Partial Plutonium Core, EURAEC-1493/WCAP-3385-54, Westinghouse Electric Corporation, December, 1965.*

9. H. C. Honeck. "The Calculation of Thermal Utilization and Disadvantage Factor in Uranium/Water Lattices," Nucl. Sci. Eng., vol. 18, p. 49. 1964.

10. M. Nelkin. "The Scattering of Slow Neutrons by Water," Phys. Rev., vol. 119, p. 791. 1960.

11. H. Takahashi. "The Generalized First-Flight Collision Probability in the Cylindricalized Lattice System," Nucl. Sci. and Eng., vol. 24, p. 60. 1966.

12. H. Brown and D. St. John. Neutron Energy Spectrum in D_2O," Savannah River Report DP-33. 1954; and H. Brown. Neutron Energy Spectrum in Water, Savannah River Report DP-64. 1956.

THREE-DIMENSIONAL ANALYSIS OF PLUTONIUM FUEL MTR CORES: PRELIMINARY RESULTS

W. W. Porath

PHOENIX FUEL PROGRAM

Serious consideration is being given to a high Pu^{240} content plutonium (Hx-Pu) burnup experiment in the MTR.[1] This experiment would form a part of the so-called "Phoenix" program which generally deals with the utilization of Hx-Pu in near-thermal, compact power reactors.

THREE-DIMENSIONAL ANALYSIS OF CYCLE 108

To assist in the planning and design of the MTR-Phoenix experiment, and to test and improve the presently available calculational methods, the results of a low Pu^{240} content plutonium (Lx-Pu) MTR burnup experiment,[2] carried out during 1958 (Cycle-108) were reanalyzed. Previous analysis of Cycle 108 had been carried out using one and two dimensional diffusion calculations.[3] However, the complexity of the experiment seems to require three-dimensional analytical techniques to properly describe the very heterogeneous MTR geometry.

To carry out 3-D calculations requires gross simplifications in the reactor model because the available codes have fairly stringent mesh point limitations. In the Cycle 108 calculations, the core was assumed to have symmetry about a central plane and the presence of the test pieces was represented in a rather approximate manner. The hollow, water-filled, cadmium sleeve control rods were represented by homogenized regions containing just enough cadmium to yield the correct rod worth. The WHIRLAWAY code,[4] a two group, three dimensional diffusion theory program was used to carry out the analysis.

RESULTS OF CYCLE 108 CALCULATIONS

One test of the usefulness of the 3-D computational model is a comparison of measured and calculated spatial activations, Figure 1 shows a comparison between a typical experimental Cycle 108 cobalt activation taken from IDO-16526[5] and the calculated activation rate from a WHIRLAWAY run. In this figure, the area under the calculated distribution has been normalized

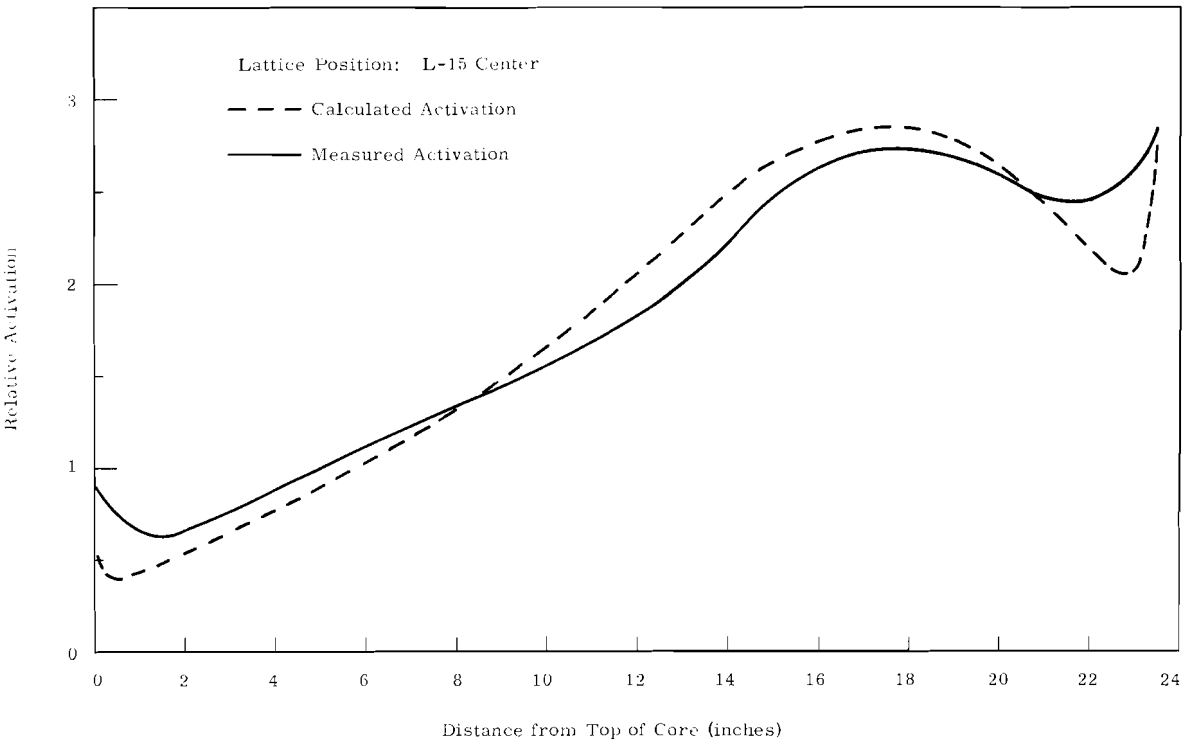

FIGURE 1. Axial Cobalt Activation

to equal that of the corresponding experimental cobalt activation. As can be seen, the agreement is quite good. Exceptions to this favorable comparison are in the fuel positions in which the control rods are located. In these positions, the calculated distributions are quite different from the measured cobalt activation. These discrepancies have been attributed to the homogenized control rod model; therefore, subsequent calculations include a more detailed rod model.

Another problem in the comparison between calculation and experiment is the overall horizontal flux distribution. The calculated fluxes lack the decided tilt of the experimental results. This may well be due to an inadequate representation of the test pieces in the reflector.

THREE-DIMENSIONAL ANALYSIS OF A PHOENIX CORE

The WHIRLAWAY code was used to analyze the MTR-Phoenix core. This core consisted of MTR type fuel plates containing 20 wt% plutonium in aluminum, the plutonium composition 76 at.% Pu^{239}, 20 at.% Pu^{240}, 3 at.% Pu^{241}, and 1 at.% Pu^{242}. The rod model contained a central water channel. It is assumed that the reflector will be free of test pieces during the Phoenix core test. The fuel boxes were located in the central 3 x 9 zone utilizing all eight control rods.

RESULTS OF PHOENIX CALCULATION

The three-dimensional analysis indicates that the highest power peaks occur in the control rod follower fuel

just below the active core zone. Previous calculations indicated that the maximum power peaks were at the core--beryllium reflector interface. The total worth of the control system is some what less in the 3-D calculation than in a 2-D analysis.

CONCLUSIONS

Cycle 108

While the results of the initial 3-D analysis of Cycle 108 are not particularly favorable, the possibility of making worthwhile improvements in this analysis appears to exist. It will be necessary to obtain a more detailed reflector representation and an improved geometric representation of the control rods to improve the reactor model.

PHOENIX CORE

The Phoenix core presents a considerable design problem with regard to power peaking along the bottom of the core and in the follower fuel. The unfavorable power peak in the follower fuel is particularly bad because, as the core burns and the control rods are withdrawn, relatively fresh fuel will be moving into a region of high thermal flux. Hence, the large power peak below the core may persist during the life of the core.

If the operating power level is reduced to a value which will permit safe operation, the core residence time will be considerably lengthened. If the bottom of the core is poisoned in some manner to lower the thermal flux peak in the bottom reflector, the life of the core may be shortened and the desired degree of burnup of initial fuel might not be attained. Hence, some compromise may be in order so that the object of the experiment can be demonstrated.

REFERENCES

1. *R. H. Holeman and P. L. Hofman. Nuclear Design Calculations for an Hx-Pu Fueled MTR, HW-84575, General Electric Company, Richland, Washington. December 15, 1964.*

2. *D. R. deBoisblanc and R. S. Marsden. Operation of the MTR on a Plutonium Loading, IDO-16508, Idaho Operations Office. December 22, 1958.*

3. *J. J. Regimbal. Analysis of MTR Cycle 108-Low Exposure Plutonium Cores, HW-83431, General Electric Company, Richland, Washington. November 19, 1964.*

4. *T. B. Fowler and M. L. Tobias. WHIRLAWAY-A-Three-Dimensional, Two Group Neutron Diffusion Code for the IBM-709 Computer, ORNL-3150 Oak Ridge National Laboratory. August, 1961.*

5. *L. J. Harrison. Operating Parameters and Neutron Flux Profiles for MTR Plutonium Core, IDO-16526. Idaho Operations Office. July 31, 1959.*

MEASUREMENTS OF k_∞ FOR A Pu-Al THORIA SUPERCELL

N. A. Hill

The PCTR technique[1] has been extended to include infinite neutron multiplication factor (k_∞) measurements of supercell lattices. Values of k_∞ have been measured for a mixed lattice of Pu-Al fuel and thoria target in alternating cells. The combination of one Pu-Al cell and one thoria cell is called a supercell.

The presence of plutonium in the system required a careful review of the definition of k_∞. The values of k_∞ in this experiment are defined as the normalized subcadmium absorption rates in the poisoned supercell plus the corrected copper epicadmium absorption rate divided by the normalized subcadmium absorption rates in the unpoisoned supercell. These values of k_∞, when multiplied by the appropriate leakage terms from a two group analysis, yield values of k_{eff} defined as the total neutron production divided by the sum of the total neutron loss due to absorption and leakage.

Two unique cells in a supercell required a modification to existing techniques in determining the proper neutron energy distribution. A method was developed to determine the buffer configuration surrounding the test cells which provided a matched energy distribution in the supercell. The measured values of k_∞ were more sensitive to a mismatch in the neutron energy distribution near the thoria than to a mismatch near the Pu-Al.

The null reactivity technique was used to determine the masses of copper required for unity neutron multiplication in the matched conditions. The compositions and geometries of the properly poisoned supercells are shown in Figure 1.

The relative reaction rates of the supercell components were also determined in the matched conditions. The fission rates in the plutonium were measured by inserting Pu-Al foils into the fuel which were made from the fuel material. The effective subcadmium (0.64 eV) absorption rates in the 1/v absorbers were monitored with copper foils whose activities were corrected for epicadmium activity by measured cadmium ratios. The subcadmium absorption rates in all cell components were normalized to the total production rates in the cells for both the poisoned and unpoisoned cases. A small correction is included for the epicadmium absorption in the copper which is multiplied by an estimated resonance escape probability and normalized to the total productions for the poisoned cases. The effective subcadmium capture to fission cross section ratio for Pu^{239} was calculated by the THERMOS[2] computer code using experimentally determined boundary conditions.

The values of k_∞ were deduced from the masses of copper and the relative

SUPERCELL COMPOSITION

THORIA CELL			PuAl CELL		
Th^{232}	71.9	g/cm	Pu^{239}	1.366	g/cm
Oxygen	10.00	g/cm	Pu^{240}	0.1387	g/cm
Aluminum	4.51	g/cm	Pu^{241}	0.0159	g/cm
Water	2.752	g/cm	Aluminum	28.18	g/cm
Zirconium	9.70	g/cm	Water	3.357	g/cm
Graphite	639.8	g/cm	Zirconium	9.645	g/cm
			Graphite	641.9	g/cm

COPPER DISTRIBUTED ON BOTH CELLS

Dry Coolant Channels	6.929 g/cm
Wet Coolant Channels	1.125 g/cm

SUPERCELL GEOMETRY

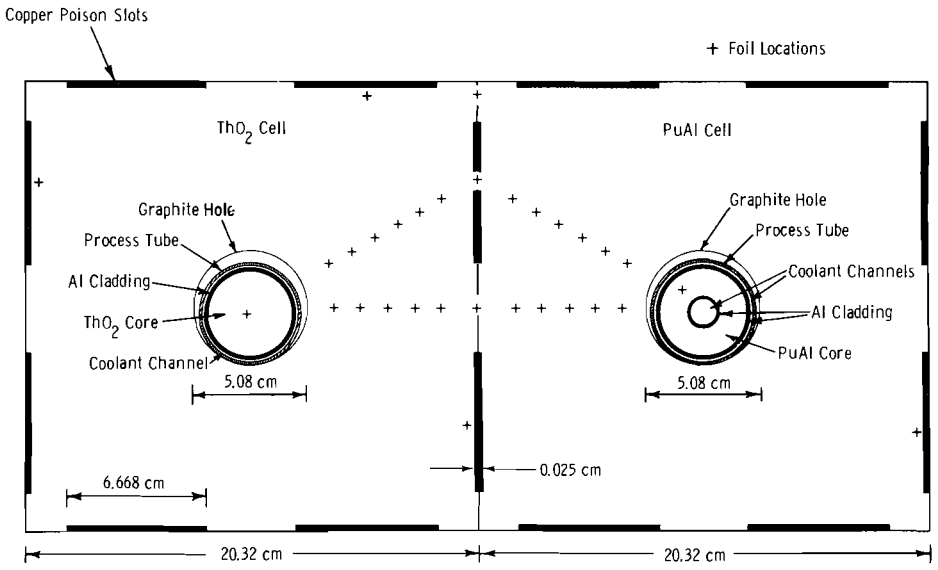

FIGURE 1. Supercell Geometry and Composition

reaction rates in the matched conditions. The numerical results were 1.014 ± 0.002 and 1.092 ± 0.01, respectively, for the wet and dry cases.

REFERENCES

1. *D. J. Donahue, et al. "Determination of k_∞ from Critical Experiments with the PCTR," Nucl. Sci. Eng., vol. 4, pp. 297-321. 1958.*

2. *H. Honeck. THERMOS, A Thermalization Transport Theory Code for Reactor Lattice Calculations, BNL 5826, Brookhaven National Laboratory. 1961.*

A THERMAL COLUMN STUDY IN THE PCTR

G. E. Hanson and N. A. Hill

INTRODUCTION AND SUMMARY

The PCTR thermal column is an irradiation facility outside of the reactor core which provides a thermal spectrum of neutrons, independent of the reactor loading, and is used to activate foils for normalization between irradiations. A series of experiments investigating the characteristics of the thermal column have been completed. Bare and cadmium covered gold foil activation measurements were obtained along the horizontal and vertical directions of the thermal column for each of the three column configurations: (1) solid graphite stack; (2) solid graphite stack reflected by 1.5 in. of polyethylene and Lucite from the outside; and (3) the reflected stack with a 3.5 x 3.5 x 8 in. void in the center.

The reflector increased the thermal flux and decreased the flux variation in both horizontal and vertical directions. Also, the cadmium ratio was increased. The addition of the void in the center of the column gave an additional decrease in the flux variation across that region, but the decrease was limited by the small horizontal dimensions of the void.

The results of this study indicate that the standard foil irradiation position should be moved about 12 in. further from the PCTR core. The reflected thermal column gives an improvement in both the increased thermal flux and the decreased epithermal flux. The void creates only a slight change in the sensitivity of foil activation to vertical position. If a large decrease in sensivitiy is desired, a larger void than the one investigated should be used.

DESCRIPTION OF EXPERIMENT

The thermal column shown in Figure 1 is an approximate cube of graphite blocks 36.5 x 37.5 x 38.5 in. high, and located on top of the stationary section of the PCTR. The thermal column serves as a normalization facility for foils irradiated in the reactor core.[1] Ideally, the column would have a completely thermal spectrum, and the flux across the region where the foils are irradiated would not vary, making the repositioning of foils not extremely critical. At the start of the experiments the foil rotator, an 8 in. long graphite cylinder with three levels for foils 2 in. apart, was operating with its bottom 35 in. below the top of the thermal column. It was located in a shaft in the exact center of the column.

PROCEDURE

There were six irradiations in all, three with bare foils and three with foils covered with 0.040 in. thick cadmium. These occurred in pairs, the first pair with the column unchanged, the second pair with the reflector in

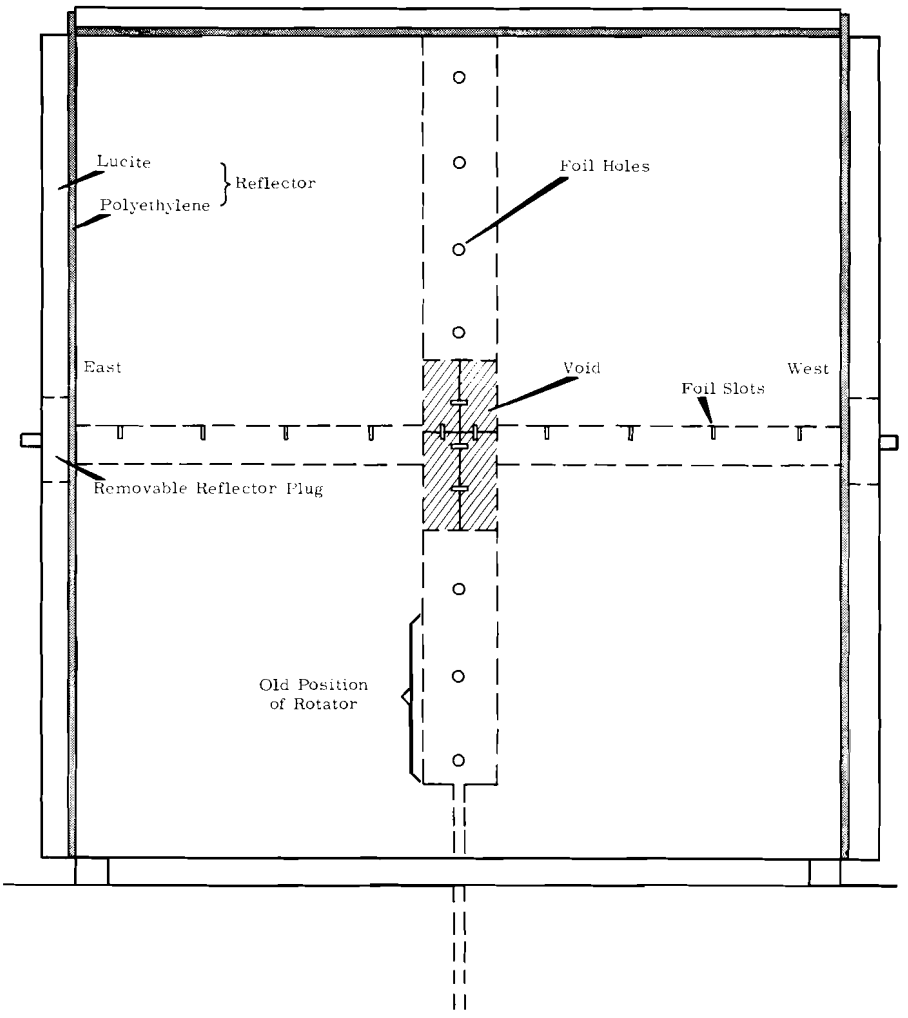

FIGURE 1. Cutaway of Center of Thermal Column Looking in from the North (Appearance is that of final two irradiations.)

place, and the third pair with both reflector and void present. All bare irradiations were for 1000 W-min, while the cadmium-covered irradiations were for 18,000 W-min.

One-half inch diameter, 5-mil thick gold foils were used for all of the traverses. The monitor foil used in each irradiation to normalize between bare and cadmium-covered irradiations was one-half mil thick. The monitor foils were placed on the outside of the reactor, just above the north hole plug. The measured foil count rates were used together with computer code APDAC-III to obtain the specific activity of each foil relative to the monitor foil. Cadmium ratios were computed by dividing bare specific activities by cadmium-covered specific activities.

RESULTS

The graphs in Figures 2 and 3 compare the total and epicadmium flux in both horizontal and vertical directions before and after the reflector was

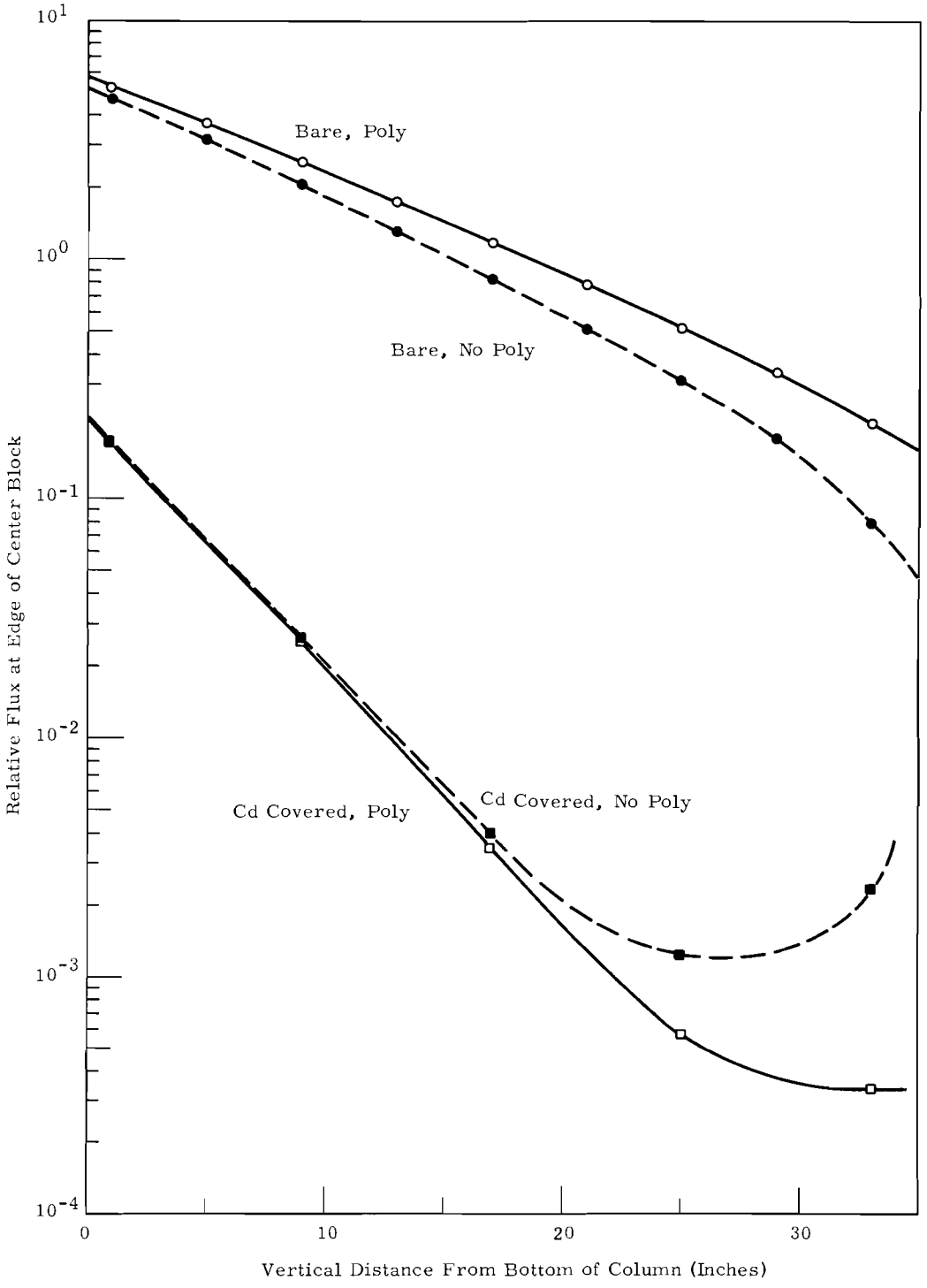

FIGURE 2. Effects of Poly Reflector on Thermal Column

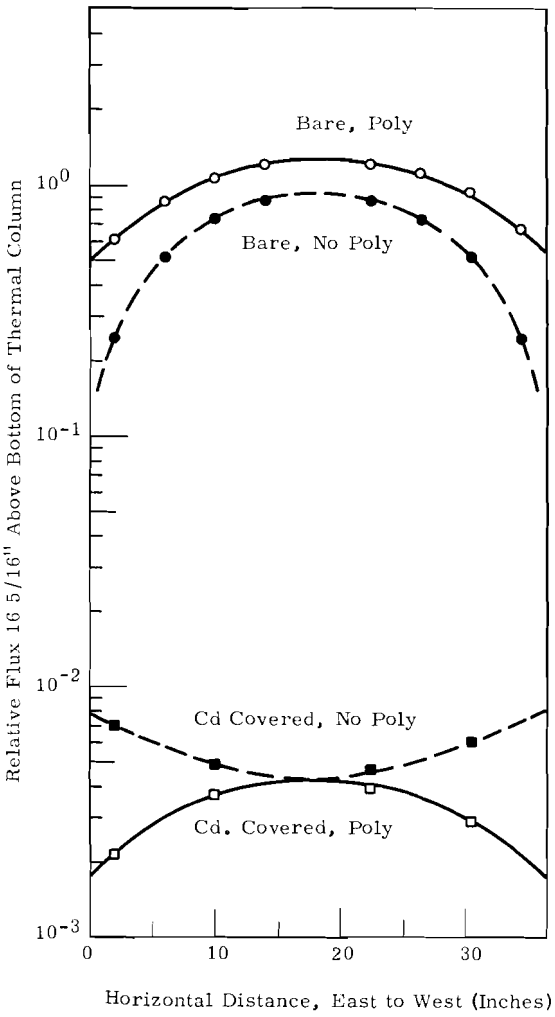

FIGURE 3. Effects of Poly Reflector on Thermal Column

added. The total flux increased slightly and flattened, while the epicadmium flux decreased greatly near the edges of the thermal column. The curvature in the horizontal direction is completely reversed (see Figure 3). The fast neutrons reflected from the concrete walls and ceiling of the reactor room into the thermal column account for the rising of the epicadmium flux near the edges of the column, and the reflector practically eliminates this effect.

As can be seen in Figures 4 and 5, the cadmium ratio is increased significantly with the addition of the reflector. Also, the cadmium ratio is now almost a constant across the horizontal dimensions. That the cadmium ratio is now not symmetric but rises slightly from east to west can probably be explained by the fact that the reflector extends some 5 in. lower on the west than on the east. This is due to the presence of a catwalk around the thermal column which runs directly along the east side and prevents the use of reflector below its level.

The changes which occur in the total flux with the addition of the void (see Figure 1) are shown in Figures 6 and 7. There is significant flattening of the flux across the void region. If a linear slope is assumed in the void region for both cases of Figure 6, a graph like that of Figure 8 is obtained where the two lines represent the respective flux variations from bottom to top of the void. Figure 8 shows a 26% decrease in the flux variation across the void where a 100% decrease would indicate no flux variation.

In Figures 9 and 10 a comparison is shown between the epicadmium flux with and without the void. The flattening of the vertical epicadmium flux again occurs, but there is a sharp peak in the horizontal epicadmium flux in the void. This phenomenon can best be explained by examining Figure 9 closely. At the horizontal traverse position 19 13/16 in. above the bottom of the column, both vertical and horizontal plots agree that the epicadmium flux in the voided case is 50% higher than the

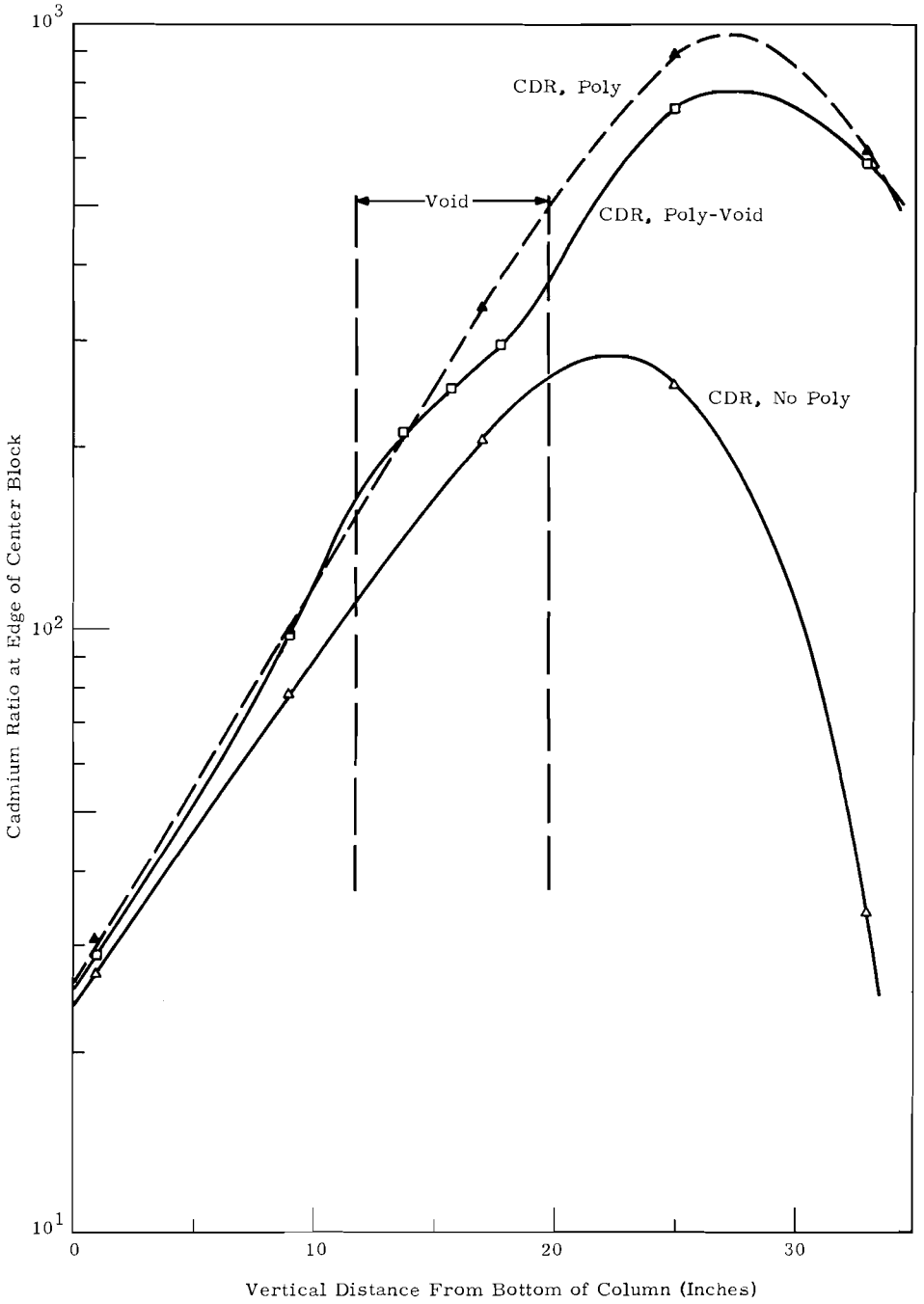

FIGURE 4. Cadmium Ratios

unvoided case. Thus, there is a streaming of fast neutrons up the void, but the epicadmium flux falls off sharply as the sides of the void are approached. A larger void, especially in horizontal dimensions, would cause the flux, both total and epicadmium, to be much flatter, but would also cause a greater peak in the horizontal flux and a greater dip in the cadmium ratio across this region (See Figure 5).

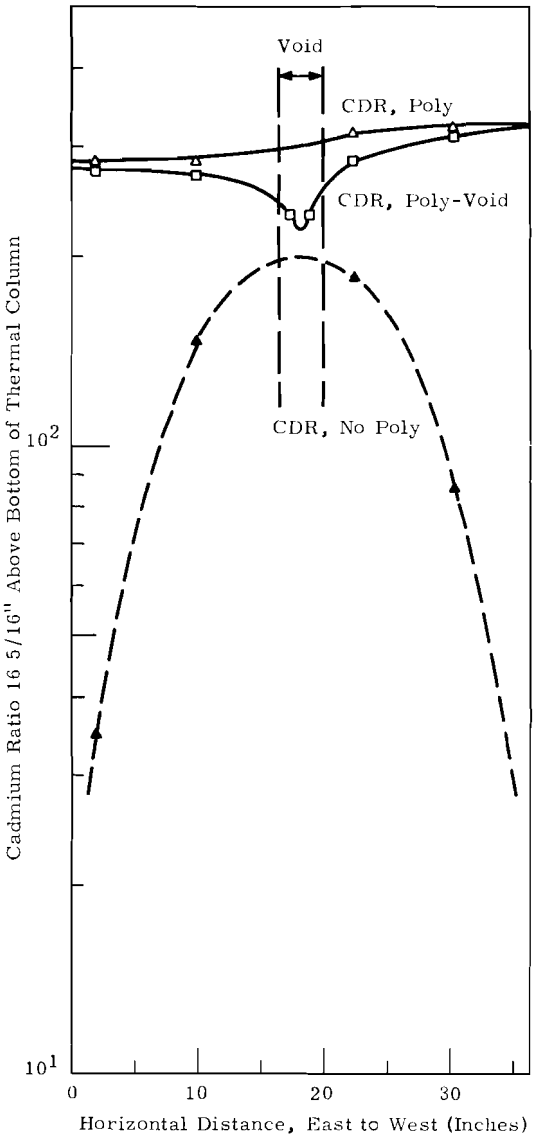

FIGURE 5. Cadmium Ratios

CONCLUSIONS

One change which has already been made, in addition to permanently adopting the reflector, has been to raise the rotator from its old position to the position where the void was investigated, 11 3/4 in. higher. The total flux there is only 1/3 of its value at the old position, but is still sufficient to activate any foils normally used in the thermal column. A slightly longer irradiation time may be necessary in some cases, such as copper foils. The advantages of such a move are readily seen by examining Figure 4. The cadmium ratio is increased to approximately 7 times its value in the old unreflected position. Also, the presence of the reflector increases the cadmium ratio to 50 to 70% over the unreflected value across the new rotator position. Thus, the foils are now irradiated in a much more thermal spectrum (cadmium ratio 200 to 300 for 5-mil thick gold foils).

The use of a void of the dimensions investigated (3.5 x 3.5 x 8 in.) is not recommended. The advantage of the 26% decrease in activation sensitivity to vertical position (See Figure 8) is offset by the large fluctuation in the epicadmium flux horizontally across the void, and the corresponding dip in the cadmium ratio. However, with a larger void (especially in horizontal dimensions) both total and epicadmium flux would be essentially flat over a large region of the void. In this case, the use of the void and an aluminum foil rotator would be an improvement.

REFERENCES

1. *R. I. Smith. "An External Thermal Column for the PCTR," Physics Research Quarterly Report, October, November, December, 1961, HW-72586, General Electric Company, pp. 28-34. January 31, 1962.*

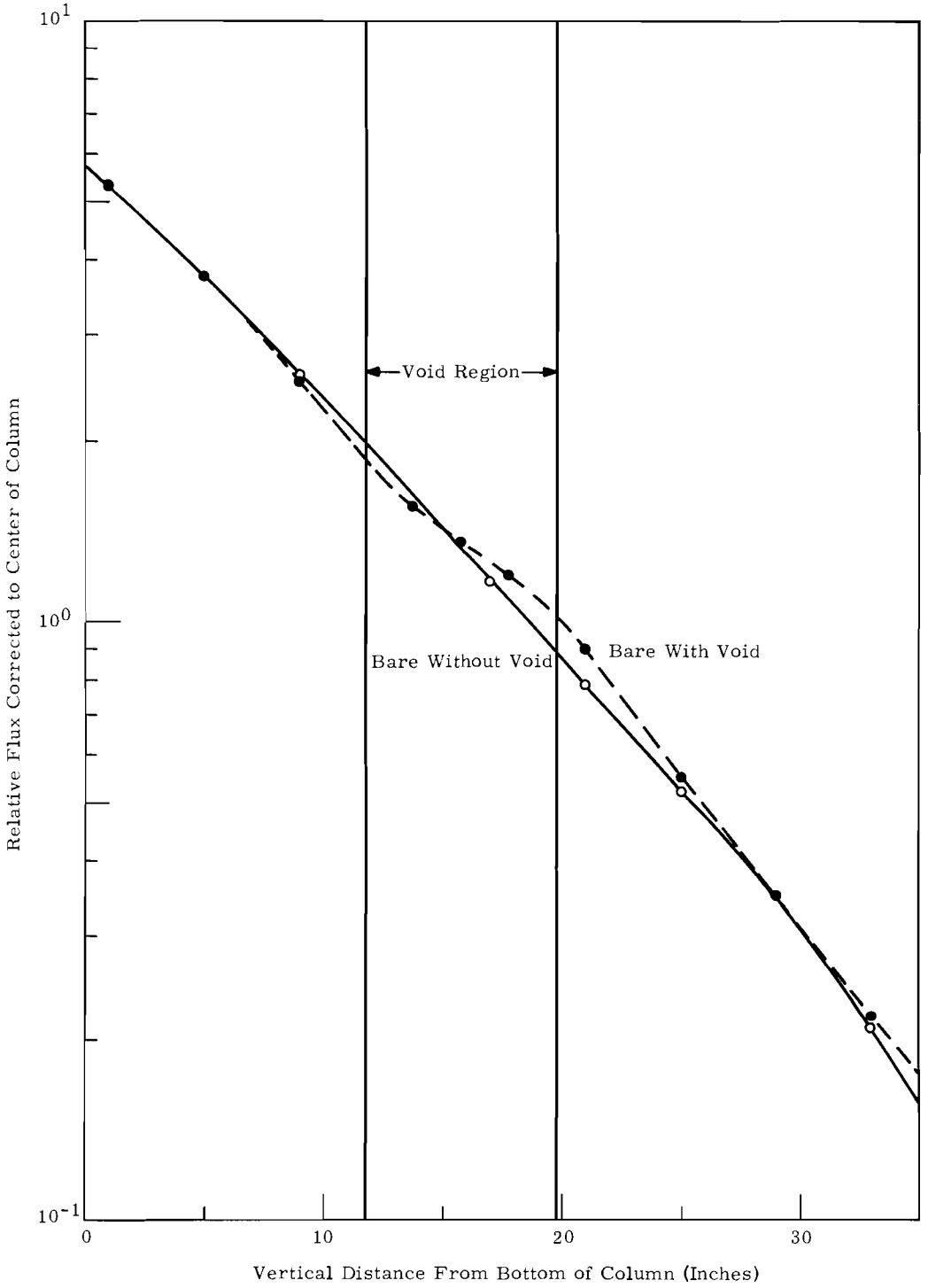

FIGURE 6. Thermal Column with Reflector--Effects of Void

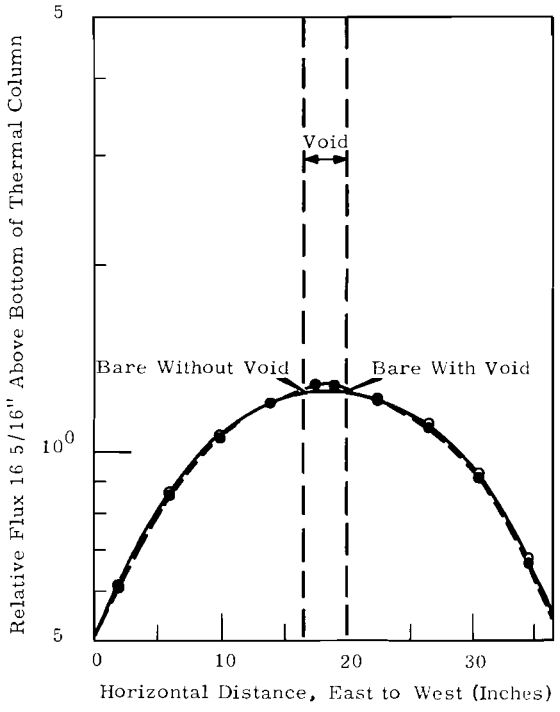

FIGURE 7. Thermal Column with Reflector--Effects of Void

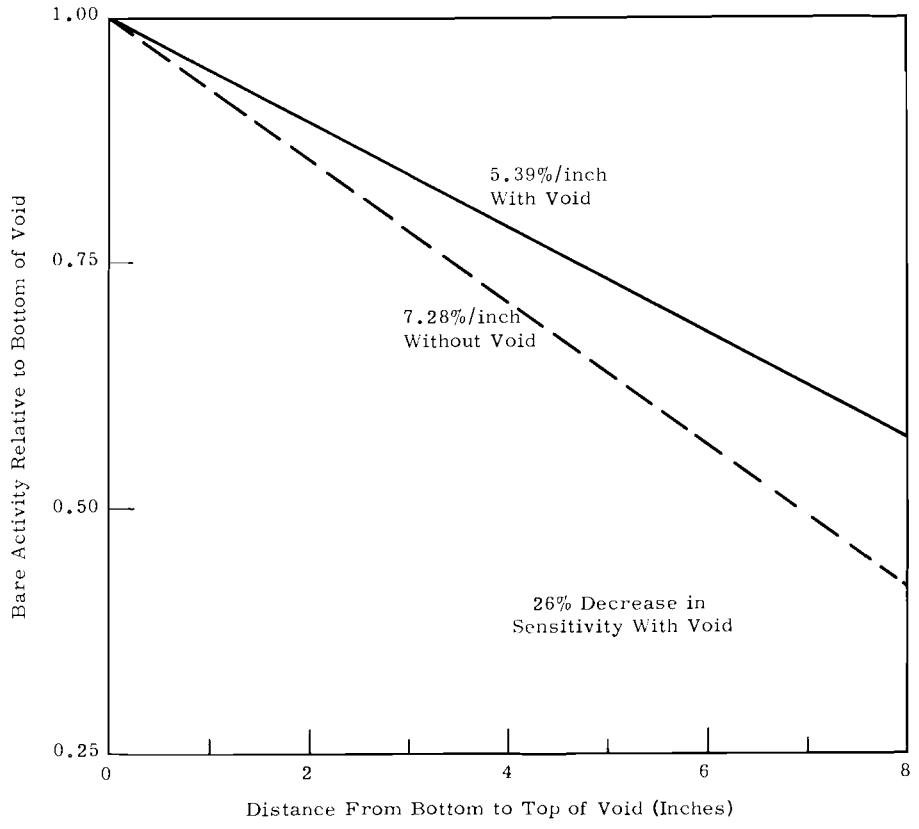

FIGURE 8. Percentage Decrease in Flux Across Void Region

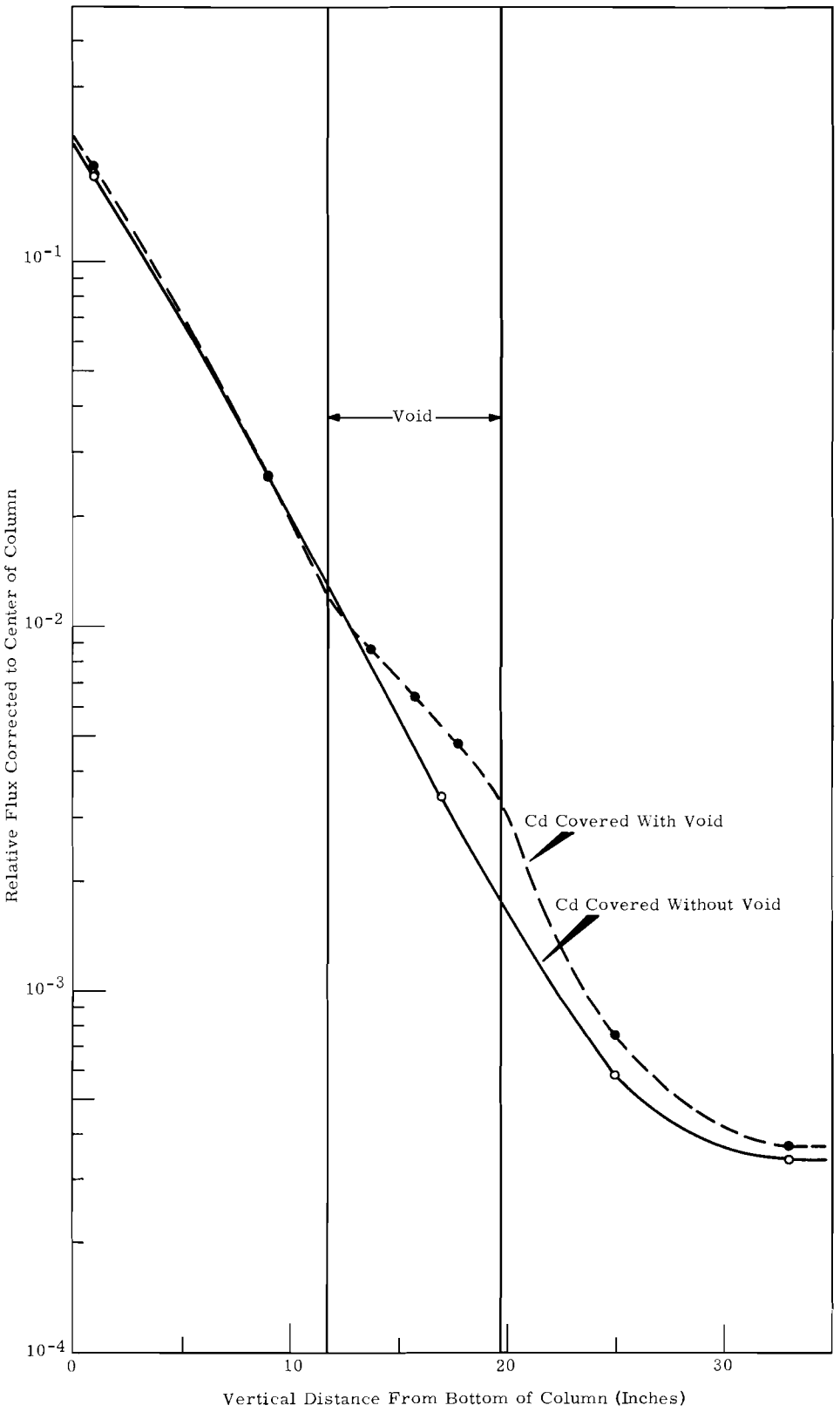

FIGURE 9. Thermal Column with Reflector--Effects of Void

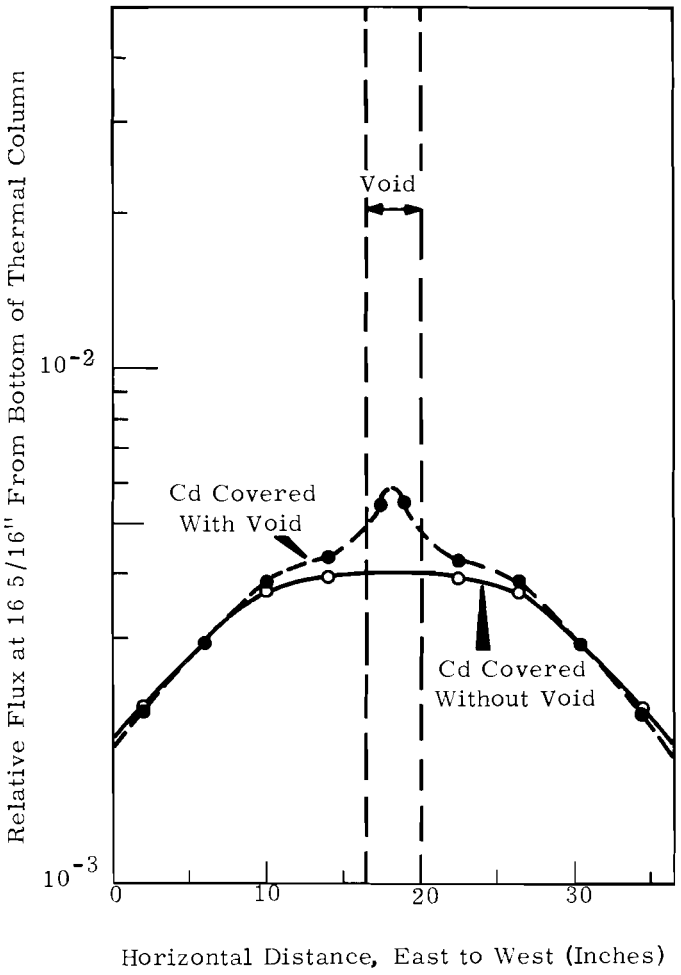

FIGURE 10. Thermal Column with Reflector--Effects of Void

FAST REACTORS

PHYSICS CHARACTERISTICS OF AN 800 LITER OXIDE FTR REFERENCE CORE

R. W. Hardie

Neutronics calculations were performed for an 800 liter, PuO_2-$U^{238}O_2$ core (L/D = 0.8). The following parameters were determined: critical mass, reactivity coefficients, flux, flux spectra, breeding ratio, sodium worth, and Doppler coefficient. All computations were performed using a modified version of the Russian 26-group cross-section compilation; shielding factors were generated using the FCC fundamental mode code. The one-dimensional runs were done using LASL's 1-D code, DTF-IV (S_4 option).

The principal statics characteristics of the ceramic reference reactor are described in Table I. Critical mass calculations were done in cylindrical geometry; axial leakage was simulated using a reflector savings of 12 cm on each end. The reactor was assumed to consist of a homogeneous core surrounded by a 30 cm Inconel radial reflector.

Table II summarizes some of the important kinetics parameters. Spherical

TABLE I. Neutronics Characteristics of an 800 Liter Oxide Reactor

Parameter	Values
k_{eff}	1.04
vol% PuO_2	5.66
vol% $U^{238}O_2$	19.34
vol% Stainless Steel	25.0
vol% Sodium	45.0
vol% void	5.0
Mass Pu^{239}, kg	412
Mass Pu^{240}, kg	46
Mass U^{238}, kg	1495
Φ_T, n-cm^{-2}-sec^{-1}	0.55×10^{16} ($\overline{P}$ = 0.5 MW/liter)
ϕ_{peak}/ϕ_{av}	1.76
ϕ(>1.4 MeV)/ϕ_T	0.10
ϕ(>0.1 MeV)ϕ_T	0.67
ϕ(>0.01 MeV)ϕ_T	0.94
Reactivity Life (days, δk = -0.03)	86 ($\overline{P}$ = 0.5 MW/liter)
Breeding Radio	0.49

TABLE II. Kinetics Parameters

Parameter	Value
Doppler Coefficient (Tdk/dT)	
Reference Core	-3.89×10^{-3}
Reference Core (no sodium)	-1.84×10^{-3}
"Dirty" Reference Core ($\sigma N_{F.P.} = 0.003$)	-3.26×10^{-3}
β_{eff}	0.0030
Λ_o, sec	3.9×10^{-7}
Sodium Worth	
Reference Core, Total	+0.0130
Reference Core, r < 10 cm	-0.0002
"Dirty" Reference Core, Total ($\delta N_{F.P.} = 0.003$)	+0.0093
"Dirty" Reference Core, r < 10 cm	- 0.0003

geometry was used for sodium worth calculations instead of cylindrical geometry because the shift in spectrum due to sodium loss causes a change in reflector savings.

PRELIMINARY EVALUATION OF CROSS-SECTION DATA

W. W. Little, L. L. Maas, and R. W. Hardie

All FTR neutronics calculations are based on a modified version of the Russian 26-group data compilation. To assess the accuracy of this cross-section set, numerous critical assemblies have been analyzed. A partial list of the assemblies studied, which cover a wide range of flux spectra, is given in Table I. The prominent spectrum characteristics of these assemblies are tabulated in Table II.

One method of checking cross-section data is to compare calculated and experimental fission ratios. Tables III and IV give the Pu^{239}/U^{235} and U^{238}/U^{235} fission ratios for the

TABLE II. Calculated Critical Assembly Characteristics

Assembly	% of Flux Above Indicated Energy 0.01 MeV	0.1 MeV	1.4 MeV	Critical Buckling, $B^2 \times 10^3$
ZPR-III 14	94.4	74.7	22.2	5.58
29	97.2	75.2	11.8	2.42
34	97.2	74.5	11.3	2.01
35 (FERMI B)	97.0	75.9	10.1	1.80
38	99.9	85.0	8.9	3.22
39	99.5	83.4	13.1	2.14
44 (RAPSODIE)	99.5	87.1	22.1	8.55
45A	93.2	67.2	10.0	1.07
46B (FARET)	99.1	85.7	20.2	5.88
47 (SEFOR)	89.3	61.0	10.3	2.40
48	92.0	67.2	12.1	2.54
ZPR-VI 2	96.7	73.5	11.4	2.08
ZEBRA 1	99.9	87.1	10.8	5.62
2	92.8	66.5	11.8	2.59
5	99.8	87.3	12.0	8.29
6A	90.9	67.1	14.6	3.27

TABLE I. Central Core Compositions

Core	U^{235}	U^{238}	Pu^{239}	Pu^{240}	Be	C	O	Na	Al	Cr	Fe	Ni	Mo	Cu
ZPR-III														
14	0.4500	0.0350	-	-	-	5.3000	-	-	-	-	0.790	-	-	-
29	0.2390	0.4800	-	-	-	-	1.3900	-	1.470	-	2.110	-	-	-
34	0.2250	0.4950	-	-	-	0.7600	-	-	1.540	-	2.110	-	-	-
35 (FERMI B)	0.1954	0.0141	-	-	-	-	0.3994	0.7825	-	0.7556	3.180	0.2975	-	-
38	0.3638	3.5052	-	-	-	-	-	-	-	0.1507	0.572	0.0716	-	-
39	0.2792	0.4576	-	-	-	-	-	-	1.410	0.3969	1.507	0.1887	-	-
44 (RAPSDIE)	0.5034	0.3365	0.1558	0.0074	-	-	1.9570	-	1.031	0.1831	1.439	0.0908	-	-
45A	0.0015	0.7230	0.1070	0.0051	-	0.8330	-	1.0580	-	0.2030	0.757	0.1000	-	-
46B (FARET)	0.3392	0.5599	0.1565	0.0074	-	1.1080	-	0.8421	-	0.2856	1.064	0.1407	-	-
47 (SEFOR)	0.0015	0.7744	0.1480	0.0132	0.568	0.3360	1.5660	0.6630	0.699	0.2731	1.045	0.1080	0.0515	-
48	0.0016	0.7406	0.1654	0.0106	-	2.0765	-	0.6230	0.011	0.2658	0.990	0.1308	0.0206	-
ZPR-VI 2	0.2285	0.9853	-	-	-	1.2900	-	0.7910	-	0.2983	1.038	0.1590	-	-
ZEBRA 1	0.4700	3.4000	-	-	-	-	-	-	-	0.1100	0.410	0.0420	-	-
ZEBRA 2	0.2400	1.5000	-	-	-	3.8000	-	-	-	0.1000	0.380	0.0390	-	-
ZEBRA 3	0.0230	3.1000	0.3820	0.0180	-	-	-	-	-	0.1100	0.420	0.0430	-	0.4600
ZEBRA 6A	0.0046	0.6353	0.1895	0.0144	-	2.9590	-	0.4474	0.2504	0.1270	0.4525	0.0443	-	0.0829

TABLE III. Central Reaction Rate Ratios

Assembly	Experimental	Calculated PNL	C/E
	$\sigma_f^{U^{238}} / \sigma_f^{U^{235}}$		
ZPR-III 14	1.050	1.089	1.037
29	1.060	1.080	1.019
34	1.067	1.088	1.020
35 (FERMI B)	1.090	1.084	0.994
38	1.170	1.185	1.013
39	1.180	1.181	1.001
44 (RAPSODIE)	1.186	1.235	1.041
45A	1.047	0.969	0.926
46 (FARET B)	--	1.212	--
47 (SEFOR)	0.916	0.900	0.983
48	0.976	0.959	0.983
ZPR-VI 2	1.090	1.074	0.985
ZEBRA 1	1.198	1.208	1.009
2	0.987	1.003	1.016
3	1.190	1.212	1.018
6A	0.961	0.949	0.988

TABLE IV. Central Reaction Rate Ratios

Assembly	Experimental	Calculated PNL	C/E
	$\sigma_f^{U^{238}} / \sigma_f^{U^{235}}$		
ZPR-III 14	0.060	0.071	1.182
29	0.038	0.040	1.053
34	0.037	0.039	1.054
35 (FERMI B)	0.031	0.034	1.100
38	0.033	0.035	1.061
39	0.048	0.050	1.042
44 (RAPSODIE)	0.082	0.086	1.049
45A	0.028	0.029	1.036
46 (FARET B)	--	0.078	--
47 (SEFOR)	0.026	0.026	1.000
48	0.031	0.034	1.097
ZPR-VI 2	0.036	0.038	1.056
ZEBRA 1	0.041	0.043	1.049
2	0.032	0.035	1.094
3	0.046	0.048	1.043
6A	0.036	0.040	1.111

assemblies listed in Table I. In general, the computed fissile fuel fission ratios are in reasonable agreement with experiment, whereas the computed U^{238}/U^{235} fission ratios are consistently higher than experimental values.

Cross sections can also be evaluated by comparing calculated and experimental reactivity coefficients. Table V gives the reactivity worth of various materials in the SEFOR critical assembly in terms of δk; Table VI gives reactivity worths in the ZEBRA assemblies in terms of σ_p. Note that fuel worths are predicted well, whereas the calculated light-element worths--especially B^{10}--exhibit rather large discrepancies with experimental values.

TABLE V. ZPR-III 47 (SEFOR) Reactivity Coefficients

Sample Material	Sample Mass, g	Reactivity Worth, mk Experimental	Reactivity Worth, mk Calculated
Pu-SS-Al	69.1	0.297	0.295
Enriched UAL	72.1	0.223	0.213
Depleted U	2460.1	-0.535	-0.719
B_4C, Enriched	32.4	-1.445	-1.416
Na	91.2	-0.031	-0.043
SS	1026.1	-0.114	-0.146
Fe	1028.0	-0.099	-0.141
Be	240.7	0.082	0.036

TABLE VI. Central Perturbation Cross Sections in Zebra Assembly

Sample	ZEBRA 1 E	ZEBRA 1 C	ZEBRA 2 E	ZEBRA 2 C	ZEBRA 3 E	ZEBRA 3 C
U^{235}	2.043	2.070	2.282	2.293	2.049	2.088
Pu^{239}	3.343	3.391	3.236	3.330	3.299	3.420
U^{238}	-0.104	-0.111	-0.177	-0.170	-0.103	-0.110
B^{10}	-1.100	-0.846	-3.136	-2.178	-1.091	-0.805
C	-0.012	-0.013	+0.010	+0.006	-0.041	-0.035
Na	-0.013	-0.015	+0.005	+0.004	-0.026	-0.029
Fe	-	-0.034	-0.019	-0.028	-	-0.040
Ta	-0.327	-0.307	-0.790	-0.734	-0.312	-0.318
Al	-0.015	-0.022	-0.009	-0.013	-0.028	-0.034

ALOGRITHMS FOR COLLAPSING FAST REACTOR CROSS SECTIONS

W. W. Little, Jr., and R. W. Hardie

Fast reactor cross sections are often compiled in multigroup arrays--the number of groups usually lying between 15 and 40. Since many design calculations--especially multidimensional calculations--do not require such fine detail, a study was made of the methods, applicability, and errors involved in collapsing fine group cross sections. The collapsing problem is of special interest in the analysis of large sodium cooled breeder reactors. In these reactors, the sodium reactivity coefficient depends on a precarious balance between spectral and leakage terms. Thus, if few group cross sections are used to calculate sodium worth, the collapsed cross sections must preserve both spectral and leakage effects.

For the calculation of k_{eff}, reaction rates, etc., the usual flux weighting recipe--with reciprocal weighting of the transport cross section--was found to be most suitable. The accuracy of this collapsing method for a large oxide fueled breeder reactor is illustrated in the first four columns of Table I. The parameters in Table I were computed using the one-dimensional DTF-IV transport code[1] and the FCC fundamental mode code.[2] Collapsed cross sections were generated by the FCC code. Observe that reaction rates, fuel coefficients, and poison coefficients are well described by the few group cross sections.

It can be seen from Table I, however, that the collapsed cross sections computed by flux weighting are totally inadequate for calculating the reactivity coefficient of a moderator (e.g., beryllium or sodium). For such calculations, a new collapsing algorithm was devised. This algorithm, which employs both flux

TABLE I. Parameters Computed from Exact and Collapsed Cross Sections[a]

Parameter	Number of Energy Groups: 20 ("Exact")	12	8	4	4 (Perturbation Cross Sections)
k_{eff} - 1	0.0	+0.00009	+0.00356	+0.00517	--
$\bar{\sigma}_f^{Pu^{239}}$	2.01493	2.01494	2.01684	2.01678	--
Worths, δk					
Pu^{239} (+ 10%)	+0.05321	+0.05392	+0.05366	+0.05377	+0.05311
B^{10} ($\delta N = 2 \times 10^{-4}$)	-0.07663	-0.07489	-0.07550	-0.07579	-0.07798
Na (- 20%)	-0.00126	-0.00090	-0.00104	-0.00077	-0.00121
Be ($N = 10^{-3}$)	+0.00060	-0.00072	-0.00084	-0.00152	+0.00062

[a] Calculations for large oxide fueled fast reactor.

and adjoint flux, is obtained by conserving the fundamental mode reactivity coefficients. This is most conveniently accomplished by introducing a pseudo absorption cross section in each coarse group. The last column in Table I demonstrates that a four-group model using such "perturbation" cross sections is much more accurate for computing moderator reactivity coefficients than corresponding models using flux weighted cross sections.

Many other numerical experiments using these and alternate algorithms have been performed. In general, the two algorithms mentioned were found most appropriate, although other collapsing recipes may yield better results for specific reactors.

REFERENCES

1. *K. D. Lathrop. DTF-IV, A FORTRAN-IV Program for Solving the Multigroup Transport Equation with Anisotropic Scattering, LA-3373. November, 1965.*

2. *W. W. Little, Jr. and R. W. Hardie. FCC, A Fundamental Mode Code for Fast Reactor Analysis, BNWL-234. March, 1966.*

PLANNING OF FTR CRITICAL EXPERIMENT PROGRAM

R. A. Bennett and R. A. Harris

Critical experiments in support of FTR design will consist of two separate but related programs: an engineering mockup program; and a premockup or "clean" experiment program. The mockup experiments will consist of an extensive experimental study of the reference FTR core.

The purpose of the premockup experiments is to obtain early experimental information regarding in-core and reflector control characteristics for systems whose neutronics resemble those of the PuO_2-UO_2 FTR core. These experimental data are to be used as tests of calculational models presently employed in the design of FTR.

It is tentatively planned that the premockup experiments will be carried out in the ZPR-III facility at ANL, Idaho. In the present program, under way in the ZPR-III facility, six plutonium assemblies (P_1 to P_6) are to be investigated. To determine which of these assemblies would be most useful for FTR purposes, a series of calculations was performed.

Fundamental mode calculations yielded the parameters shown in Table I for the plutonium assemblies and the 800 liter PuO_2-UO_2 ceramic FTR core.

The plutonium assembly which appears to most consistently duplicate the flux spectra of the FTR ceramic core is P_1 (Assembly 48). Other assemblies, such as P_2, could be utilized if the need arose.

Fairly detailed design calculations are now being carried out for Assembly 48. Spatial distributions of neutron reaction rates have been calculated for several possible detector materials. Further, since it is presently planned to use an Inconel reflector on the FTR, calculated worths of control rods on the core periphery of Assembly 48 were compared for a U^{238} reflected and an Inconel reflected system.

For the U^{238} and Inconel reflected systems, the worths of an annular shell of B_4C (equivalent in volume to four, 2 in. by 2 in. rods) on the core periphery were found to be 3.27\$ and 9.47\$ (ρ = 0.00345), respectively.

Since an Inconel reflector on Assembly 48 would more closely simulate the spectral conditions of the FTR and in view of the significant increase in rod worth, experiments with an Inconel reflector are more appropriate than experiments with a U^{238} reflector. However, complete replacement of the U^{238} reflector of Assembly 48 with Inconel is costly, time consuming, and perhaps not necessary. It may be possible to do experiments of pertinence to the design of FTR control rods using a partial Inconel reflector in the form of a sector, as small as 90°. Calculations are presently under way to establish the required size of an adequate Inconel sector.

TABLE I. Fundamental Mode Parameter

Core	Fraction of Total Flux Above Given Energies					Spectrum Averaged Cross Sections		
	800 keV	100 keV	10 keV	1 keV	0.1 keV	$\sigma_f^{Pu^{239}}$	$\sigma_f^{Pu^{240}}$	$\sigma_f^{U^{238}}$
P_1	0.225	0.677	0.925	0.988	1.000	1.899	0.479	0.0678
P_2	0.236	0.696	0.933	0.993	1.000	1.852	0.500	0.0704
P_3	0.227	0.607	0.861	0.973	0.998	2.113	0.465	0.0709
P_4	0.256	0.598	0.833	0.957	0.996	2.296	0.503	0.0827
P_5	0.256	0.653	0.890	0.974	0.999	2.053	0.516	0.0803
P_6	0.268	0.668	0.896	0.982	1.000	1.987	0.537	0.0838
800 liter FTR	0.182	0.663	0.935	0.989	1.000	1.864	0.420	0.0571

FTR SHIELD CALCULATIONS

D. R. Marr, W. L. Bunch

The removal-diffusion attenuation code MAC has been used to compare four different axial shield arrangements for the Fast Test Reactor (FTR). This code calculates the energy and spatial distribution of both the neutron and gamma flux throughout the shield. In the present version of MAC, geometry is limited to slab core and shield regions that are infinite in extent. Up to 18 slab shield regions can be used in a calculation, with the material in each slab being homogeneous. Streaming or channeling effects due to penetrations through the shield cannot be taken into account by the code. The basic advantage of the code for survey calculations is speed. The time required for a Monte Carlo or transport calculation would be orders of magnitude greater. Thus, these latter codes will only be used for more detailed shield design.

Table I summarizes the compositions and dimensions of the various regions assumed in the four cases. The thermal barrier between the sodium pool and the cover plate could probably contain special neutron shielding material, subject to the environmental conditions that will exist. The results (see Table II) indicate that some neutron shielding material will be required in this region. The filler materials that were assumed in each case would be adequate; however it will be necessary to determine how these materials might be included within the barrier and if they would be able to withstand the temperature and radiation environment. Study programs have been proposed to determine the environmental conditions in which these materials might be used.

TABLE I. Assumed Axial Shield Composition

Shield Arrangement 1

Region	Name	Composition (Volume %)
1,2	Core 1, Core 2	50% SS, 5% PuO_2, 40% Na
3	Sodium Pool 1, Part 1	2.2% 304 SS, 97.8% Na
4	Sodium Pool 1, Part 2	1.7% 304 SS, 98.3% Na
5	Upper Tube Sheet	97.6% 304 SS, 2.4% Na
6	Sodium Pool 2	7.7% 304 SS, 92.3% Na
7	Thermal Barrier, Part 1	3.5% 304 SS
8	Thermal Barrier, Part 2	3.5% 304 SS
9	Cover Plate, Part 1	3.5% 304 SS, 92.7% Cast Iron
10	Cover Plate, Part 2	3.5% 304 SS, 92.7% Cast Iron
11	Nozzle Area	3.3% 304 SS
12	Gamma Shield	100% Cast Iron

Shield Arrangement 2

Same as (1) except Thermal Barrier, Regions 7 and 8, also contain 30% iron serpentine (1.38 g/cm^3) concrete (TS-265).

Shield Arrangement 3

Same as (1) except Thermal Barrier, Regions 7 and 8, also contain 70% graphite (1.11 g/cm^3).

Shield Arrangement 4

Same as (1) except Thermal Barrier, Regions 7 and 8, also contain 80% bulk serpentine (1.38 g/cm^3).

TABLE II. Results of MAC Calculations for FTR Axial Shield Arrangements

Case	Calculated Exposure Rate Through Shield, mrem/hr	
	Neutrons	Gamma
1	7×10^{1}	2×10^{1}
2	7×10^{-2}	1×10^{-2}
3	3×10^{-2}	7×10^{-3}
4	5×10^{-3}	9×10^{-4}

SHIELD ANALYSES FOR IRRADIATED FTR FUEL HANDLING

W. L. Bunch

The computer program ISOSHLD has been used to determine basic shielding requirements for a number of components of the FFTF (Fast Flux Test Facility) in which the fuel irradiated in the FTR will be handled or processed. ISOSHLD performs gamma ray shielding calculations for a wide variety of source and shield configurations. Taylor Buildup factors are incorporated in the calculations based on the number of mean free paths traversed and the effective atomic number of the basic shield region. Also incorporated as a subroutine is the program RIBD, which calculates fission product inventory as a function of irradiation conditions and decay time. It was necessary to develop a fast reactor library for use with this code to incorporate fast fission yield factors and fast neutron absorption (burnup) cross sections.

Facilities for which preliminary shielding requirements have been calculated include the "rabbit" irradiation facility, the gas-cooled interim examination facility, the gas-cooled disassembly cell, the gas-cooled "pin" examination cell, and the underwater examination facility. In addition, the program RIBD has been used to calculate decay heat in FTR fuel following shutdown. These studies have all been reported in internal reports to serve as bases for conceptual design of the several facilities. More detailed shielding calculations will be required for these and other facilities to assist in evolving the final design.

A STUDY OF A FAST-THERMAL REACTOR EXPERIMENT

R. M. Humes and D. A. Bitz

Major emphasis is being placed on fast reactor development as a method of conserving the nation's supply of fissionable material. In view of the past and present usefulness of the Physical Constants Test Reactor (PCTR) in the development of thermal reactors, it was anticipated that experiments similar to those performed on these thermal systems could also be done for fast systems utilizing both the PCTR and the new High Temperature Lattice Test Reactor (HTLTR). To provide insight into the needed experimental conditions and also the possible uncertainties to be expected in such experiments,[1] the set of calculations described here were begun.

The calculations are being performed on the Univac 1107 utilizing the multigroup transport program, DTF-IV. A 26 neutron energy group set of cross sections proposed by the Russians and averaged over the SEFOR core 1A

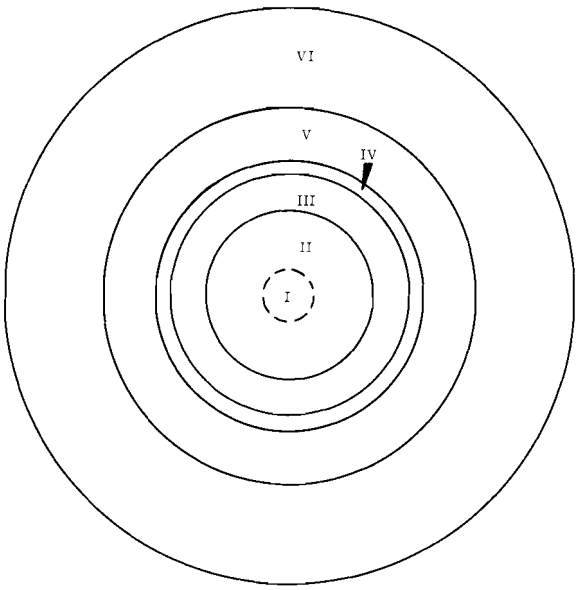

FIGURE 1. Reactor Model for DTF-IV

spectrum have been used in all of the calculational runs.[2]

To provide a reference, a calculation was made on the SEFOR-1A core with an artificial boundary at a radius of 8 cm.

The experimental fast-thermal system is represented by a sphere containing six regions as shown in Figure 1. Regions I and II are composed of the SEFOR-1A material. The boundary between these regions is at a radius of 8 cm in all cases, and thus represents the test cell in the experiment. Region III is a natural uranium buffer-decoupler region. Region IV is a narrow, 5 cm, zone of graphite. The highly enriched uranium drivers of the test reactor are represented by Region V; and a graphite reflector, Region VI, surrounds the entirety.

Six configurations, in addition to SEFOR, have been examined thus far. Representing these by X + Y where X = outer radius of Region II, Y = thickness of natural uranium buffer-decoupler region, these configurations are:

a) 15 + 10 cm
b) 20 + 5 cm
c) 30 + 0 cm
d) 30 + 5 cm
e) 30 + 10 cm
f) 30 + 15 cm

The purpose behind this series of calculations was to determine if the neutron energy distribution of an operating fast breeder reactor could be attained, while still keeping as small a test core as possible and staying within the standard PCTR safety limitations. It is believed that the PCTR type of experiments can be made on very low leakage test material (i.e., $k_\infty \simeq 1.000$).

The calculations discussed here are for a rather high leakage test material and thus represents a severe test of the possibilities of accomplishing such experiments. One of the proposed experiments for this highly reactive fuel is to measure the adjoint weighted neutron leakage, with a suitable normalization, for the equilibrium fast reactor medium under investigation. The quantity most nearly corresponding to this which can be obtained from the computer printouts is (Net Leakage)/(Total Absorption). Hence, for each configuration this ratio for Region I is the quantity which has been compared with the value for SEFOR. The values obtained are shown in Table I and Figure 2.

Care must be taken in drawing conclusions from these results. The

TABLE I. (Net Leakage)/(Total Absorption) in Region I

Loading (Fast Region) + (Decoupler)	L/A
SEFOR	0.4662
15 + 10	0.4656
20 + 5	0.4726
30 + 0	0.1926
30 + 5	0.4046
30 + 10	0.4205
30 + 15	0.5477

major pitfall is a result of the algebraic nature of the leakage for each energy group. The net leakage is the sum of the leakages for the 26 groups, and may thus produce a value which appears to be in excellent agreement with the reference value although detailed examination of each group provides an entirely different picture.

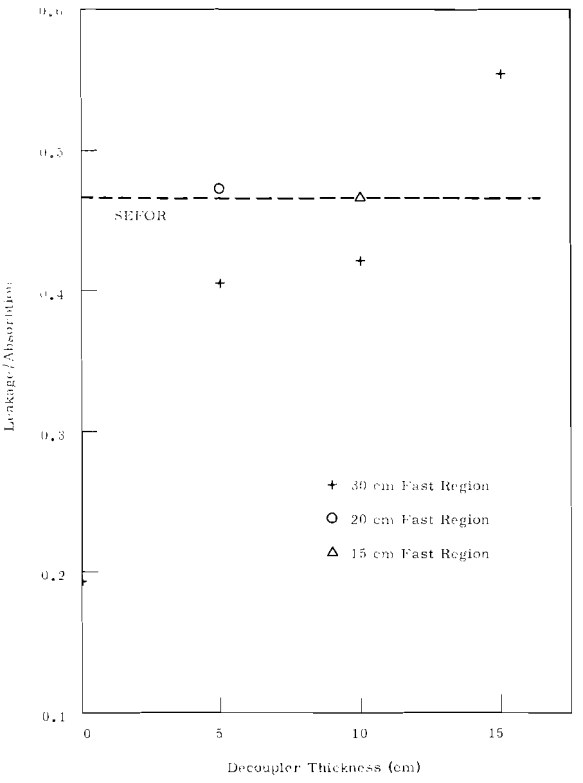

FIGURE 2. Leakage/Absorption in Region 1

TABLE II. Leakage/Absorption by Group in Region 1 Core

Group	SEFOR	15 + 10	20 + 5	30 + 0	30 + 5	30 + 10	30 + 15
				L/A			
1	1.15	1.79	1.11	0.15	1.04	1.23	1.58
2	1.05	2.10	1.10	0.01	0.97	1.21	1.51
3	0.90	2.30	1.09	-0.05	0.87	1.08	1.33
4	0.79	1.73	0.85	-0.10	0.68	0.87	1.09
5	1.00	0.85	0.89	0.02	0.90	1.12	1.45
6	0.94	-0.43	0.66	0.30	0.78	0.85	1.14
7	0.83	-0.27	0.64	0.51	0.66	0.62	0.83
8	0.58	0.23	0.58	0.48	0.47	0.39	0.51
9	0.41	0.46	0.50	0.40	0.35	0.28	0.34
10	0.32	0.68	0.47	0.31	0.29	0.24	0.29
11	0.28	0.90	0.47	0.24	0.28	0.26	0.30
12	0.15	0.62	0.27	0.11	0.16	0.17	0.19
13	0.08	0.31	0.13	0.03	0.08	0.09	0.10
14	0.12	0.50	0.15	0.01	0.13	0.16	0.18
15	0.08	0.30	0.05	-0.06	0.08	0.12	0.14
16	0.06	-0.15	-0.09	-0.10	0.06	0.10	0.13
17	0.04	-0.09	-0.13	-0.11	0.03	0.06	0.08
18	0.02	-0.23	-0.15	-0.11	0.00	0.03	0.05
19	0.03	-0.34	-0.43	-0.21	0.01	0.05	0.07
20	0.01	-0.14	-0.21	-0.12	0.01	0.02	0.03
21	0.01	-0.08	-0.30	-0.17	0.01	0.02	0.03
22	0.06	-2.12	-2.08	-1.94	-1.78	-1.42	-0.84
23	0.01	-0.39	-0.13	-0.27	-0.25	-0.21	-0.16
24	0.00	-0.34	-0.16	-0.00	-0.00	0.01	0.02
25	0.00	0.04	0.01	-0.04	-0.04	-0.03	-0.03
26	0.00	-0.10	0.00	-0.02	-0.02	-0.02	-0.01

This is well illustrated by the values for the 15 + 10 case. Table I shows a value of L/A = 0.4656 which compares quite favorably with the SEFOR value of 0.4662. Examination of the leakage/absorption by group and comparison of the spectrum as shown in Table II (p. 41) and Figure 3 respectively, however, indicates that this is not a well designed configuration.

From the calculations to date, it is tentatively concluded that it would be possible to conduct meaningful reactivity experiments on fast cores in PCTR and HTLTR in support of the fast reactor program.

REFERENCES

1. *See for example: KFK-217, "The Karlsruhe Fast Thermal Argonaut Reactor Concept", H. Meister, K. H. Beckurts, W. Häfele, W. H. Köhler, K. Ott, June 1964.*

2. *Fast Flux Test Reactor - Critical Experiment Program, BNWL-SA-909, R. A. Bennett, P. L. Hofmann, W. W. Little, L. L. Maas, Sept. 1966.*

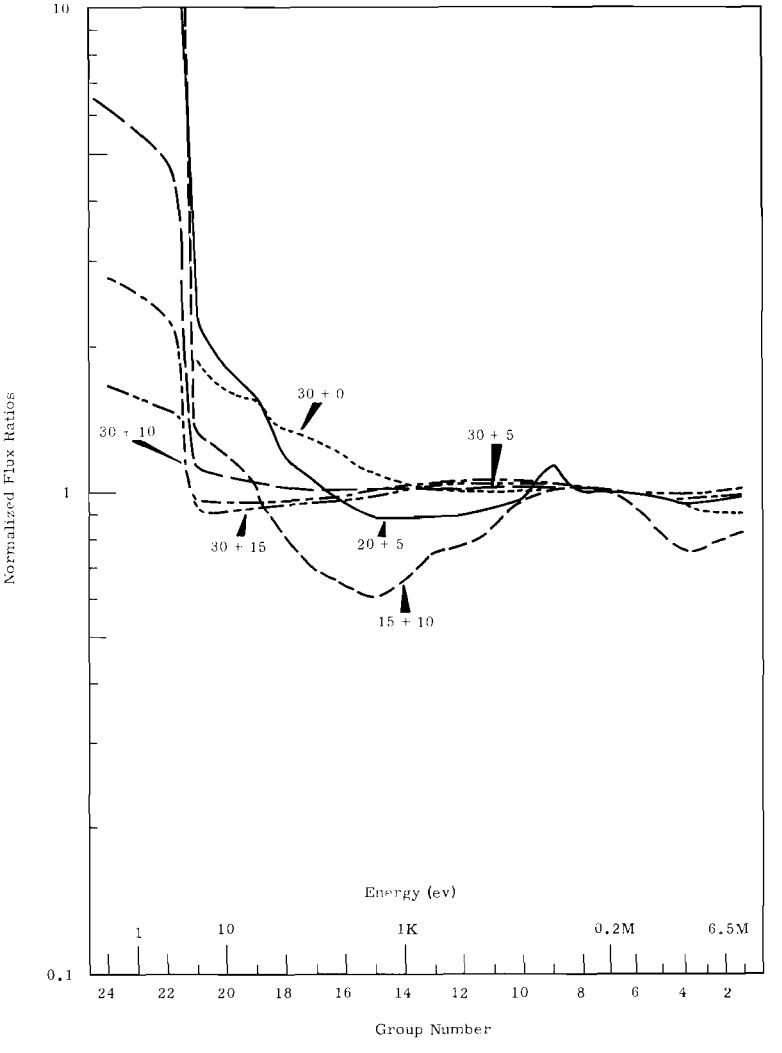

FIGURE 3. Model Flux/SEFOR Flux at r = 0 for Several Fast-Thermal Configurations

CRITICAL MASS PHYSICS

RESOLVING TIME OF A PULSED NEUTRON SOURCE DATA ACQUISITION SYSTEM

S. R. Bierman and K. L. Garlid*

In making pulsed neutron source measurements, counting rates of such magnitude are often encountered that the characteristics of the data acquisition system must be properly identified before corrections for coincidence losses can be accurately made. To account properly for coincidence losses at very high counting rates, it is necessary to determine how closely a perfectly paralyzable or completely nonparalyzable system represents the real detection system used in the measurements.

A detection and counting system is never a perfectly paralyzable type or a completely nonparalyzable type,[1] but lies somewhere in between these two possible extremes. Either type system fails to count events spaced more closely than the system's resolving time. In a perfectly paralyzable system, each event spaced less than a resolving time after a counted event will extend the inability of the system to count another event for a resolving time. In a completely nonparalyzable system, the events spaced less than a resolving time after a counted event will have no effect; and the system will continue to function as if they had never occurred.

For a paralyzable system counting random events the observed number of events per unit time, N_o, are related to the resolving time, t_r, of the system and the true number of events per unit time, N_T;

$$N_o = N_T e^{-N_T t_r} \quad . \tag{1}$$

For a nonparalyzable system counting random events, the true number of events are related to the resolving time and observed events by

$$N_T = \frac{N_o}{1 - N_o t_r} \quad . \tag{2}$$

The maximum observed counting rate for a paralyzable system is limited to

$$\max N_o = \frac{1}{(t_r e)} \quad . \tag{3}$$

However, for a nonparalyzable system, the maximum number of true events can approach infinity; and the detection system will ignore all except those spaced one resolving time apart. Thus, for a nonparalyzable system, the maximum observed counting rate is limited to

$$\max N_o = \frac{1}{t_r} \quad . \tag{4}$$

---

* *K. L. Garlid, Department of Nuclear Engineering, University of Washington, Consultant to Battelle-Northwest Critical Mass Laboratory*

With these relationships, it becomes a fairly simple matter to bracket the resolving time of a system by merely observing the maximum count rate that a system is capable of.

This approach was employed to bracket the resolving time of the data acquisition system used in making pulsed neutron source measurements at the Critical Mass Laboratory of Battelle-Northwest. The system consisted of a B^{10} loaded organic liquid scintillator and an RCA 6810 photomultiplier tube as the detection device, a linear amplifier with no discrimination circuit, and a Technical Measurements Corporation pulsed neutron logic unit 212 used in a TMC 256 channel analyzer. The maximum count rate that could be ob-observed by this system was determined by placing the detector on the top face of a plutonium fueled assembly and subjecting the assembly to repetitive bursts of 14 MeV neutrons from a Kaman A-810 neutron generator. By selecting a proper time scale on the time analyzer, it was possible to observe at what value the counts, stored in the analyzer's memory, went through a maximum.

The maximum observed count rate averaged 2,200,000 counts/sec over a series of measurements on six different assemblies, each at three or more different fuel loadings. Based on these data the resolving time of the entire data acquisition system lies somewhere between 0.17 ± 0.03 μsec and 0.46 ± 0.03 μsec, depending on how near the system is to being a paralyzable or nonparalyzable type, respectively.

The actual resolving time of the data acquisition system can be obtained by inspecting the time characteristics[2] (Stever's Pattern) of the components external to the analyzer and by employing a nonrandom pulse technique in the analyzer. The shape of the output pulse from the scintillator-detector device indicated that this component of the data acquisition system had a resolving time no greater than 0.04 μsec. Similarly, the detector and amplifier combined were found to have a resolving time of 0.08 μsec.

To determine the resolving time associated with sorting the counts in time and storing them in the memory of the TMC channel analyzer, a technique employing nonrandom pulses separated by a finite time interval was used. Pulses having a total width of less than 0.1 μsec, including rise and fall times, were fed directly from a high speed pulse generator into the pulsed neutron logic unit of the analyzer. The pulse repetition rate was increased step-wise until the analyzer failed to count properly. Since each arithmetic binary circuit in the analyzer divides the count rate in half, the first binary limits the counting speed of the analyzer. Therefore, the true number of counts in the first channel width were observed, along with the channel width, on an oscilloscope. The true number of

counts entering the binary may thus be compared with the number stored in the memory of the analyzer by digital readout of the memory. Based on these results, the analyzer was found to be limiting the resolving time of the data acquisition system to 0.23 μsec.

Thus, the resolving time for this particular data acquisition system lies between the allowable limits as established by the "maximum count rate" technique. Corrections for coincidence losses should therefore not be made on the basis that the system is either a nonparalyzing or a paralyzing type. Instead, the corrections should be made on a weighted basis that reflects the relative position of the real system with respect to the paralyzable and nonparalyzable type systems. A comparison between the real system and the nonparalyzing and paralyzing type counting systems as a function of count rate is shown graphically in Figure 1 for the measured resolving time of 0.23 μsec. The curve depicting the real system was obtained by linearly interpolating between the two perfect systems on the basis of resolving times; that is, the count rate for the real system lies approximately one-fifth of the way between the two perfect systems. It should be noted that only above about 10^6 counts/sec do the two systems begin to differ. Thus, at the more normally encountered counting rates, it makes no difference whether the system is assumed to be perfectly paralyzable or completely nonparalyzable.

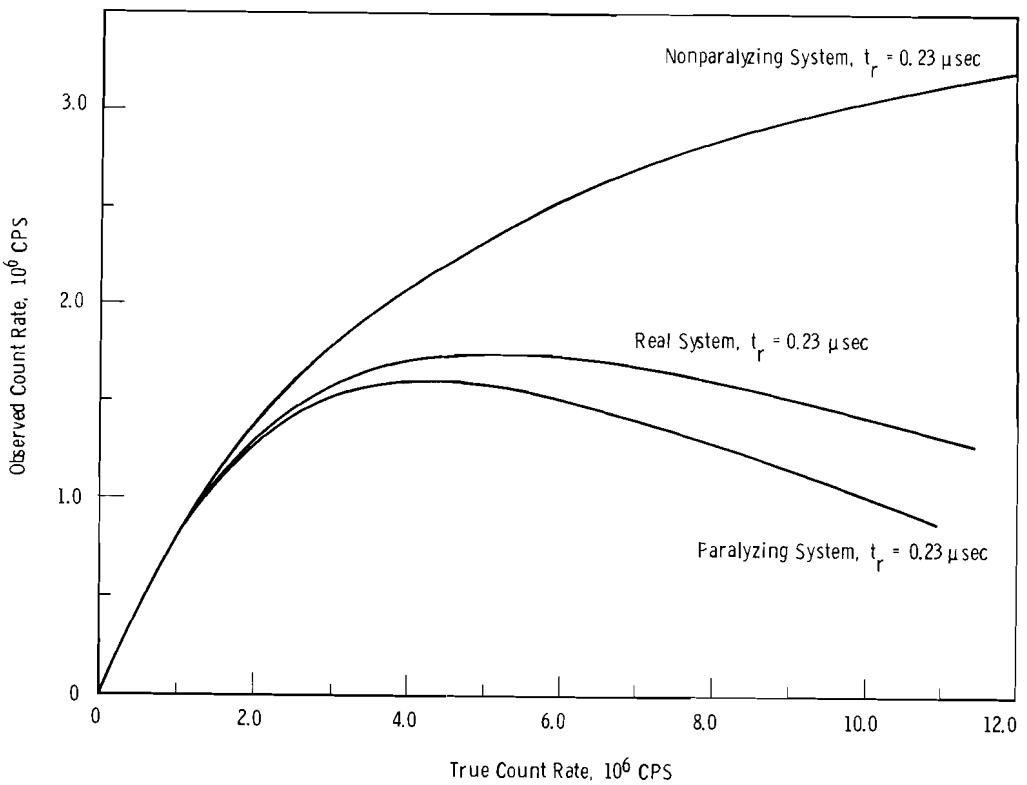

FIGURE 1. Comparison of Nonparalyzing and Paralyzing Counting Systems as Function of Count Rate

REFERENCES:

(1) *Jerome Kohl, René D. Zentner, and Herbert R. Lukens. Radioisotope Applications Engineering, D. Van Nostrand Company, Inc., New York, London, and Toronto, 1961. Page 168.*

(2) *J. B. Hoag. Nuclear Reactor Experiments, Edited by J. B. Hoag, D. Van Nostrand Company, Inc., New York, London, and Toronto, 1958. Page 32.*

NEUTRON SPECTRA EXPERIMENTS

S. R. Bierman, L. E. Hansen, G. L. Woodruff*, R. C. Lloyd, and G. M. Hess III

Measurements were completed on three experiments designed to permit studying fundamental behavior of neutrons in plutonium fueled critical assemblies. Each of the assemblies had different H/Pu atomic ratios, but all were parallelepipeds having uniform cells of PuO_2-polystyrene and Lucite.

In addition to the critical approach and pulsed neutron source measurements, foil activation measurements were made to determine the intracellular distribution of the Pu^{239} fission rate, the In^{115} (n,γ) reaction, the In^{115} (n,n') In^{115m} reaction, and the Cu^{63} (n,γ) reaction. The critical approach and pulsed neutron data at critical are summarized in the Table I below:

Preliminary results of the Cu^{63} activation have been obtained. The copper foils were placed throughout the lattice cell, and along the axis of the assemblies. The activation distribution along the axis was used to correct the intracellular activation of bare and cadmium covered foils, whose relative positions were offset axially. This correction is necessary due to the flux

**G. L. Woodruff, Department of Nuclear Engineering, University of Washington, Summer Faculty Appointment Program Professor at the Critical Mass Physics Laboratory.*

TABLE I. Summary of Criticality and Pulsed Neutron Source Measurements on PuO_2-Polystyrene Cubes 2.2 wt% Pu-240, 150.06 g Pu/2.036 in. Cube

Experiment Number	Assembly	H/Pu atomic	Length, cm	Width, cm	Delayed Critical Height, cm	Prompt Critical Height, cm	B/ℓ, sec^{-1}	Delayed Critical Mass, kg
2-015-240	Alternate 2-in. Rows of Fuel and Lucite.	35	51.10	41.57	35.56 ± 0.07	35.98 ± 0.05	135 ± 5	24.95 ± 0.05
2-015-242	Alternate 3-in. Rows of Fuel and 1-in. Rows of Lucite.	22	31.04	31.75	33.43 ± 0.08	33.47 ± 0.05	302 ± 45	26.44 ± 0.05
2-015-243	Alternate 1-in. Rows of Fuel and 1 1/2 in. Rows of Lucite. [a]	59	56.05	50.61	28.15 ± 0.05	--	146 ± 7	24.29 ± 0.04

[a] Some fuel containing 8 wt% Pu-240 was used to achieve a critical loading. It was positioned to minimize its effect on the flux in the unit cell containing the foils and to permit correction being made for its presence.

peaking on the side of the assembly nearest the control rod (see Figures 1 and 2), which is located near the back face of the assemblies.

The ratio of the thermal ($E \leq \sim 0.6$ eV) to fast neutron densities, for the first two assemblies, are shown in Figures 3 and 4 as a function of the position in the lattice cell.

The integral neutron spectrum data for all of the assemblies are currently being analyzed, and an error analysis of the data shown in Figures 3 and 4 is being made.

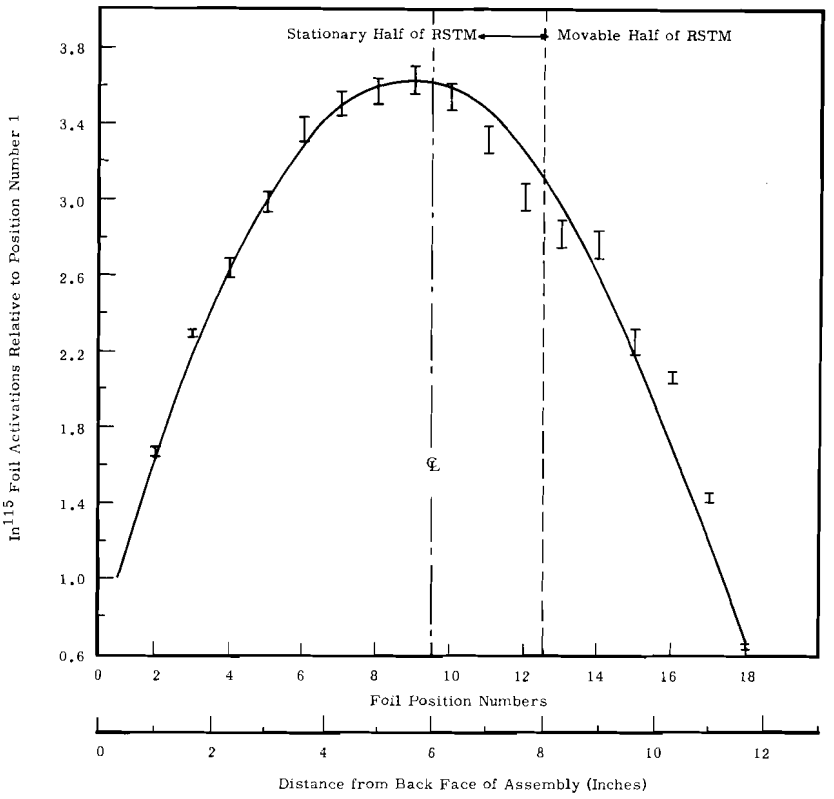

FIGURE 1. Experiment Number 2-015-240, Control Rod Effects on In^{115} Specific Activations Across the Assembly

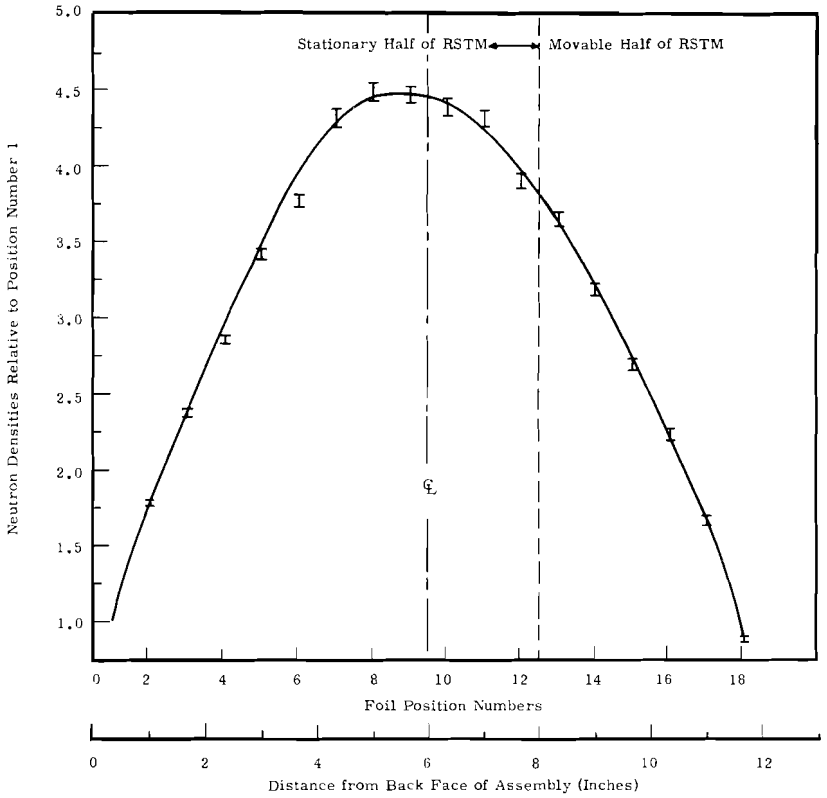

FIGURE 2. Experiment Number 2-015-141, Control Rod Effects on Neutron Densities Across the Assembly

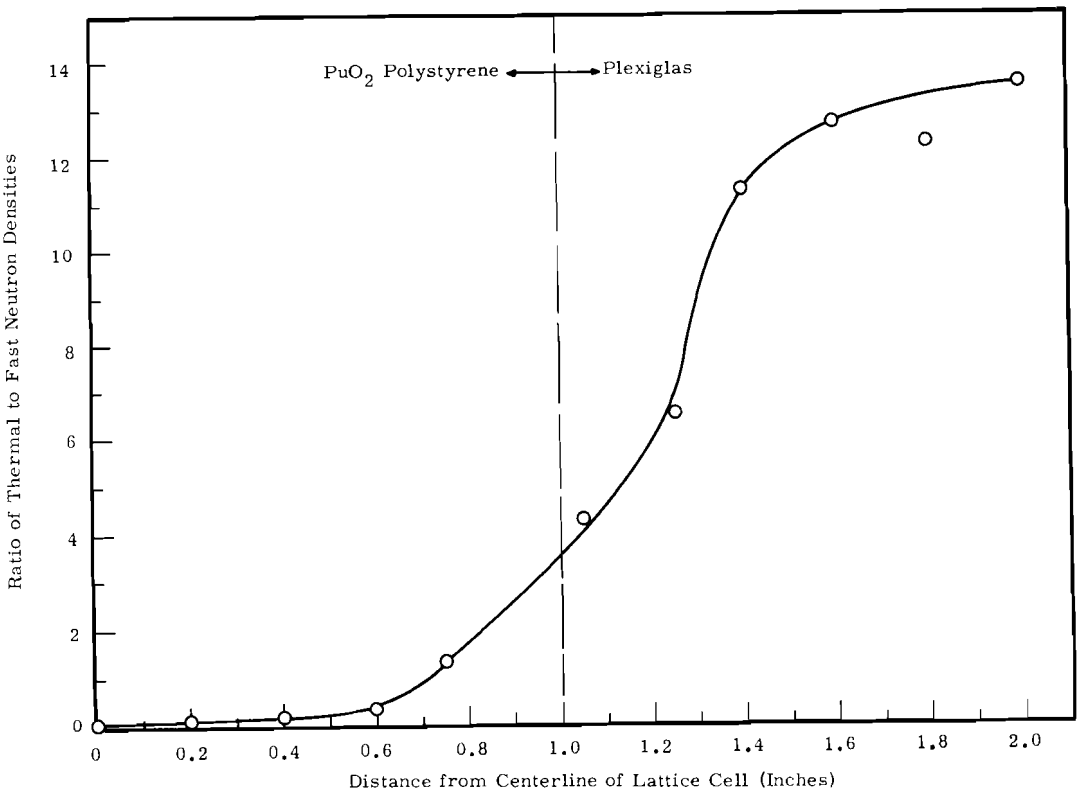

FIGURE 3. Experiment Number 2-015-240, Lattice Cell Neutron Density Distributions

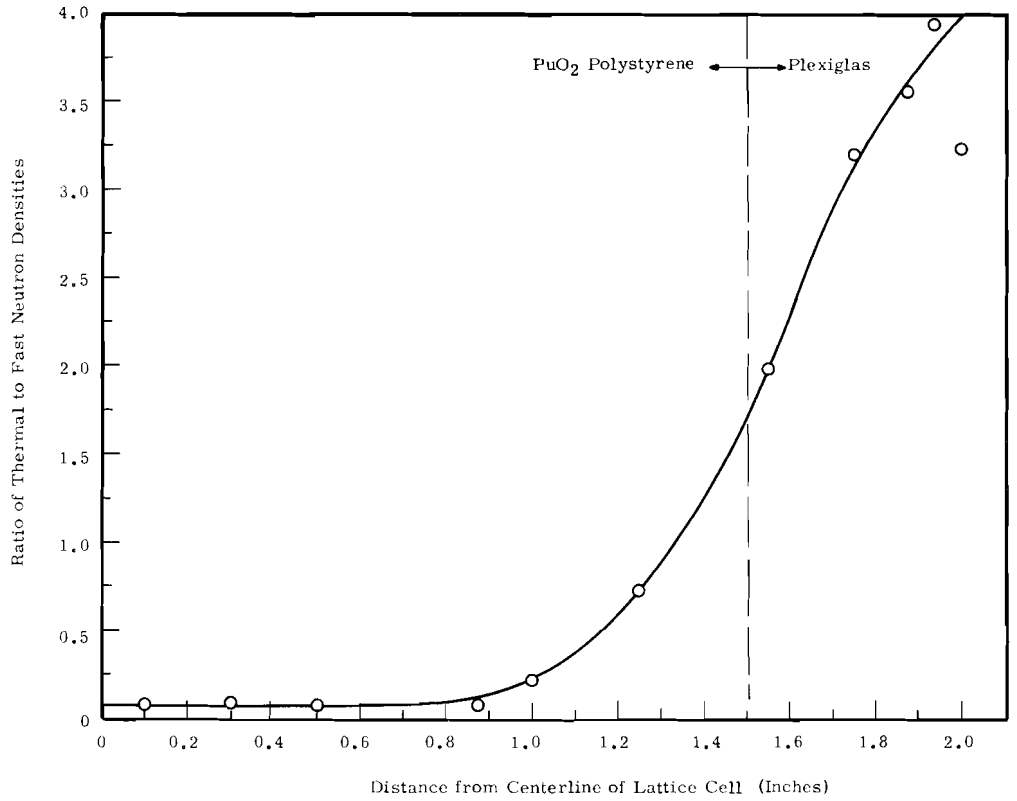

FIGURE 4. Experiment Number 2-015-242, Lattice Cell Neutron Density Distributions

PULSED NEUTRON SOURCE MEASUREMENTS - $Pu(NO_3)_4$ SOLUTIONS

G. M. Hess III, S. R. Bierman

Pulsed neutron source experiments were performed concurrently with the criticality experiments on plutonium nitrate solution in the expandable slab tank. Analysis of the data taken on the fully reflected tank at a width of 4.6 in. have been completed and the results are shown in Table I. The plutonium concentration was approximately 58 g/liter and the length of the tank was 42 in.

The errors shown are the least-squares fitting errors only. That is, the experimental values of the decay constant, α, used to determine the delayed critical α were least-squares fit without regard for the error in these numbers. By recognizing these errors, an experimental error of $\pm$ 3 is found for the delayed critical decay constant. This range encompasses the experimental values.

The same reasoning applies to the delayed critical height as determined by inverse multiplication;

and, indeed, recognition of the errors in the fitted points may account for the difference in this height shown by experiments 3-4.6-2-356 and 3-4.6-2-359.

Chemical analyses of the solutions used in these experiments are listed in the section containing the criticality experiments.

TABLE I. Slab Tank Results

Experiment	PULSE NEUTRON: Delayed Critical α, sec^{-1}	PULSE NEUTRON: Prompt Critical Height in.	PULSE NEUTRON: Delayed Critical Height in.	Inverse Multiplication Delayed Critical Height in.	Difference $Pulse_{DC}$-$Inverse_{DC}$
3-4.6-2-356	95.3 ± 0.8	33.525 ± 0.017	31.864 ± 0.01[illegible]	31.891 ± 0.006	-0.027 ± 0.023
3-4.6-2-358	96.0 ± 2.4	32.538 ± 0.186	30.96 ± 3.74	30.963 ± 0.005	-0.003 ± 3.745
3-4.6-2-359	98.1 ± 0.4	32.897 ± 0.041	31.301 ± 0.041	31.298 ± 0.016	+0.003 ± 0.057

LEAST-SQUARES DATA REDUCTION CODE

G. M. Hess III

The quantity of pulse neutron and reactor noise data taken at the Critical Mass Laboratory has pointed out the need for a least-squares code that may be used routinely in the reduction of these data. Such a code should (1) have a simple input format, (2) be time economic, (3) provide for pre- and postprocessing, and (4) have accuracy comparable to that of the experimental data.

MISFIT-III[(1)] is a generalized least-squares code incorporating second order iterative logic and is thus capable of converging with fewer iterations than a first order code. A code, LSDR, has been assembled which is specific to the pulse and noise applications using MISFIT-III as a base to take advantage of this convergence ability. MISFIT-III is in fact too detailed for these applications. The convergence criteria is a 36 bit requirement, which is overly stringent for reduction of the experimental data. LSDR converges when the difference of the misfits between two iterations is 1/2% of the misfit. The 36 bit convergence may be used on option.

The second order statistical analysis provided by MISFIT-III is more than that required routinely; LSDR eliminates portions of this analysis with a corresponding saving in run time. The complete error analysis may be had on option.

When used with pulse neutron data, LSDR performs a deadtime correction using an input deadtime. The time scale is set using the channel width input and the inactive analyzer time accounted for. The data is then least-squares fit.

If desired, further fits may be made by eliminating portions of the data to observe the effect on the fitted parameters.

A kβ/ℓ reactivity evaluation may also be performed using the Garelis-Russell[2] approach.

Reactor noise data may be input in a number of ways, multiple record averaged, normalized, the spectrum calculated, the data least-squares fit, and renormalized. The amplitude and/or power spectrum may be obtained, depending on the input data.

The input to LSDR consists of two blocks of data in the Namelist format and three identification cards. One input block is essentially that of MISFIT-III, the other is particular to the pulse or noise applications.

The input is detailed and further explanations are given in Reference 3.

REFERENCES:

(1) *Physics and Instruments Department Monthly Report, BNWC-86b, June 1965, Preliminary Report.*

(2) *E. Garelis and J. L. Russell. "Theory of Pulse Neutron Source Measurements," Nuclear Science and Engineering, vol. 16, p. 263 1963.*

(3) *G. M. Hess. A Least Squares Code for Pulse Neutron and Reactor Noise Data Reduction, BNWL-CC-805. September 1966.*

NEUTRON INTERACTION EXPERIMENTS WITH BOTTLES OF U^{233} SOLUTIONS

R. C. Lloyd and E. D. Clayton

Subcritical neutron interaction experiments were performed with bare and Lucite reflected arrays of bottles of U^{233} solution. The effect on criticality of adding Lucite moderator between the bottles was also studied. These experiments provide data for nuclear safety guidance in handling, storage, and shipment of this material and for checking interaction calculations.

The U^{233} was in the form of uranyl nitrate hexahydrate--$UO_2(NO_3)_2 + 6H_2O$)--at a concentration of about 330 g U^{233}/liter; the uranium was contained in three-liter polyethylene bottles. The molarity of the solution was about 0.53. The bottles were 17.75 in. high, 4.7 in. OD, with a wall thickness of 0.100 in. The average solution height was about 11.5 in.--960 g uranium/bottle. Since the bottles varied in content, Table I lists averages for each experiment.

The bottles were placed in arrays on the Remote Split-Table Machine and inverse multiplication techniques were used to estimate the number of bottles for criticality. Extrapolations were also made on spacing to determine critical spacing for fixed number square arrays of the bottles. Arrays were single tier, except in one experiment where a double tier array was used.

TABLE I. Averages for Actual Bottles Used in Experiments

Experiment Number	Solution Height, in.	U, g	Volume, liter	Concentration, g/liter
1	11.78	946	2.98	318.3
2	11.67	951	2.94	323.1
3	11.59	947	2.93	323.0
4	11.40	961	2.89	332.5
5	11.77	947	2.95	321.1
6	11.72	062	2.95	326.2
7	11.71	934	2.94	318.1
8	11.71	934	2.94	318.1
9	11.71	934	2.94	318.1
10	11.71	934	2.94	318.1
11	11.71	934	2.94	318.1
12	11.64	947	2.95	323.2
13A	11.67	951	2.94	323.1
13B	11.59	947	2.94	323.0
14	11.59	947	2.94	323.0
15	11.59	947	2.94	323.0
16	11.59	947	2.94	323.0
17	11.59	947	2.94	323.0
18	11.40	961	2.89	332.5
19	11.40	961	2.89	332.5
20	11.40	961	2.89	332.5
21	11.25	895	2.87	312.6

In the reflected arrays, the Lucite was placed touching the outside surface of the bottles; i.e., boxing in the array. The thickness of the top and bottom Lucite reflector was 4.5 in. and the side reflectors were 6 in. Low density aluminum honeycomb was used to provide accurate spacing between bottles and to provide assurance of bottles remaining upright for safety. In the bare assemblies, stability of the outer bottles was maintained by aliminum frames which were magnetically mounted on a 0.03 in. steel base plate. Aluminum honeycomb was used to support the baseplate and reduce neutron reflection.

The results obtained from extrapolation of the data are presented in Table II. A single row of nine bottles unreflected was not critical, and extrapolation of the inverse neutron multiplication curves indicated an infinitely single line would probably be subcritical. The reflected curve extrapolated to between two and three bottles for criticality. Three bottles in line with surface-to-surface (S-S) spacing of 0.6 in. would be critical when reflected. S-S spacings for criticality were determined for the bare lattices of 2 x 3, 3 x 3, and 4 x 4 bottles in single tier arrays and for reflected 2 x 2 and 3 x 3 bottle arrays.

TABLE II. Interaction Data for Bottles of U^{233} Solution

Experiment	Description	Configuration	Number Bottles	Estimated Critical S-S Spacing, in.	Remarks
U^{233}-1	Bare Single Row	1 x 9	9	0	
U^{233}-2	Bare Double Row	2 x 3	6.1	0	
U^{233}-3	Bare Lattice	3 x 3	9	0.60	
U^{233}-4	Bare Lattice	4 x 4	16	1.10	
U^{233}-5	Reflected Single Row	1 x 2	2	0	2.8 Bottles
		1 x 3	3	0	Table stopped at 0.9 in.
U^{233}-6	Reflected Single Row	1 x 5	5	0.6	
U^{233}-7	Reflected Lattice	2 x 2	4	2.18	
U^{233}-8	Reflected Lattice/$\frac{1}{2}$ in. Moderator	2 x 2	4	2.48	$\frac{1}{2}$ in. Lucite Moderator Between Bottles
U^{233}-9	Reflected Lattice/$\frac{3}{4}$ in. Moderator	2 x 2	4	2.58	$\frac{3}{4}$ in. Lucite Moderator Between Bottles
U^{233}-10	Reflected Lattice/1 in. Moderator	2 x 2	4	2.66	1 in. Lucite Moderator Between Bottles
U^{233}-11	Reflected Lattice/1$\frac{1}{2}$ in. Moderator	2 x 2	4	2.80	1$\frac{1}{2}$ in. Lucite Moderator Between Bottles
U^{233}-12	Reflected Lattice	3 x 3	9	3.98	
U^{233}-13A	Bare/1 in. Lucite Moderator	2 x 3	6.3	1.00	1 in. Lucite Moderator Between Bottles
U^{233}-13B	Bare/1 in. Lucite Moderator	3 x 3	9	1.60	1 in. Lucite Moderator Between Bottles
U^{233}-14	Bare/$\frac{1}{2}$ in. Lucite Moderator	3 x 3	9	1.17	$\frac{1}{2}$ in. Lucite Moderator Between Bottles
U^{233}-15	Bare/1$\frac{1}{2}$ in. Lucite Moderator	3 x 3	9	1.78	1$\frac{1}{2}$ in. Lucite Moderator Between Bottles
U^{233}-16	Bare/1$\frac{3}{4}$ in. Lucite Moderator	3 x 3	9	1.87	1$\frac{3}{4}$ in. Lucite Moderator Between Bottles
U^{233}-17	Bare/2 in. Lucite Moderator	3 x 3	9	1.90	2 in. Lucite Moderator Between Bottles
U^{233}-18	Bare/2 in. Lucite Moderator	4 x 4	16	2.50	2 in. Lucite Moderator Between Bottles
U^{233}-19	Bare/2$\frac{1}{2}$ in. Lucite Moderator	4 x 4	16	2.47	2$\frac{1}{2}$ in. Lucite Moderator Between Bottles
U^{233}-20	Bare/1$\frac{1}{2}$ in. Lucite Moderator	4 x 4	16	2.42	1$\frac{1}{2}$ in. Lucite Moderator Between Bottles
U^{233}-21	Bare - Double Tier	3 x 3 x 2	18	0.75	

Effect of Lucite moderation was determined by placing Lucite plates of different thicknesses between bottles of the arrays. This was done for the 2 x 2 bottle reflected array and for the 3 x 3 and 4 x 4 bottle bare array.

A S-S spacing for criticality of 0.75 in. was measured for the double tier 3 x 3 bottle bare array, which compares with a 0.60 in. spacing for the 3 x 3 bottle single tier array. The double tier array had a spacing of 7.0 in. between the fuel of the upper and lower tiers.

Figure 1 shows a plot of the number of bottles for criticality versus S-S separation. It is seen that the critical number of bottles is much more sensitive to spacing for the bare array than for the reflected array. Points determined for optimum moderation are also shown for comparison. Figure 2 shows a plot of critical S-S spacing versus thickness of added Lucite moderator for a four-bottle reflected array. Figures 3 and 4 show plots of critical S-S Spacing versus added Lucite moderator for bare arrays of 9 and 16 bottles. This moderator thickness peaks at about 2 in. as determined from extrapolation of the bare array.

Pictured in Figures 5 and 6 are two of the experimental loadings of bottles. Figure 5 shows the bare 16 bottle array. Figure 6 shows the reflected 9 bottle array.

A paper summarizing the analyses of these experiments, including the results of calculations to be performed on the arrays, is being prepared.

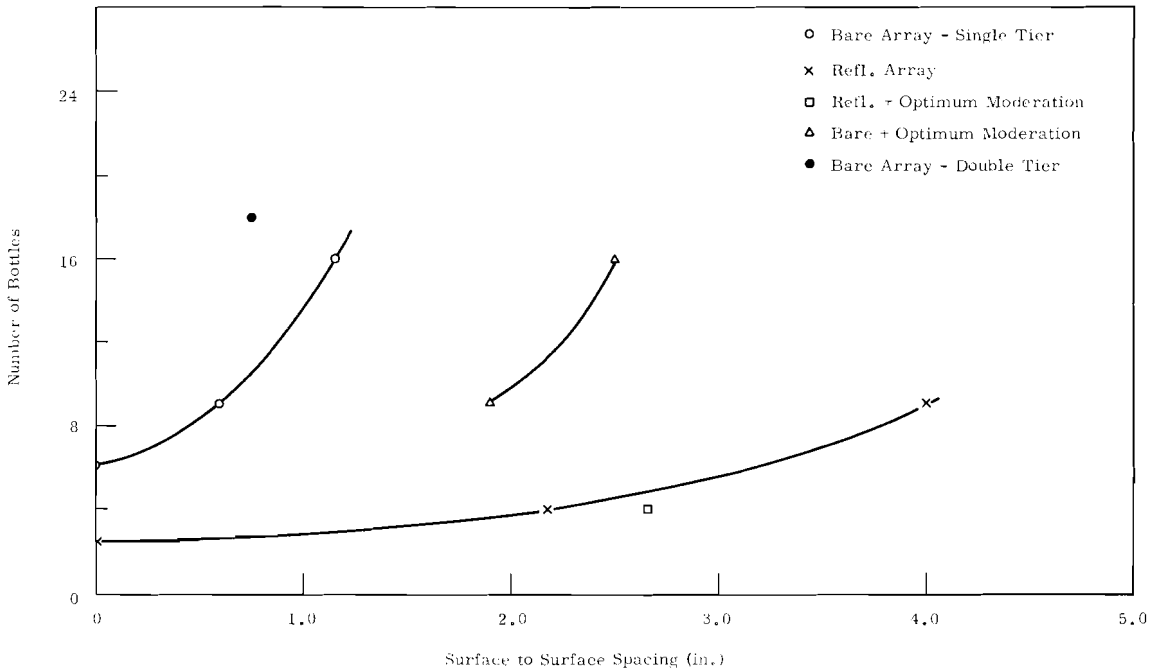

FIGURE 1. Criticality of U^{233} Solution in Polyethylene Bottles

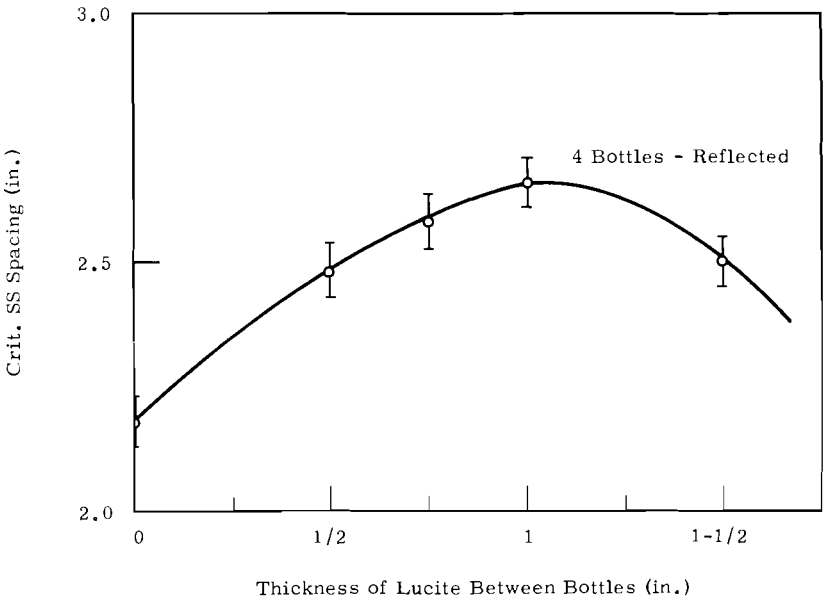

FIGURE 2. Effectiveness of Moderation Between Bottles of U^{233}

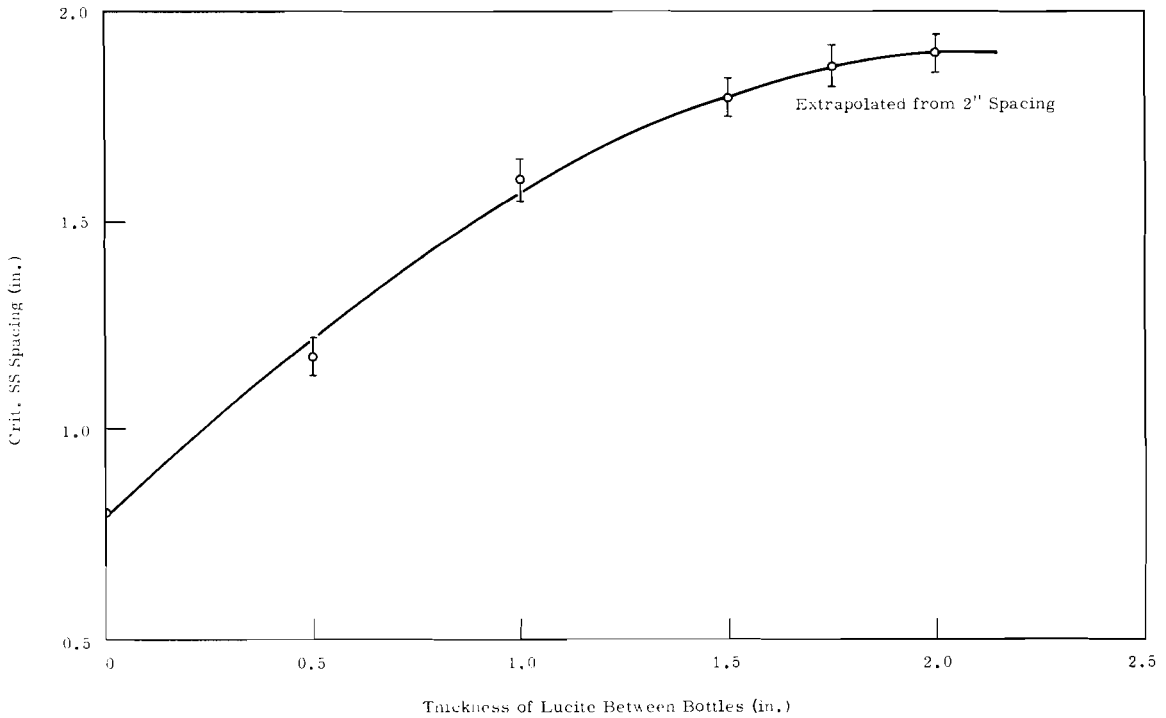

FIGURE 3. Effectiveness of Moderation Between Bottles of U^{233} Solution, 9 Bottle Array

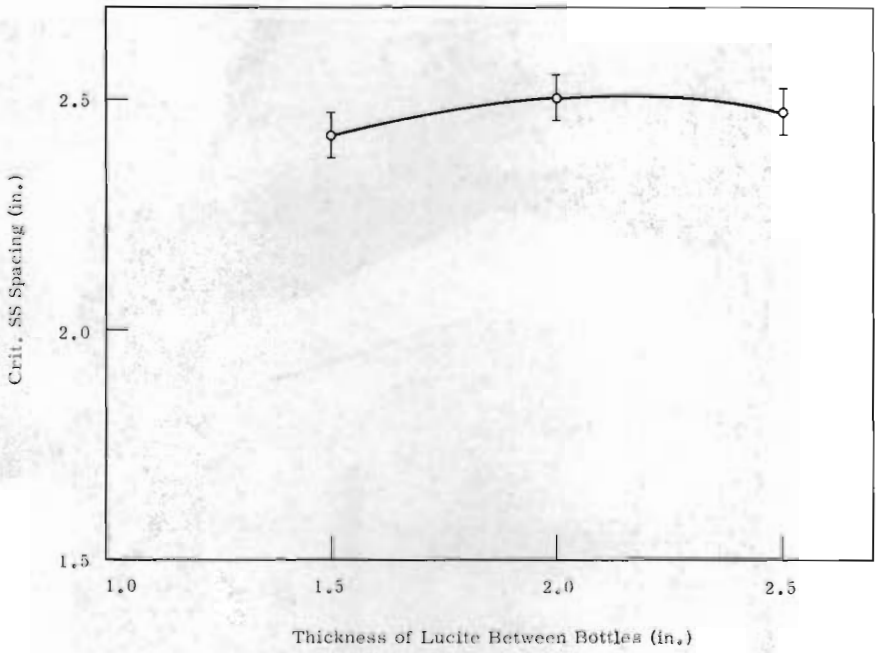

FIGURE 4. Effectiveness of Moderation Between Bottles of U^{233} Solution, 16 Bottle Array

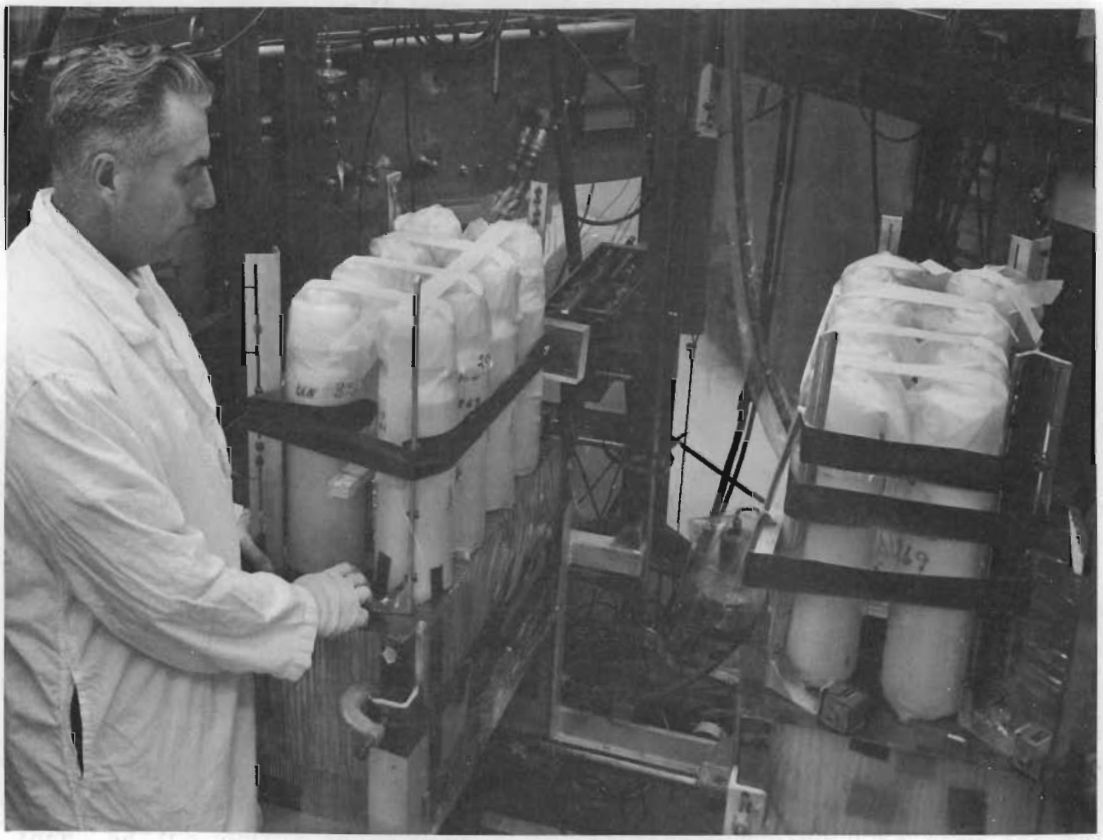

FIGURE 5. Bare Sixteen Bottle Array

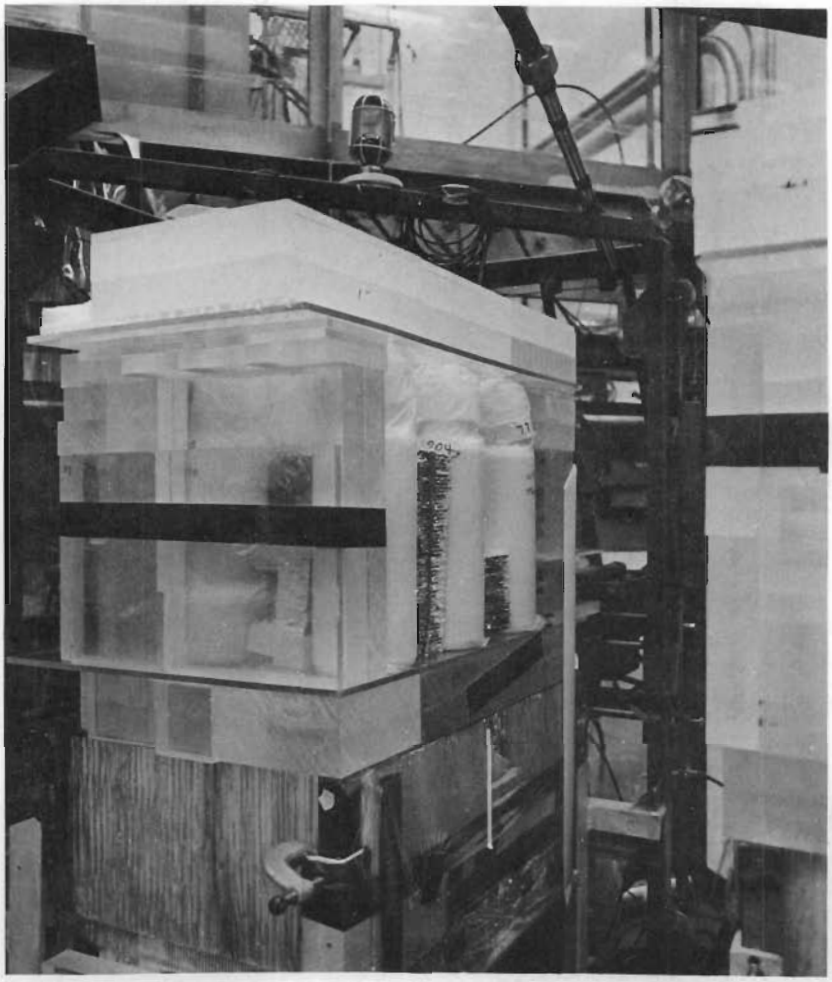

FIGURE 6. Reflected Nine Bottle Array

BASIC CRITICALITY EXPERIMENTS WITH PLUTONIUM NITRATE SOLUTIONS IN SLAB GEOMETRY

R. C. Lloyd and E. D. Clayton

A criticality vessel of unique design was installed at the Critical Mass Laboratory. It is a slab vessel such that its thickness can be varied throughout a range of 3 to 9 in., which is made possible by use of a welded stainless steel bellows. The sides of the slab are made of 0.062 in. stainless steel sheet welded to the bellows. Structural rigidity over the slab's large thin sides (42 x 42 in.) is accomplished by means of a low density lattice reinforcement. Accurate adjustment of the slab thickness is obtained by use of a single crank geared to adjustment screws on the edges of the

vessel. The vessel is mounted in the upright position to provide greatest measure of safety in fuel addition and in entry of the control and safety blades into the solution. The system is also equipped with solution dump and liquid reflector dump mechanisms.

Criticality experiments are being carried out with the adjustable slab assembly to determine critical thicknesses of bare and water reflected "infinite" slabs of plutonium nitrate solutions. These data are needed 1) to specify critical thickness of slab tanks more accurately, 2) to check computational methods, and 3) to check shape or buckling conversions between spherical[1] and slab geometry. In addition to application of these data to process vessels, the results will be useful in assessing criticality of plutonium solutions in sumps.

Criticality experiments, bare and water reflected, have been completed over a thickness range of 4.5 to 6.5 in. for plutonium nitrate solution containing ∿58 g plutonium/liter with an acid molarity of 2.4. The plutonium had 4.6 wt% Pu^{240}. The slab vessel was not critical when the vessel was adjusted to 6 in. thickness and filled with plutonium nitrate (162 liters.)

Critical thickness settings for the bare and water reflected slab and chemical analysis data of the solutions are given in Table I.

Effective extrapolation lengths were estimated for the bare and water reflected systems by means of constant buckling conversions. These calculations were made using three critical bare systems and six critical reflected systems of the slab vessel having different geometrical dimensions. These

TABLE I. Criticality of Plutonium Nitrate Solutions in Slab Geometry

Exposure Number	Date	Reflector Status	Plutonium Concentration, g/liter	Acid Molarity	Specific Gravity	H_2O[a] g/liter	Total NO_3 g/liter	H/Pu Atomic Ratio	Critical Slab Thickness, in.	Critical Volume, liter	Critical Height, in.	Critical Mass, kg
347	5-25-66	Bare	60.0	2.37	1.1754	895	215.5	405.6	6.0	- -	- -	- -
348	5-27-66	Bare	57.7	2.41	1.1721	900	211.6	423.9	6.5	122.85	27.80	7.090
349	6-2-66	Bare	57.7	2.38	1.1711	901	209.1	424.4	6.4	139.61	32.09	8.059
350	6-3-66	Bare	57.3	2.29	1.1692	903	206.0	427.9	6.3	164.09	38.33	9.403
351	6-8-66	Tamper Tank[b] Sides On	57.1	2.32	1.1690	905	204.6	429.9	6.3	141.70	33.11	8.102
352	6-9-66	Water Reflector[c]	57.3	2.29	1.1692	912	196.9	432.1	6.3	48.68	11.34	2.790
353	6-9-66	Water Reflector	57.3	2.29	1.1692	912	196.9	432.1	5.8	52.07	13.18	2.984
354	6-14-66	Water Reflector	58.2	2.32	1.1714	913	197.4	425.9	5.3	59.42	16.47	3.459
355	6-14-66	Water Reflector	58.2	2.32	1.1714	913	197.4	425.9	4.8	78.66	24.10	4.579
356	6-15-66	Water Reflector	58.6	2.32	1.1733	911	200.5	422.2	4.6	99.74	31.89	5.847
357	6-20-66	Water Reflector	58.1	2.40	1.1746	915	200.4	427.4	4.5	121.00	39.61	7.027
358	6-21-66	Water Reflector	58.3	2.33	1.1731	914	198.3	425.5	4.6	96.84	30.96	5.647
359	6-24-66	Water Reflector	58.3	2.33	1.1731	914	198.3	425.5	4.6	97.89	31.30	5.709
360	6-24-66	Water Reflector	58.3	2.33	1.1731	914	198.3	425.5	4.8	77.57	23.76	4.524
361	6-27-66	Water Reflector[d] Tamper Tank Equal to Sol.	58.1	2.37	1.1723	911	200.4	425.7	4.6	99.09	31.69	5.761
362	6-28-66	Water Reflector	58.1	2.37	1.1723	911	200.4	425.7	4.6	99.52	31.82	5.786

[a] Water content calculated assuming 100% material balance.
[b] Tamper tank sides were 0.25 in. stainless steel, tamper tank width is 27 in.
[c] Water reflector was at the top of slab tank.
[d] Water reflector increased as solution increased.

preliminary values, including the infinite slab thicknesses are given in Table II.

During the course of the experiments, solution began leaking through a faulty weld in the storage tank which supplies solution for the experiments. The contaminated weld was rewelded without spread of contamination. In fact, the welder's gloves or rod holder were not contaminated during the rewelding operation. This was accomplished by controlling the air flow in the area of the welding arc.

TABLE II. Preliminary Values for Bare and Water Reflected Systems

Reflector Condition	λ[(a)] cm	Buckling 10^{-6} cm^{-2}	Infinite Slab Thickness, cm
Bare	3.9	19,000	15.0
Water Reflected	6.2	18,800	10.5

(a) For the assembly as mounted in hood.

REFERENCES

(1) *Lloyd, R. C., et al., "Criticality Studies of Plutonium Solutions," Nuclear Science and Engineering, 25, 165 (June 1966).*

NEUTRON PHYSICS

EXISTENCE OF THE 2.86 MeV LEVEL IN B^{10}

D. W. Glasgow and D. G. Foster, Jr.

Kurath[1] has applied the individual-particle model with intermediate coupling to the nuclear 1p-shell. The theory predicts the first five confirmed levels in B^{10} with surprising success; however, it does not predict a level at 2.86 MeV. The status of this energy level has been reviewed in the compilation by Lauritsen and Ajzenberg-Selove.[2] Dyer and Bird[3] and Génin[4] presented some evidence for its existence from a study of the neutron spectrum from the $Be^9(d,n)B^{10}$ reaction. Dyer and Bird used a thick target, E_d = 0.60 MeV, and a nuclear emulsion detector, while Génin used a thin target, E_d = 0.57 MeV, and a nuclear emulsion detector. Reid[5] studied the neutron spectrum from this reaction; using a target of unspecified thickness, E_d = 0.75 MeV, and a triple-coincidence proportional-counter telescope; and reported the level. Coombe and Walker[6] reported the level after studying the neutron spectrum from this same reaction. They used a thick target, E_d = 0.08 MeV, and a diffusion cloud chamber to measure the proton recoils produced by the neutrons. All of these attempts to detect the level have been seriously hampered by low signal-to-background ratios and poor energy resolution.

Maydan and Vass[7] have recently reported a search for this level by observing the neutron spectrum resulting from the $Be^9(d,n)B^{10}$ reaction. Their study was performed using a time-of-flight spectrometer, deuteron energy of 600 keV, and 0.3 cm thick target. The signal-to-background ratio of the neutron groups corresponding to the 3.58 and 2.15 MeV states was 4:1 and 9:1, respectively, while the energy resolution in this region was 0.32 MeV. Improvements were made in the signal-to-background ratio (18:1 and 30:1) and the energy resolution (0.16 MeV) by operating the time-of-flight spectrometer in coincidence with the gamma rays resulting from de-excitation of the various levels. The conclusion of the study was that there were no indications of a neutron group in coincidence with the appropriate gamma ray and, hence, no evidence for the 2.86 MeV level.

The excitation of the compound system B^{11} is equal to or greater than 15 MeV for all deuteron energies. At these high excitations, the number of open channels should be quite large; and, hence, excited states of either parity and of a broad range of angular momenta should be formed in B^{11}. Therefore, neutron groups corresponding to all of the levels in B^{11} should be observed. However, if the competition between the various modes of neutron emission is sufficiently unfavorable

to the 2.86 MeV level, then the corresponding weak neutron group might escape detection. It is obvious that a detecting system with lower background and better energy resolution must be used in order to provide a more positive answer to the question of the existence of this level.

During the course of a large-scale measurement of fast-neutron total cross sections by the time-of-flight technique,[8] we have repeatedly used the spectrum of neutrons from the $Be^9(d,n)B^{10}$ reaction to determine the form of the resolution function. Our spectra were obtained with deuteron energies ranging from 1.5 to 2.0 MeV. Our apparatus provides signal-to-background ratios of 40:1 and 100:1 for the neutron groups associated with the 3.58 and 2.15 MeV groups, respectively, and an energy resolution (FWHM) in the critical region of 0.07 MeV. These improvements over the experimental conditions of Maydan and Vass[7] prompted us to review our data for more definitive evidence regarding the existence of the 2.86 MeV state.

The experimental method has been described previously in full detail[8]; therefore, only a brief summary will be given here. Deuterium ions were accelerated in a 2 MeV Van de Graaff accelerator which was equipped with a postacceleration pulsed-beam system to produce 1.5 nsec bursts of ions on a target. A beam-alignment and -focusing system was used to reduce the background radiation and produce a small beam spot on the target. The target consisted of a beryllium film deposited onto a 0.03 cm thick platinum support. The film was 93 keV thick to 1.7 MeV deuterons. The detector consisted of type NE-213 liquid organic scintillator contained in a glass cell, which was coupled to an Amperex 58-AVP photomultiplier. Pulse shape discrimination was used to reduce the effects of interfering radiations. The detector was encased in lead and foamed polystyrene and was mounted in a shielded enclosure whose concrete walls and ceiling were 1.2 m thickness. The target assembly was viewed through a collimator which pierced a water shield of 1.2 m thickness. The detector was located 6.17 m from the target at a laboratory angle of 25°. The electronics consisted of a fast start-stop system coupled to a circulating-line vernier chronotron, a memory-control system, a beam current monitor system, and a system that provided a check on the stability of the entire experiment.

Neutron spectra suitable for the present analysis were obtained at deuteron energies of 1.7 and 2.0 MeV. A typical spectrum is shown in Figure 1, which illustrates our resolution and signal-to-background ratio. The quality of the resolution dictates the use of a relativistic energy scale. An additional spectrum was obtained with the pulse-shape circuit disabled to determine the centroids of the synchronous gamma rays. The gamma rays, which were located at channels 24.33 and 233.43, were used to make the relativistic calculation of the velocity at the centroids of the neutron groups. The relativistic form of the reaction energies was then used to determine the excitation energies of the various

levels. The arrows mark the levels calculated from the data. The calculated position at which the neutron group corresponding to the 2.86 MeV level should occur is channel 115.1; however, it is conspicuously absent in Figure 1.

A statistical analysis was performed to verify its absence. Three energy regions were of interest, the 11-channel region centered on channel 115 and the two flanking regions of 11 channels each. The difference between the average number of counts per channel taken over the central region and the average background count per channel taken over the flanking regions was 0.63 counts/channel with a standard deviation of 2.1 counts/channel. This provides no indication of a neutron group. From Poisson statistics, the probability that, in a repetition of the measurements, the sample variance would exceed the observed dispersion is 0.84 and 0.43 for the central and flanking regions, respectively. In the central region the population standard deviation estimated from the residuals was 1.35 counts/channel, which is to be compared to 1.81 counts/channel for the population standard

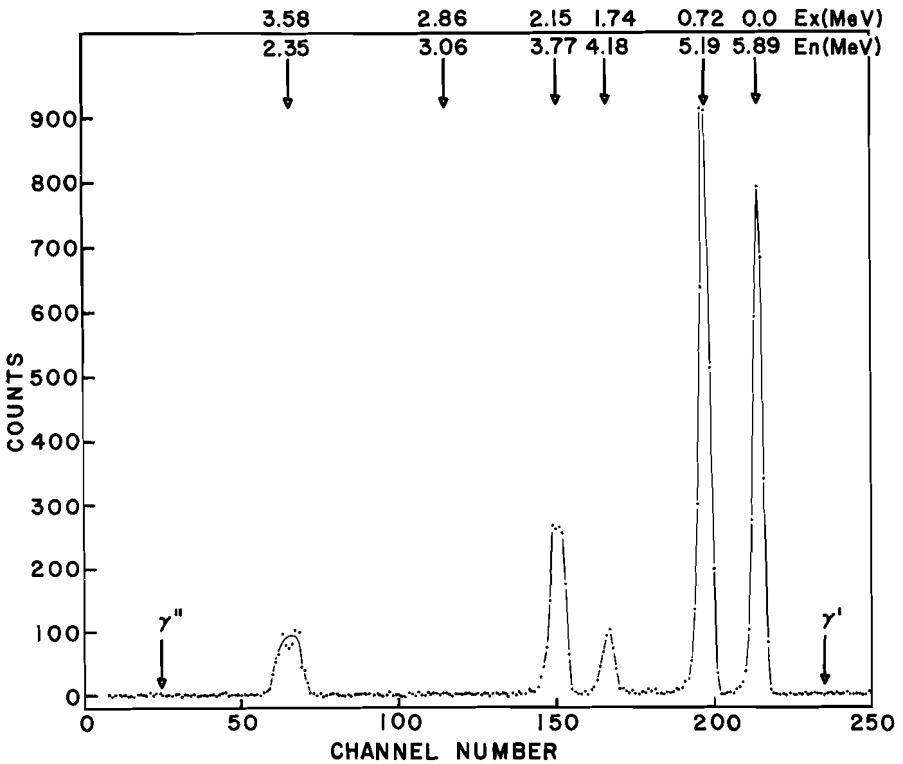

FIGURE 1. Time-of-Flight Spectrum of the $Be^9(d,n)B^{10}$ Reaction (The upper and lower energy scales indicate the excitation energies in B^{10} and the corresponding neutron energies. $\theta_\ell = 25°$, $E_d = 1.7$ MeV, flight path = 6.17 m, channel width = 0.72 nsec, and the repetition period = 150.15 nsec.)

deviation calculated for a Poisson distribution. In the flanking regions, the corresponding values are 1.65 and 1.63. Thus, our data are entirely consistent with the complete absence of a neutron group at this position.

For the particular detecting system and bias used in the experiment, we estimate that the detection efficiency should be about the same for 3.06 and 2.35 MeV neutrons. We assume that a 3.06 MeV neutron group would have a shape intermediate between that of the 3.77 and 2.35 MeV neutron groups. A comparison of the integrated count in the 3.06 and 2.35 MeV neutron groups then allows us to place an upper limit of 1% on the intensity of the neutron group associated with a 2.86 MeV level relative to the group associated with the 3.58 MeV level.

A similar analysis was performed on the spectrum associated with a deuteron energy of 2.0 MeV with essentially the same results.

Within the limitations of the experiment, we found no evidence for a 2.86 MeV state in B^{10}. This result does not disagree with the conclusions derived from the study of intermediate coupling in the 1p-shell.[1]

REFERENCES

1. *D. Kurath. Phys. Rev., vol. 101 p. 216. 1965.*
2. *T. Lauritsen and F. Ajzenberg-Selove. Nuclear Physics, vol. 78 p. 1. 1966.*
3. *A. J. Dyer and J. R. Bird. Aust. J. Phys., vol. 6, p. 45. 1953.*
4. *J. Génin. Compt. Rend., vol. 246, p. 1028. 1958.*
5. *G. C. Reid. Proc. Phys. Soc., vol. A67, p. 466. 1954.*
6. *R. A. Coombe and J. Walker. Proc. Phys. Soc., vol. 80, p. 1218. 1962.*
7. *D. Maydan and D. G. Vass. Proc. Phys. Soc., vol. 86, p. 817. 1965.*
8. *D. G. Foster, Jr. and D. W. Glasgow. Nucl. Instr., vol. 36, p. 1. 1965.*

THE n-d TOTAL CROSS SECTION, THE Di-NEUTRON, AND CHARGE INDEPENDENCE*

D. W. Glasgow and D. G. Foster, Jr.

The neutron total cross section of deuterium was measured continuously over the energy range 2.25 to 15.0 MeV using a time-of-flight technique[1] with an energy resolution ranging from 2.5 to 4.5%. The cross-section results were obtained with a precision of 0.5 to 2.0% per resolution interval and an absolute accuracy of $\leq \pm$ 2%.

Calculations predict that a cusp anomaly will occur in the total cross section near the energy threshold for di-neutron production if a stable state of the di-neutron exists and the n-d scattering length in the doublet state is large.[2] The observed total cross section in this energy region was subjected to rigorous analysis to put an upper limit on the magnitude of any possible structure. This analysis shows that any fluctuation in the cross section must be less than 1%.

*Summary of a paper being submitted for publication.

Recent three-body calculations of Aaron, et al.[3] and Phillips[4] predict that the n-d scattering length is small in the doublet state and large in the quartet state in agreement with experimental values (a_d = 0.7 fm, a_q = 6.38 fm).[5] The small-doublet case would produce a scarcely visible cusp even if the di-neutron is stable.[2]

Since we find no evidence in the total cross section for the existence of a stable di-neutron, we conclude either that this particle does not exist or that, if it does, then the quartet scattering length is larger than the doublet or both. Our results are entirely consistent with the recent calculations[4] which predict both the small doublet scattering length and the nonexistence of the di-neutron.

REFERENCES

1. *D. G. Foster, Jr. and D. W. Glasgow. Nucl. Instr., vol. 36, p. 1. 1965.*
2. *R. Alzetta, G. C. Chirardi and A. Rimini. Phys. Rev., vol. 131, p. 1740. 1963.*
3. *R. Aaron, R. D. Amado, and Y. Y. Yam. Phys. Rev., vol. 140, p. 1291. 1965.*
4. *A. C. Phillips. Phys. Rev., vol. 142, p. 984. 1966.*
5. *D. Hurst and N. Alcock. Can. J. Phys., vol. 29, p. 36. 1951.*

HIGH-RESOLUTION MONOCHROMATIZATION OF NEUTRONS AND X RAYS BY MULTIPLE BRAGG REFLECTIONS*

D. A. Kottwitz

A simple scheme for obtaining highly monochromatic, reproducible beams of slow neutrons or X rays at fixed wavelengths by means of crystal diffraction is described. The method is based on the well-known phenomenon of "umweganregung," in which a "forbidden" Bragg reflection is simulated under conditions of multiple reflection, i.e., when three or more reciprocal lattice points lie on an Ewald sphere. It is shown that there are orientations at which the Bragg angle (and wavelength) of a simulated reflection has local maxima. With only coarse collimation in the neighborhood of these extrema, perfect crystals can give wavelength resolutions of $\Delta\lambda/\lambda \simeq 10^{-4}$. Mosaic crystals would give worse resolution but greater intensity. Since the simulations of a "forbidden" reflection may interfere with each other, it is necessary to carry out systematic computer calculations to check for interference after the extrema have been located. The scheme is applicable to a large set of crystals, including several diamond-structure and hexagonal close-packed elements and compounds such as quartz and calcite.

Detailed numerical results show that germanium has about 80 potentially useful wavelengths in the range 1.2 to 5 Å (neutron energy 0.003 to 0.05 eV). The beams are shown to have a number of other interesting properties. Several

*Abstract of a paper to be submitted to Acta Crystallographica.

problems, such as order contamination and background radiation, and potential uses in neutron research are discussed briefly.

SCATTERING LAW MEASUREMENTS FOR LIGHT WATER AT 95 °C*

R. B. Smith

Measurements have been made of the double-differential scattering of slow neutrons from H_2O at 95° using the Hanford triple-axis spectrometer. Scattering cross section values were obtained by normalization to the measured scattering from Vanadium and were obtained for neutron energy changes of 0.04 to 0.175 eV and scattering angles of 4 to 70°.

During the course of these measurements several sources of systematic errors in triple-axis spectrometer measurements were investigated. These included spatial nonuniformities in neutron beam intensity and in analyzer sensitivity as well as multiple diffraction in beryllium monochromator crystals. Simulated (0003) reflections were noted. The magnitudes of these effects and methods of minimizing their contributions are discussed.

Abstract of a formal report to be published.

COMPUTER CODE ABSTRACTS

COMPUTER CODE - CALX

1. NAME OR DESIGNATION OF CODE - CALX
2. COMPUTER FOR WHICH CODE IS DESIGNED AND OTHER UPON WHICH IT IS OPERABLE - UNIVAC 1107
3. NATURE OF PHYSICAL PROBLEM SOLVED - The isotope concentration equations are integrated as a function of time using a modified zero-dimensional model of the reactor. Emphasis is on calculational speed for survey type applications.
4. METHOD OF SOLUTION - The one-group parameters for the time step integrations are determined at specified time intervals from spectrum calculations based on a two region diffusion theory model of up to nine groups. The time step integrations use a fourth order Runge-Kutta scheme.
5. RESTRICTIONS ON THE COMPLEXITY OF THE PROBLEM -
   No. energy groups for in-burnup spectrum calculation ≤ 9
   No. fuels (fissile and fertile) ≤ 30
   No. nonfuels ≤ 100
   No. burnable regions ≤ 2
6. TYPICAL RUNNING TIME - Approximately 20 sec per typical case.
7. UNUSUAL FEATURES OF THE PROGRAM - CALX is linked to GAM and TEMPEST for cross section generation. End point searches can be made in time, reactivity, or exposure. Fuel cycling is permitted. Isotope transmutations can be followed through reactor outages. Initial conditions can be matched by addition of poison or enrichment mixtures. Graded exposure cases can be run.
8. RELATED AND AUXILIARY PROGRAMS - None.
9. STATUS - Coding Completed. 90% debugged.
10. REFERENCES - None.
11. MACHINE REQUIREMENTS - UNIVAC 1107, 64k core, 6000000_8 word drum storage (exclusive of system requirements), 2 tape units, on-line printer and card reader, clock.
12. PROGRAMMING LANGUAGE(S) USED - 100% FORTRAN IV.
13. OPERATING SYSTEM - CSC EXEC II, Package B
14. OTHER INFORMATION - None.

15. NAME AND ESTABLISHMENT OF AUTHOR

J. R. Lilley (formerly Hanford Laboratories) and
D. R. Marr - Code Authors

D. R. Marr - Abstract
Battelle-Northwest; P.O. Box 999; Richland, Washington 99352

16. MATERIAL AVAILABLE - Authority has been granted to release the following material for use subject to further testing [CALX Source Program (4000 cards)]. The material can be obtained directly from the author. Magnetic tape is preferred for transmittal.

COMPUTER CODE - HRG

1. NAME OR DESIGNATION OF CODE - HRG (Hanford Revised GAM)
2. COMPUTER FOR WHICH CODE IS DESIGNED AND OTHERS UPON WHICH IT IS OPERABLE: IBM 7090; UNIVAC 1107. Code has been adapted at other sites to CDC-1604, IBM 7040, Philco-2000.
3. NATURE OF PHYSICAL PROBLEM SOLVED - As in the original GAM code, this code computes the slowing-down spectrum in either the B-1 or P-1 approximation, using 68 groups of neutrons with a constant group width of delta u = 0.25. The calculated flux and current spectra are used to reduce the original 68-group cross section data to average values over as many as 32 broad groups.
4. METHOD OF SOLUTION
   (a) A subroutine will calculate resonance integrals for special nuclides from the resonance parameters for each group, using the quantitative methods developed by L. W. Nordheim.
   (b) The energy-angle correlation is retained for slowing down in all isotopes. That is, the P0 and P1 components of the scattering kernel are treated rigorously.
   (c) The code contains an extensive library. At present, the library tape contains data for 197 nuclides; obtained with but few exceptions from the BNW Master Library.[1] The library tape contains all of the data needed in the calculation for each of the 68 subgroups.
   (d) Inelastic scattering and (n,2n) processes are explicitly included.
   (e) The code contains an option that will calculate the neutron age in an infinite medium by the moments method.
   (f) Both microscopic and macroscopic broad group average cross sections can be obtained for as many isotopes as are on the data tape for any specified group structure.
   (g) Self-shielding factors can be included for any nuclide, if desired.
   (h) Eight different source spectra are included as options.

5. RESTRICTIONS ON THE COMPLEXITY OF THE PROBLEM - Number of broad groups $\leq$ 32. Broad group boundaries must coincide with one of the 68 fine group boundaries. Energies must lie between 10 MeV and 0.414 eV.

6. TYPICAL RUNNING TIME - One minute.

7. UNUSUAL FEATURES OF THE PROGRAM - HRG differs from GAM in the following features:

   (a) Details of the resonance integral calculation have been modified to: (1) extend the method to nuclides other than Th-232 and U-238, (2) include fission resonance integrals formally, (3) provide consistent space and energy self-shielding in calculating effective fine group cross sections for resonances, (4) extend and add tables, revise interpolation formulae, and change unresolved resonance treatment logic to speed calculations and make the code more compatible with data obtained from the BNW Master Library.

   (b) Microscopic broad group average transport cross sections are calculated from current-weighted broad group averages for consistency with the GAM definition of the macroscopic diffusion coefficient.

   (c) P1 cross section is defined as mu x PO (1/3 the GAM values).

   (d) Output printout has been revised for convenience of the user and options for punching or writing data for subsequent use have been added.

8. RELATED AND AUXILIARY PROGRAMS -

   (a) GAM-I

   (b) NUTAPE-II, updates and/or prints the HRG data tape. Updating can be done from either tape or card input.

   (c) BARNS-II and TRANS, calculate cross sections from BNW Master Library data and prepare tape input for NUTAPE-II for automated updating of HRG data tape.

9. STATUS - In use.

10. REFERENCES -

    (1) K. B. Stewart, BNW Master Library. BNWL-CC-325. Document on HRG in preparation.

11. MACHINE REQUIREMENTS - IBM 7090: 32k memory; minimum of 6 tapes, including system (1 or 2 additional tapes needed, depending on option). UNIVAC 1107: 64k memory; drum, 1 tape, excluding system.

12. PROGRAMMING LANGUAGE(S) USED - IBM 7090: Fortran-II (95%), FAP (5%). FAP subroutines are associated with punch option only and are easily removed. UNIVAC 1107: Fortran-IV.

13. OPERATING SYSTEM OR MONITOR UNDER WHICH PROGRAM IS EXECUTED - IBM 7090: IBM Fortran-II Monitor. UNIVAC 1107: CSC EXEC-II, Package B.

14. ANY OTHER PROGRAMMING OR OPERATING INFORMATION OR RESTRICTIONS - HRG input is compatible with GAM-1 input in format.

15. NAME AND ESTABLISHMENT OF AUTHOR -

J. L. Carter
Battelle-Northwest; P.O. Box 999; Richland, Washington 99352

16. MATERIAL AVAILABLE - Authority has been granted to release the following material for use subject to further testing

HRG Source Program (2500 cards)
NUTAPE-II Source Program (1000 cards)
Date Tape
Test Case

This material can be obtained directly from the author. Magnetic tape is required for transmission.

PUBLICATIONS

1. J. Lewins and R. D. Benham. Time Optimal Xenon Shutdown on the Xenon Boundary, BNWL-186. May 1966.
2. W. W. Little, Jr. and R. W. Hardie. Neutronics Characteristics of Selected Compact Reactors, BNWL-283. July 1966.
3. E. D. Clayton, C. R. Richey, R. C. Lloyd, S. R. Bierman, and L. L. Carter. "Criticality Research on Plutonium," Criticality Control of Fissile Materials, Proceedings of a Symposium, Stockholm, Sweden, November 1-5, 1965, International Atomic Energy Agency, Vienna, May 1966.
4. R. C. Lloyd, C. R. Richey, E. D. Clayton, and D. R. Skeen. "Criticality Studies of Plutonium Solutions," Nuclear Science and Engineering, vol. 25. June 1966
5. O. K. Harling. "Slow-Neutron Width of the 200 meV Vibration Level in H_2O," Physics Letters, vol. 22, no. 15. July 25, 1966.
6. O. K. Harling and B. R. Leonard, Jr. "A Multiphonon Neutron Scattering Study of Hydrogen Bonding in Zirconium Hydride," Symposium on Inelastic Scattering of Neutrons by Condensed Systems, BNL-940, Brookhaven National Laboratory, (C-45), pp. 96-104.
7. O. K. Harling. "Phased Rotating Crystal and Chopper for Time-of-Flight Neutron Spectroscopy," Rev. Sci. Instr., vol. 37, pp. 697-709. 1966.

PAPERS ACCEPTED FOR PRESENTATION

1. W. W. Little, Jr. and P. L. Hofmann. Neutronics Characteristics of Cermet, Oxide, and Carbide Driver Fuels for the Fast Test Reactor, to be presented at the ANS Winter Meeting Pittsburgh, Pa. October 31-November 3, 1966.
2. V. O. Uotinen. Measurement of the Reactivity Worth of Hafnium Oxide Rods in a PuO_2-UO_2-H_2O Lattice, to be presented at the ANS Winter Meeting, Pittsburgh, Pa. October 31-November 3, 1966.
3. J. W. Kutcher, J. H. Lauby, W. L. Purcell, L. C. Schmid, L. D. Williams, and J. R. Worden. Critical Experiments with PuO UO_2 Fuel and D_2O Moderator, to be presented at the ANS Winter Meeting, Pittsburgh, Pa. October 31-November 3, 1966.
4. N. A. Hill. k_∞ Measurements of a Pu-Al Thoria Supercell, to be presented at the ANS Winter Meeting, Pittsburgh, Pa. October 31-November 3, 1966.

PAPERS ACCEPTED FOR PUBLICATION

1. *W. W. Little, Jr. and R. W. Hardie. "FCC - A Fundamental Mode Code for Fast Reactor Analysis," Computer Code Abstract accepted for Publication in Nuclear Science and Engineering.*

2. *W. W. Little, Jr. and R. W. Hardie. "Neutronics Characteristics of Cermet and Ceramic Driver Fuels for the Fast Test Reactor," accepted for publication in Nuclear Applications.*

3. *C. L. Brown and R. C. Lloyd. "Measurements of Material Bucklings for 1.002 wt%, 1.25 wt%, and 1.95 wt% U-235 Enriched Uranium Tube Lattices in Light Water," accepted for publication in Nuclear Science and Engineering.*

4. *K. L. Garlid and S. R. Bierman. "Applications of Pulsed Neutron Measurements in Very Large Systems," to be published in Nuclear Applications, vol. 2, no. 5. 1966.*

5. *S. R. Bierman, K. L. Garlid, and J. R. Clark. "Resolving Time of a Pulsed Neutron Source Data Acquisition System," to be published in the December issue of Nuclear Applications.*

DISTRIBUTION

No. of Copies

5 Argonne National Laboratory
- Reactor Physics Constants Center (4)
- R. Avery (1)

11 Atomic Energy Commission, Wash.
- Assistant Director for Civilian Reactors, DRD (1)
- Reactor Physics Branch, DRD, Chief (1)
- H. Honeck (1)
- Division of Production, F. P. Baranowski (1)
- Division of Licensing and Regulations, C. D. Luke (1), R. J. Odegaarden (1)
- Physics and Mathematics Programs, K. G. Kolstad (1)
- Reactor Products, Division of Production, J. L. Schwennesen (1)
- Advanced Reactor Technology, E. E. Sinclair (1)
- Water Reactor Branch, DRD (2)

1 Babcock and Wilcox Company
- D. H. Roy

1 Bettis Laboratory, Westinghouse Electric Company
- J. J. Taylor

1 Brookhaven National Laboratory
- J. Chernick

1 California Institute of Technology
- H. Lurie, Engineering Division

CNEN-Centro Studi-Nucleaire CASACCIA
Rome, Italy
- Augusto Gardini

1 Combustion Engineering, Nuclear Division
- S. Visner

1 Computer Sciences Corporation
- E. Z. Block

3 Cornell University, Ithaca, N. Y.
- R. T. Cuykendall, Eng. Physics
- M. Nelkin
- R. R. Witson, Physics Dept.

No. of Copies

5 Douglas-United Nuclear, Inc.
- T. W. Ambrose
- C. E. Bowers
- R. O. Gumprecht
- R. Nilson
- G. F. Owsley

280 Division of Technical Information Extension

1 Donald W. Douglas Laboratories
- J. Greenborg

2 Duke University
Durham, N. C.
- H. W. Newson, Physics Dept.
- W. J. Seeley, School of Eng.

3 E. I. du Pont de Nemours & Co., Inc., Savannah River Laboratory
- J. L. Crandall
- G. Dessauer
- E. J. Hennelly

2 General Atomic
- L. W. Nordheim
- H. B. Stewart

1 General Electric Company
Knolls Atomic Power Laboratory
- R. Ehrlich

10 General Electric Company
Richland, Washington
- D. W. Constable
- R. L. Dickeman
- G. C. Fullmer
- M. M. Hendrickson
- M. C. Leverett
- W. S. Nechodom
- D. R. Oden, Jr.
- R. J. Shields
- R. E. Trumble
- GE File Copy

2 General Electric Company
San Jose
- S. Levy
- R. Kanne

2 General Electric Company
Vallecitos Atomic Laboratory
- L. P. Bupp
- T. M. Snyder

No. of Copies

1 Institute of Atomic Physics
Applied Radioactivity Laboratory
Bucuresti, CP 35, Rumania
Ing. E. Gaspar

8 Isochem Inc.
O. F. Beaulieu
O. F. Hill
H. H. Hopkins
G. R. Kiel
R. J. Sloat
A. E. Smith
R. E. Tomlinson
File Copy

1 Japan Atomic Energy Research Institute (JAERI)
Tokai-mura, Naka-gun, Ibaraki-ken, Japan
Hjime Sakata

1 Kansas State University
Manhattan, Kansas
W. R. Kimel, Nuclear Eng.

1 Los Alamos Scientific Laboratory
G. E. Hansen

1 Manhattan College
Riverdale, New York, N.Y.
Brother Gabriel Kane

1 Massachusetts Inst. of Technology
Prof. Irving Kaplan

1 North American Aviation Science Center
E. R. Cohen

1 North Carolina State College
R. L. Murray

2 Oak Ridge National Laboratory
F. C. Maienschein
A. M. Perry

1 Phillips Petroleum Company
R. G. Fluharty

1 Purdue University
P. N. Powers, Nucl. Eng. Dept.

1 Rensselaer Polytechnic Institute
E. R. Gaerttner

No. of Copies

15 Richland Operations Office
M. J. Carrothers
J. T. Christy
C. D. Compton
W. Devine, Jr.
G. R. Gallagher
P. G. Holsted
H. A. House
R. L. Plum
R. G. Rader
M. J. Rasmussen
M. R. Schneller
R. K. Sharp
Technical Information Library

1 Savannah River Operations Office
Robert Thorne

1 Union Carbide Corporation (ORNL)
C. A. Preskitt

1 United Nuclear Corporation
White Plains, N. Y.
G. Sofer

1 University of Arizona
Tucson, Arizona
Monte V. Davis, Nucl. Eng. Dept.

1 University of Florida
Gainesville, Florida
R. E. Uhrig, Nucl. Eng.

1 University of Illinois
Urbana, Illinois
Frederick Seitz, Physics Dept.

1 University of Minnesota
Minneapolis, Minnesota
H. S. Isben, Chem. Eng. Dept.

1 University of Nevada
Reno, Nevada
T. V. Frazier, Physics Dept.

1 University of Notre Dame
Notre Dame, Indiana
E. W. Jerger, Dept. of Mech. Eng.

1 University of Oregon
Eugene, Oregon
J. L. Powell, Physics Dept.

No. of Copies

2 University of Tennessee
Knoxville, Tennessee
A. H. Nielsen, Physics Dept.
P. F. Pasqua, Nucl. Eng. Dept.

1 University of Toledo
Toledo, Ohio
J. J. Turin

1 University of Washington
Seattle, Washington
A. L. Babb, Dept. of Nucl. Eng.

1 University of Wisconsin
Madison 6, Wisconsin
M. W. Carbon, Nucl. Eng. Com.

1 U. S. Atomic Energy Commission, DNR
A. Radkowsky

1 Virginia Polytechnic Institute
Blacksburg, Virginia
Andrew Robeson, Physics Dept.

1 Washington State University
Pullman, Washington
J. P. Spielman, Col. of Eng.

1 Westinghouse Electric
H. W. Graves

115 Battelle-Northwest
F. W. Albaugh
Q. L. Baird
C. A. Bennett
C. L. Bennett
R. A. Bennett
S. R. Bierman
C. L. Brown
W. L. Bunch
S. H. Bush
G. J. Busselman
J. J. Cadwell
J. L. Carter
L. L. Carter
D. E. Christensen
R. G. Clark
E. D. Clayton
R. E. Dahl
G. M. Dalen
F. G. Dawson (6)
D. R. de Halas
R. F. Dickerson
B. H. Duane
G. W. R. Endres

No. of Copies

Battelle-Northwest (contd)
S. L. Engstrom
E. A. Eschbach
S. L. Fawcett
J. R. Fishbaugher
D. G. Foster
H. A. Fowler
G. C. Fullmer
J. J. Fuquay
A. G. Gibbs
D. W. Glasgow
V. W. Gustafson
C. E. Haines
L. E. Hansen
S. E. Hanson
R. W. Hardie
O. K. Harling
R. A. Harris
H. Harty
R. A. Harvey
C. M. Heeb
R. E. Heineman
H. L. Henry
G. M. Hess III
N. A. Hill
R. J. Hoch
P. L. Hofmann
R. H. Holeman
R. M. Humes
U. P. Jenquin
R. L. Junkins
E. L. Kelley, Jr.
D. A. Kottwitz
J. W. Kutcher
C. R. Lagergren
D. D. Lanning
J. H. Lauby
B. R. Leonard,Jr.
W. R. Lewis
R. C. Liikala
C. W. Lindenmeir
E. P. Lippincott
W. W. Little
R. C. Lloyd
L. L. Maas
D. R. Marr
R. P. Matsen
D. D. Matsumoto
G. C. Moore
D. F. Newman
R. E. Nightingale
T. J. Oakes
L. J. Page
H. M. Parker
R. S. Paul
R. E. Peterson
W. W. Porath
W. L. Purcell
W. A. Reardon
J. J. Regimbal
C. R. Richey
W. C. Roesch

Battelle-Northwest(contd)

J. T. Russell
R. E. Schenter
J. E. Schlosser
L. C. Schmid
J. D. Smith
R. B. Smith
R. I. Smith
K. B. Stewart
W. P. Stinson
J. J. Stoffels
D. H. Thomsen
C. R. Tipton, Jr.
V. O. Uotinen
A. D. Vaughn
E. E. Voiland
M. T. Walling, Jr.
A. E. Waltar
J. D. White
O. J. Wick
R. D. Widrig
L. D. Williams
J. R. Worden
D. C. Worlton
H. S. Zwibel
Technical Publications (2)
Technical Information Files (5)